MECHANISTIC AND STRUCTURAL STUDIES OF SALICYLATE BIOSYNTHESIS IN *PSEUDOMONAS AERUGINOSA*

BY

Qianyi Luo

Submitted to the Department of Molecular Biosciences and the
Faculty of the Graduate School of the University of Kansas
in partial fulfillment of the requirements for the degree of
Doctor of Philosophy

Chairperson – Audrey Lamb

Committee members: Roberto De Guzman

Krzysztof Kuczera

Mark Richter

Emily Scott

William Picking

Date defended: 4/22/2009

The Dissertation Committee for Qianyi Luo certifies that this is the approved version of the following dissertation:

MECHANISTIC AND STRUCTURAL STUDIES OF SALICYLATE BIOSYNTHESIS IN *PSEUDOMONAS AERUGINOSA*

Committee:

Chairperson – Audrey Lamb

Roberto De Guzman

Krzysztof Kuczera

Mark Richter

Emily Scott

William Picking

Date approved: 4/23/2009

Abstract

Iron is an essential element for most pathogenic bacteria. To survive and establish infections in host tissues, these pathogens must compete with the host organism for iron. One strategy is to excrete iron-chelator siderophores with very high affinity to ferric iron in the low iron environment of the host. The phenolate type siderophore, such as pyochelin in *Pseudomonas aeruginosa*, uses salicylate derived from chorismate as a precursor. Studies have shown that the salicylate activation by adenylation for incorporation to siderophores is associated with the growth and virulence of some pathogens. The inhibition of salicylate biosynthesis, and hence, siderophore production is considered an attractive target for the development of novel antimicrobial agents.

In *P. aeruginosa*, salicylate is derived from chorismate via isochorismate by two enzymes: isochorismate synthase (PchA) and isochorismate-pyruvate lyase (IPL, PchB). PchB eliminates the enolpyruvyl side chain from isochorismate through a biologically unusual pericyclic reaction mechanism. PchB can also perform an adventitious pericyclic reaction that rearranges chorismate to prephenate possibly due to the homology to the *E. coli* chorismate mutase (CM). The primary contribution to lower the activation energy for enzymatic pericyclic reactions is controversial and may be arise from electrostatic stabilization of the transition state, or conformational stabilization of the reactive substrate. Structural and mutational studies on a key residue, lysine 42, of the active site loop suggest that rate enhancement of the two

pericyclic reactions (IPL and CM) performed by PchB results from both the transition state stabilization and the reactive substrate conformation, but the relative contributions are different for each reaction. A mutation with less active site loop mobility, A43P indicates that the loop dynamics is related to catalysis. The I87T structure reveals a larger disordered region compared to the wild type structure, suggesting that conformational mobility may play a role in catalysis.

PchA is an isochorismate synthase (ICS) in *P. aeruginosa* that removes the C4 hydroxyl group and adds a hydroxyl group to C2-chorismate. PchA is homologous to salicylate synthases from *Yersinia* spp. and *Mycobacterium tuberculosis* that convert chorismate to salicylate without requirement of an additional lyase such as PchB in *P. aeruginosa*. A sequence comparison between PchA with salicylate synthases of known structure suggests that two conserved residues are directly involved in the general acid and base chemistry in PchA: K221 as the general base and E269 as the general acid. Replacement of K221 and E269 with alanine respectively led to catalytically inactive enzymes, suggesting that K221 and E269 are critical for ICS catalysis. Preliminary pH dependence data for PchA supports the general acid and base mechanism of PchA catalysis. Two nonconserved residues A375 and D310 were also examined. Replacement of A375 by threonine, the corresponding residue in salicylate synthase, resulted in only residual ICS activity, indicating that A375 is not associated with the IPL-deficiency in PchA. The D310E mutant leads to two additional activities, IPL and CM. The additional activities in three reactions may due to the preferential orientation of substrates in the active site.

Acknowledgments

I would like to thank everyone who helped me in my graduate education and research. I would like to acknowledge Dr. Richard H. Himes and Dr. Roberto De Guzman for their help with instrument setup for isochorismate purification. I would also like to acknowledge Dr. Richard L. Schowen for his enzymology lectures and his scientific advice in thermodynamic analyses. I am thankful to Dr. Kathy Meneely for her generous assistance in my graduate course work and my research. I would like to acknowledge all the undergraduates who helped with my projects: Krysti Spiess, Daniel Shippy, Tyler McMillen, Katie Waugh, and Allison Ho. Thank you to all of the previous and current members of the Lamb lab, Andy Haith, Dr. Lena Zaitseva, Jingping Lu, Andrew Ouellette, and Jose Olucha.

I would like to thank Dr. T. Christopher Gamblin for his kind support and guidance with the instruments used in my research. I would like to thank the Protein Structure Laboratory at the University of Kansas for PchB K42A and I87T X-ray data collection.

I would also like to thank my committee members for providing suggestions and reading this dissertation, especially Dr. Roberto De Guzman and Dr. Emily Scott who served as the readers. Finally, a very special thank you goes to my advisor, Dr. Audrey Lamb for her scientific expertise, significant guidance, continuous support, and encouragement throughout my graduate career.

Table of Contents

List of Figures

List of Tables

CHAPTER 1

Introduction

1.1 Bacterial Infections

Among millions of different kinds of bacteria, only small subsets of them cause diseases and are referred to as pathogens. The work described in this dissertation will be relevant to pathogens *Pseudomonas aeruginosa*, *Yersinia enterocolitica*, and *Yersinia pestis*.

P. aeruginosa is a ubiquitous gram-negative bacterium that widely resides in nature including soil, water, plants, and animals. This opportunistic bacterium rarely causes infection in healthy people. Immunocompromised individuals are much more susceptible to opportunistic infections by *P. aeruginosa*, such as patients with severe burn, AIDS, or cystic fibrosis (CF) disease. *P. aeruginosa* outbreaks are responsible for a death rate of ~60% in patients with severe burns who have disrupted physical barriers to pathogen invasion.[1] In AIDS patients, secondary infections caused by *P. aeruginosa* are a major cause of death.[2] CF patients provide an excellent habitat for chronic microbial colonization in the airways. *P. aeruginosa* is the major pathogen found in CF patients and causes chronic lung infections associated with high rates of illness and death in CF patients.[3] *P. aeruginosa* is also responsible for nosocomial infections. *P. aeruginosa* infections are very hard to deal with because of a variety of virulence factors produced, the formation of biofilm, and their innate resistance to

many antibiotics.

Y. enterocolitica and *Y. pestis* are gram-negative bacteria that belong to the family *Enterobacteriaceae*. *Y. enterocolitica* is a versatile enteric pathogen that usually infects hosts through contaminated food and water. *Y. enterocolitica* infections cause acute enteritis associated with fever, abdominal pain and diarrhea , particularly in children.[4] Various antibiotics are available for the treatment in patients with *Y. enterocolitica* infection.[5] *Y. pestis* is historically famous as an etiologic agent of European Black Death (the plague) during the 14th century, resulting in a loss of approximately 30 to 40% of the population.[6] *Y. pestis* is an obligate parasite and is primarily transmitted by fleas from infected rodents or other wild mammals to humans. *Y. pestis* grows in the regional lymph nodes after transmitted to humans, causing swollen lymph nodes followed by continued growth in the blood and other organs.[6] Patients with plague can be treated by antibiotics treatments, such as streptomycin, tetracycline, chloramphenical, *etc*.[6]

Bacterial drug resistant species have been documented, including *P. aeruginosa* and *Yersinia* spp. To develop new antimicrobial reagents, the iron uptake pathway is of interest due to no current reagent specifically designed to inhibit this pathway.

1.2 Bacterial Iron Uptake

The Importance of Iron

Iron is an essential element for most living organisms and a growth-limiting

factor for the majority of microorganisms. Iron can adopt two positively charged ionic forms, Fe^{2+} (ferrous iron) and Fe^{3+} (ferric iron). Many enzymes involved in metabolic processes require iron-containing cofactors, for example, iron-sulfur clusters and heme groups, as a catalytic center or an electron carrier. Thus iron is important for a variety of cellular events, including photosynthesis, respiration, the tricarboxylic acid cyclic, oxygen transport, and gene regulation.[7]

Ferrous iron is soluble in solution at pH 7.0. If this reduced ferrous form could be maintained, Fe^{2+} would be sufficient for living cells. Under anaerobic or reducing conditions, Fe^{2+} diffuses easily through porins on the outer membrane of gram-negative bacteria, and then across the cytoplasmic membrane via an ABC ferrous ion transporter.[8] However, under aerobic conditions, Fe^{2+} is unstable and is oxidized to Fe^{3+}, which releases reactive hydroxyl radicals that are toxic for most biological macromolecules.[9] At physiological pH 7, Fe^{3+} forms insoluble ferric oxide hydrate complexes, leading to a free Fe^{3+} concentration of 10^{-9} to 10^{-18} M. In mammalian hosts, ferric iron is tightly sequestered into various proteins such as hemoproteins, ferritins, lactoferrin, and transferrin. Iron homeostasis is so strictly regulated that the concentration of free iron in the mammalian hosts is only about 10^{-18} ~ 10^{-24} M.[10] Thus, in order to colonize hosts and establish infections, pathogenic bacteria must acquire iron from its host. Under conditions of iron starvation, these bacteria have evolved several elaborate mechanisms to scavenge iron from their environment through high affinity iron acquisition systems composed of siderophores, outer membrane receptors, periplasmic binding proteins, ATP-binding cassette transporters,

and the TonB-ExbB-ExbD protein complex (Figure 1-1). Iron overload is harmful to bacteria, so iron uptake is strictly regulated through repressors of genes involved in iron uptake systems.[11]

Iron Uptake from Host Transferrin/Lactoferrin

Transferrin and lactoferrin are homologous iron-binding glycoproteins. Gram-negative pathogenic bacteria, such as *Neisseria* and *Haemophilus*, have a conserved mechanism to extract ferric iron from transferrin and lactoferrin through outer membrane receptors for these two glycoproteins.[12] The extraction events take place on the cell surface via receptors TbpB/TbpA for transferrin, and LbpB/LbpA for lactoferrin.[13] TbpB and LbpB are attached to the outer membrane by a lipid anchor and function as the initial reorganization site of transferrin and lactoferrin.[14] Boulton *et al.*[15] have proposed a dynamic model in which TbpB initially recognizes and binds transferrin, which might facilitate transferrin binding to TbpA. Binding of transferrin/lactoferrin to TbpA/LbpA leads to a conformational change of transferrin/lactoferrin, and then release of iron. After transportation across the outer membrane, ferric ion binds to ferric iron binding protein (FBP) and is shuttled through the cytoplasmic membrane via an inner membrane ABC transporter (Figure 1-1).[16]

Heme as An Iron Source

In a host organism, iron is often incorporated into heme, a prosthetic group in

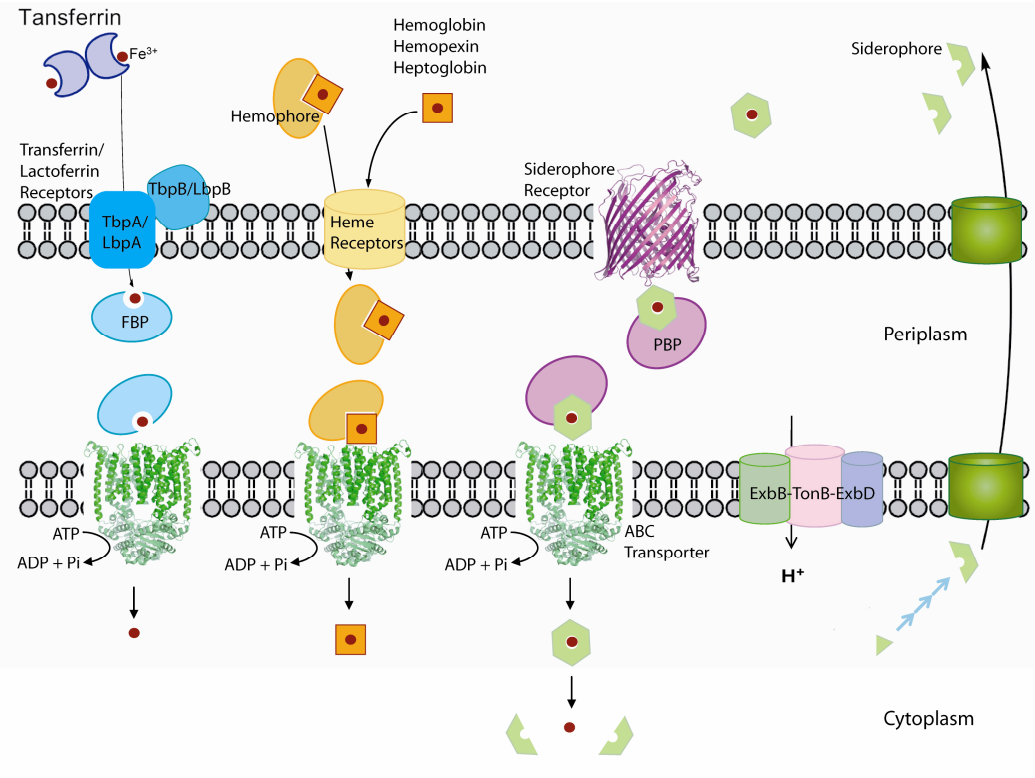

Figure 1-1. A schematic view of iron uptake in gram-negative bacteria. ABC transporters on the inner membrane are represented as BtuCD (PDB code 1L7V) and the siderophore receptor is represented as FptA (PDB code 1XKW).

many host intracellular carrier proteins. Pathogenic bacteria secrete exotoxins such as cytolysins and hemolysins to disrupt cell membranes and release heme during infection.[17, 18] Two mechanisms have been proposed for heme uptake in gram-negative bacteria (Figure 1-1). The first mechanism, the direct uptake of heme or hemoproteins requires a TonB dependent outer membrane receptor. The receptor HmbR of *Neisseria meningitides* transports hemoglobin and heme, whereas HemR of *Y. enterocolitica* is capable of transporting heme and many hemoproteins, such as hemoglobin, myoglobin, hemopexin, etc.[19] To move heme and hemoproteins into the cytoplasm, a periplasmic binding protein (PBP), and an ABC transporter are also required.[19] The second mechanism used by gram-negative bacteria is to secrete small heme-binding proteins (hemophores) that can scavenge heme from the host. This heme acquisition system [20] has been identified in several pathogens such as *P. aeruginosa* and *Yersinia* sp.[12, 21] Hemophore HasA from *Serritia marcescens* is secreted into the extracellular environment through an ABC transporter complex (HasD-HasE-HasF).[12, 20] HasA binds either free heme or extracts it from hemoproteins and then is transported through the receptor HasR that also recognizes free heme.[22] Once inside the cytoplasm, ferric iron is release upon heme degradation by heme oxygenase.[23]

Siderophores

Siderophores are low molecular weight molecules (500 ~ 1000 Da) produced in microorganisms and some plants that chelate ferric iron with particularly high

affinity (K_a range from 10^{23} to 10^{30} M^{-1}).[7] Almost 500 different siderophores from gram-negative and gram-positive bacteria have been identified.[24] Despite the diversity in their overall structures, siderophores primarily use three types of chemical groups to coordinate the ferric iron. Based on the chemical properties of these iron-chelating groups, siderophores are classified as: hydroxycarboxylate, catecholate-phenolate, and hydroxamate types (Figure 1-2). Some siderophores integrate more than one chemical group from the three classes, resulting in a mixed type siderophore. A siderophore molecule provides six coordination sites to an iron due to ferric iron's electronic configuration. The Fe-coordinating atom in siderophores is primarily oxygen.[25]

Studies have found that siderophore production is associated with virulence in several pathogenic bacteria.[4, 26-28] Siderophores regulated production of the virulence factors required for colonization and lethality during *P. aeruginosa* infection.[26, 27] Yersiniabactin, a siderophore produced by *Y. enterocolitica* was found to only be expressed in the mouse lethal strains, indicating that the virulence was strictly related to siderophore production.[28]

Nonribosomal Peptide Synthesis

Siderophores are primarily assembled by nonribosomal peptide synthetase (NRPS) machineries in the cytoplasm. NRPSs are large multifunctional enzymes that consist of modules; each module catalyzes one cycle of peptide chain elongation. A module is composed of several domains that are responsible for a single step during the

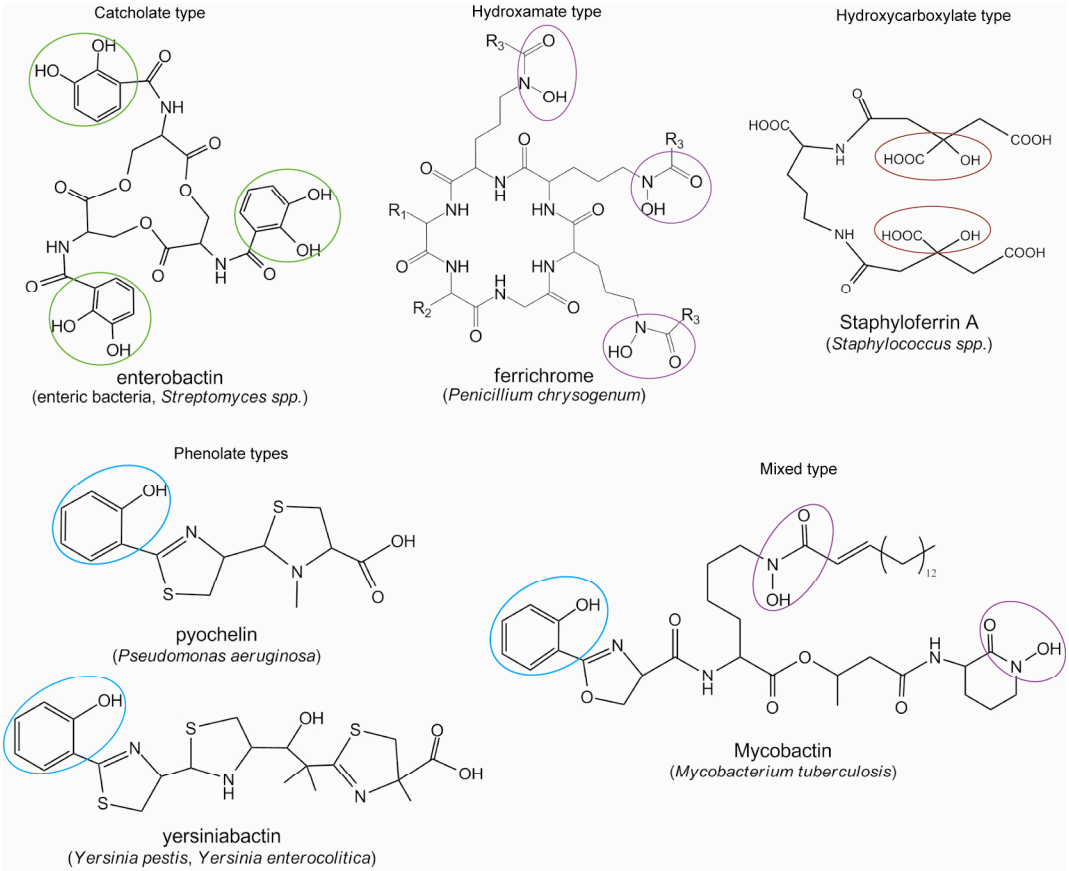

Figure 1-2: Representative siderophore structures. Catecholate-phenolate type siderophores coordinate Fe^{3+} using adjacent hydroxyl groups of catechol rings (green and blue circles); hydroxamate type siderophores bind Fe^{3+} via a carbonyl group with an adjacent nitrogen (purple circles), and citrate-derived α-hydroxy-carboxylates are circled in red in hydroxycarboxylate type siderophore.

chain elongation. The classical module has an adenylation domain (A), a peptidyl carrier domain (PCP), a condensation domain (C), and editing domains (Figure 1-3). An amino acid is adenylated by the A domain and tethered to the 4′-phosphopantetheine (Ppant) group of the PCP domain. The Ppant group shuttles the peptide intermediate between catalytic centers that catalyze peptide bond formation in the C domain and modification of the incorporated amino acid in the editing domain. The editing domains give rise to the diversity and stability of siderophores, such as epimerization L-amino acid to D-amino acid, methylation of the peptide bond, and alteration of the oxidation state in oxazoline and thiazoline rings. A thioesterase (TE) domain is usually found at the C-terminal of last module of NRPS assembly line, serving as an end point of peptide elongation through hydrolysis or cyclization.[29, 30]

Siderophore Transport

Siderophores are too big to freely diffuse across the inner and outer membranes in gram-negative bacteria, so membrane transporters are required for siderophore secretion. The mechanism of siderophore secretion is proposed to require energy. The exporters involved in the outflow of siderophores have only been identified in several bacteria. Enterobactin secretion by *E. coli* requires an efflux pump of the major facilitator superfamily (MFS) on the inner membrane and a channel protein on the outer membrane.[31] Once in the environment, the siderophore extracts iron from the host, forming a Fe^{3+}-siderophore complex that is recognized by an outer membrane receptor. Structures of several Fe^{3+}-siderophore receptors have been

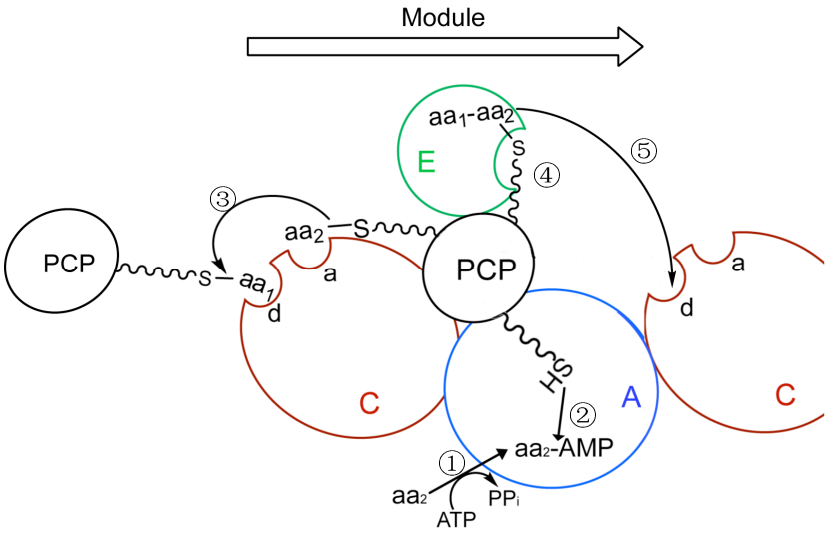

Figure 1-3: Representation of one cycle of the peptide chain elongation on a module of NRPS. ① The amino acid is activated by adenylation by the A domain. ② The activated adenylyl amino acid is covalently attached to the thiol group of the Ppant arm on the PCP domain. ③The C domain catalyzes peptide formation between the donor and acceptor amino acids. ④ Modification of the amino acid (aa_2) by the E domain in this case, to convert L- to D- configuration. ⑤ D-aa_2 is loaded to the donor site on the C domain of next module. Abbreviations: A, adenylation domain; PCP, peptidyl-carrier domain; C, condensation domain; E, epimerase domain. (Figure modified from Mootz *et al.* 2002)

determined as β-barrels. Transport of Fe^{3+}-siderophore complex across the outer membrane requires energy input from the complex ExbB-TonB-ExbD on the inner membrane (Figure 1-1),[32] followed by transport into the cytoplasm through an ABC transporter. Iron is released in the cytosol by hydrolysis of the Fe^{3+}-siderophore or reduction of Fe^{3+} to Fe^{2+} that has less affinity for the siderophore.[25]

Pyochelin Assembly

During infection, *P. aeruginosa* overcomes the iron-limiting condition in hosts by secreting two siderophores, pyochelin and pyoverdin. Pyoverdin has a very high affinity for ferric iron with an association constant of 10^{30} M^{-1}, whereas pyochelin binds ferric iron with an association constant of 10^5 M^{-1}.[24, 33] Pyoverdin is a hydroxamate siderophore composed of 6 ~ 12 amino acids. It has been shown that the virulence of *P. aeruginosa* is regulated and enhanced by the production of pyoverdin.[26, 27] Pyochelin produced by *P. aeruginosa* increased the lethality of virulent strains but not in nonvirulent strains.[34]

Pyochelin assembly by NRPS requires one salicylate, three ATPs, two cysteines, one S-adenosylmethionine (SAM), and one NADPH. The steps of pyochelin assembly are shown in Figure 1-4. Six enzymes, PchA, PchB, PchD, PchE, PchF, and PchG are involved. The pyochelin precursor, salicylate is generated in a two-step process catalyzed by the sequential action of the enzymes PchA and PchB. PchA, an isochorismate synthase, converts chorismate from the shikimate pathway into isochorismate, followed by isochorismate-pyruvate lyase, PchB to produce salicylate

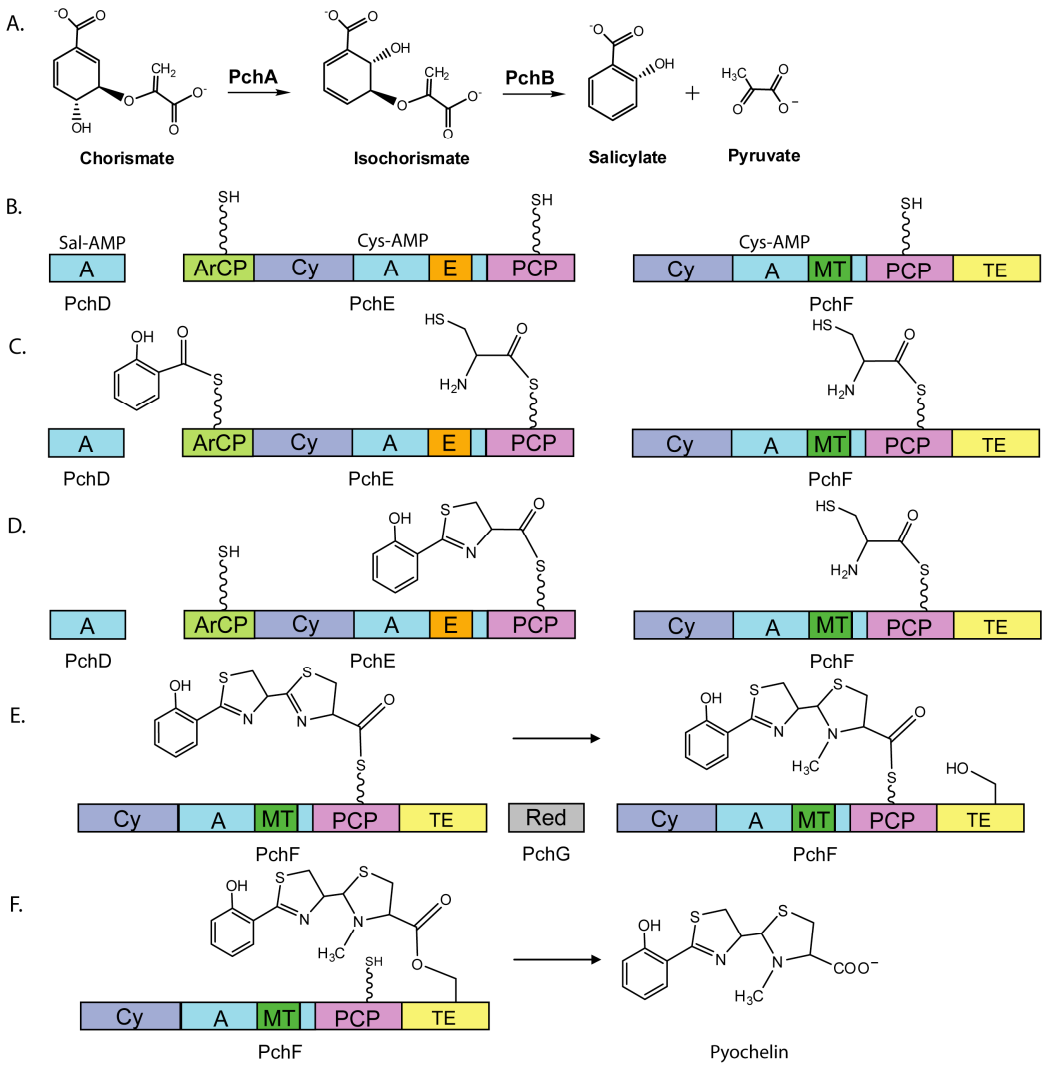

Figure 1-4: Pyochelin assembly line in *P. aeruginosa*. **A.** Salicylate formation in a two-step process. **B.** Covalent attachment of the Ppant prosthetic group to the carrier domains and activation of the building blocks through adenylation. **C** & **D.** Chain elongation through condensation and cyclization. **E.** Reduction of the second thiazoline ring by PchG and N-methylation of thiazolidine ring. **F.** Pyochelin maturation by hydrolysis and release from the last domain of PchF. Abbreviations: ArCP, aryl-carrier domain; Cy, cyclization domain; MT, methyltransferase domain; TE, thioesterase domain; Red, reductase. (Figure modified from Quadri *et al*., 1999)

and pyruvate (Figure 1-4A). The assembly of pyochelin starts with PchD, an adenylation domain that activates salicylate. PchE and PchF undergo posttranslational modification by covalent attachment of the Ppant group from coenzyme A to their PCP domains and aryl-carrier (ArCP) domains (Figure 1-4B). Activated salicylate is transferred to the ArCP domain of PchE (Figure 1-4C). The cyclization (Cy) domain of PchE condenses the salicylate with the first cysteine as well as heterocyclizes to form a thiazoline ring, which is followed by conversion of L-cysteine to D-cysteine by the epimerization (E) domain (Figure 1-4D). The peptidyl product is condensed with the second cysteine that is continuously cyclized to a thiazoline ring by the Cy domain in PchF. PchG is a NADPH-dependent reductase that reduces the second thiazoline ring to a thiazolidine ring,[35, 36] which act as a nucleophile that facilitates the methyl group transfer from SAM to the thiazolidine ring by the methyl transferase domain of PchF (Figure 1-4E). The completed pyochelin is released from PchF via the TE domain (Figure 1-4F).[37]

Yersiniabactin Assembly

Yersiniabactin (Ybt) from *Yersinia* spp. is a mixed nonribosomal peptide and polyketide with a K_a of 10^{36} M^{-1} for ferric iron.[38] Ybt assembly requires not only NRPSs but also a PKS (polyketide synthase) component (Figure 1-5).[29] Four proteins catalyze the condensation of one salicylate, three cysteines, and one malonate into a Ybt molecule with consumption of five ATPs, three SAMs as methyl group donor, and one NADPH.[39]

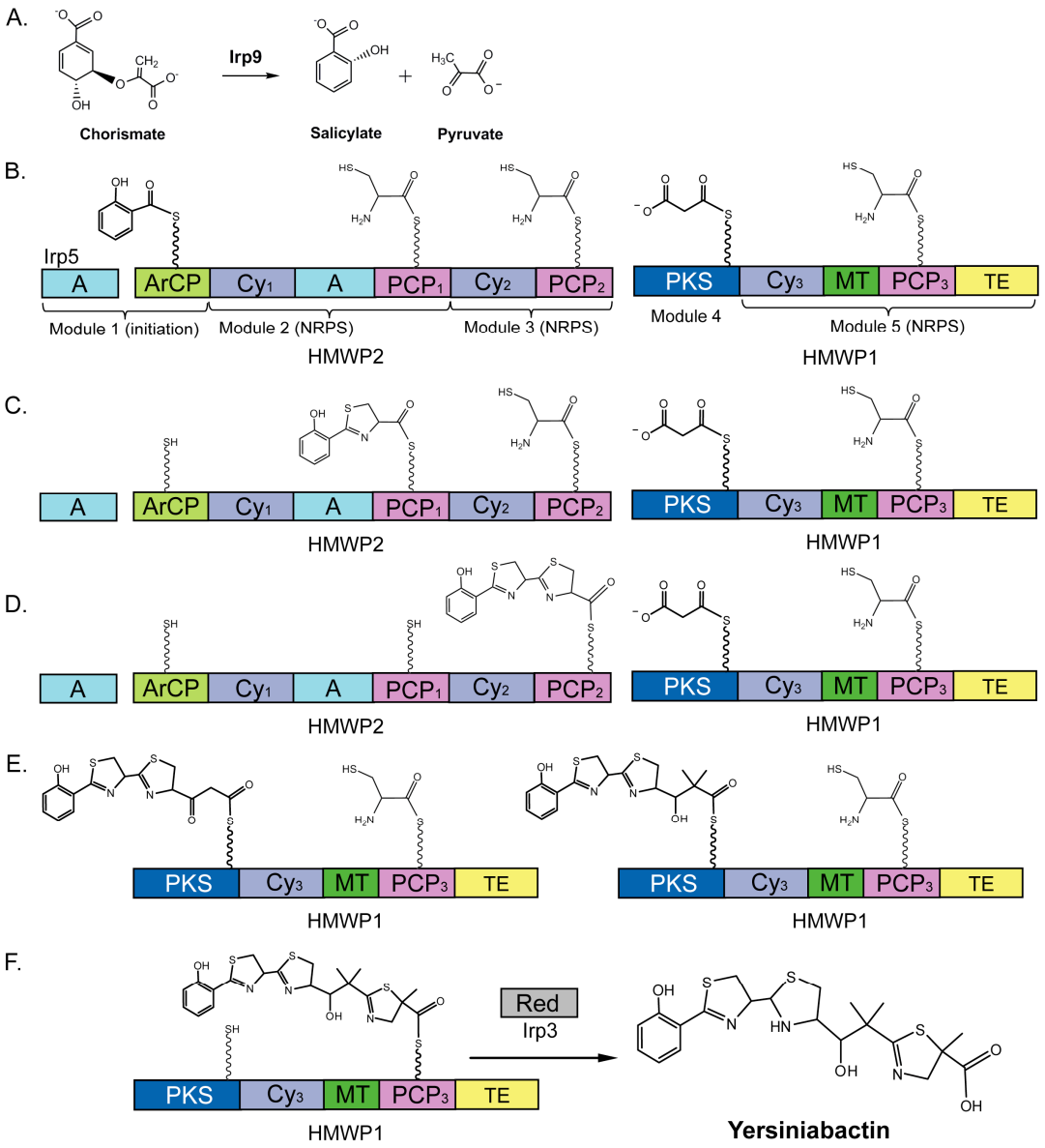

Figure 1-5: Yersiniabactin assembly in *Y. enterocolitica*. **A.** Salicylate formation from chorismate catalyzed by Irp9. **B.** Activation and covalent attachment of the acyl building blocks to the carrier domains. **C** & **D.** Chain elongation through condensation and cyclization. **E.** Peptidyl chain transfer from the last module of HMWP2 to the PKS module of HMWP1. A malonyl moiety is loaded to the peptidyl chain. Double methylation of C2 on the intermediate-PKS and incorporation of the last cysteine. **F.** Methylation of the C_α of the thiazolinyl-S-PCP_3 intermediate, reduction of the second thiazoline ring by Irp3, and hydrolysis to release of mature yersiniabactin by TE domain. The PKS module is composed of a keto synthase domain, an acyltransferase domain, a MT domain, a ketoreductase domain, and an acyl-carrier domain. (Figure modified from Miller *et al.* 2002)

Proteins involved in Ybt synthesis have very high sequence homology between *Y. enterocolitica* and *Y. pestis*. The assembly line for Ybt is composed of Irp5, high-molecular-weight proteins 1 and 2 (HMWP1 and HMWP2), and Irp3 in *Y. enterocolitica.* Prior to Ybt assembly, salicylate is generated from chorismate in a single step catalyzed by a salicylate synthase Irp9 (Figure 1-5A)[40], which is different from the two-step reaction carried out by PchA and PchB in pyochelin biosynthesis in *P. aeruginosa*. Salicylate is then adenylated and transferred to the ArCP domain of HMWP2, ready for peptidyl chain elongation (Figure 1-5B). The Ybt is assembled on the HMWP1 and HMWP2 protein complex. HMWP2 has two NRPS modules that are responsible for incorporation of two cysteine units to salicylate (Figure 1-5C and 1-5D), which is similar to the elongation steps during pyochelin synthesis. The remaining steps for the formation of Ybt take place on HMWP1. First, the intermediate tethered to the PCP_2 domain in the last module of HMWP2 needs to be transferred to the PKS module of HMWP1. Instead of an amino acid, malonate is activated and loaded onto acyl-carrier domain of PKS. The keto synthase domain of PKS catalyzes the condensation reaction to form a C-C between the intermediate on the PCP_2 domain and the malonyl group, switching from the NRPS system to the PKS system (Figure 1-5E). Second, methyl groups from SAMs are attached to the malonyl group by a MT domain and β-keto is reduced by the ketoreductase domain on PKS module (Figure 1-5E). Third, the assembly is switched back to the NRPS from the PKS, in which the last cysteinyl group is added and cyclized. The last methylation on C_α of the thiazolinyl-PCP_3 is carried out by the MT domain of the last

module on HMWP1. Finally, the middle thiazoline ring is reduced into a thiazolidine ring by the NADPH-dependent reductase Irp3, followed by the release of complete Ybt from the HMWP1 through action of the TE domain (Figure 1-5F).

1.3 Enzyme Active Site and Catalysis

Enzymes catalyze biochemical reactions in almost all physiological processes in living organisms. All known enzymes are proteins with exception of some catalytic RNAs. Enzyme catalysis can accelerate reaction rates as large as a factor of 10^{19}.[41] Under biologically relevant conditions, uncatalyzed biochemical reactions happen slowly with rate constants range from 10^{-17} to 10^{-1} s^{-1}, whereas rate constants (k_{cat}) of enzyme-catalyzed reactions range from 10 to 10^{7} s^{-1}.[42] Enzymes provide a sheltered environment, active sites, where specific substrates bind and chemical reactions take place to produce specific reaction products. Both rate enhancement and substrate specificity allow enzymes perform the chemical reactions in metabolism with efficiency and accuracy for cells.

Enzyme Active Site

During enzymatic catalysis, the formation of an enzyme-substrate complex (ES) is the first step followed by formation of an enzyme-transition state complex ($ES^{‡}$), an enzyme-product complex, and finally release of product from enzyme. All those processes take place in an active site through direct contacts between the substrate and its active site.

In the active site, amino acids side chains, cofactors, or coenzymes are arranged in a precise position that in some ways complements the structure and charge of the substrate molecule. During an enzyme-catalyzed reaction, various types of chemical reactions happen between substrates and functional groups of enzymes. Functional groups that provide chemical catalysis include metal ions, coenzymes, and the carboxyl, amino, imidazole, hydroxyl, and thiol groups of amino acid side chains. These functional groups are involved in hydrogen bonding and electrostatic interactions with substrates and also serve as acid-base, nucleophilic, and electrophilic catalysts. A transient covalent bond may be formed between catalytic functional groups and a substrate to promote the reaction, or a group may be transiently transferred from the substrate to the enzyme in the active site. Covalent interactions between enzymes and substrates provide an alternative reaction pathway to lower the activation energies of reactions, leading to rate enhancement.[43]

Conformational Mobility in Enzyme

An enzyme is a structurally dynamic system in which internal motions are important for its function. Some motions may associate with global conformational change.[44] Enzymes were thought to be rigid molecules that must have an active site shape that exactly complements to that of the substrate, known as the lock and key model. However, the interactions between the enzyme and substrate are far more complex. In most cases, the active site does not have the exact shape of substrate. When the substrate approaches the active site, the enzyme is induced to slightly

change its active site conformation to best fit the substrate. This change also puts strains on the substrate molecule, promoting bond-breaking and bond-making towards the transition state. This type of interaction is described as an induced-fit model.[45] In other words, the enzyme's active site best accommodates the structure of substrate at the transition state rather than the ground state. Motions of the active site help with transition state formation and also provide stabilization to the transition state.[46]

Transition State Theory for Enzyme Catalysis

For a chemical reaction, the transition state is the unstable species that has the characteristics of partially broken and partially formed covalent bonds. The transition state is at the highest point on the reaction coordinate diagram and is a key factor that would affect the reaction rate ($E^{\ddagger}$ in Figure 1-6). Enzyme-catalyzed reaction differs from its counterpart reaction in solution in the formation of ES binary complex and the transformation into the $ES^{\ddagger}$.

The binding of a substrate to an enzyme (formation of the ES complex) is most likely noncovalent through hydrogen bonding, hydrophobic, electrostatic, and van der Waals interactions. These weak, noncovalent interactions between the enzyme active site and substrate are considered the major source of the energy required to lower the activation free energy barriers of reactions. In 1946, before structural information was available, Linus Pauling[47] proposed that enzymes bind the transition state (TS) better than the corresponding ground state. This means that interactions between the enzyme active site and the transition state are optimized for

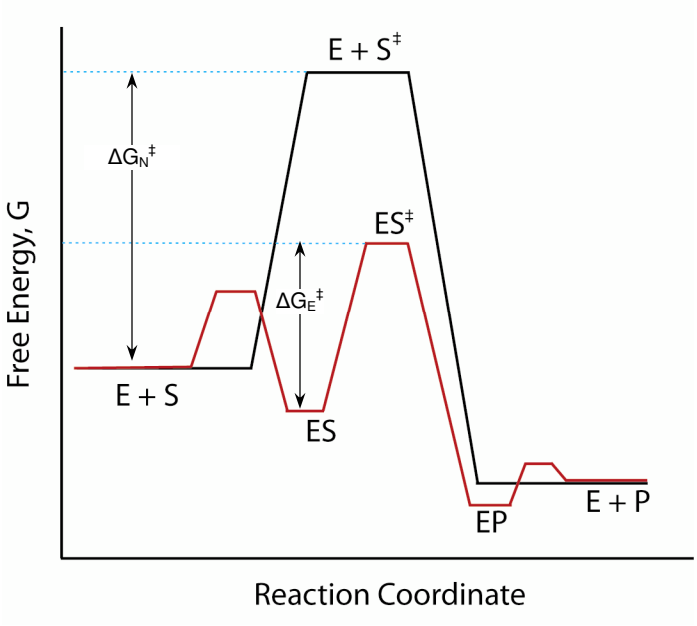

Figure 1-6: Reaction diagram for a single-substrate reaction in solution (black) and catalyzed by an enzyme (red). The terms $\Delta G_N^{\ddagger}$ and $\Delta G_E^{\ddagger}$ correspond to the activation energies for the uncatalyzed reaction in solution and its counterpart catalyzed by the enzyme, respectively. (Figure modified from Voet *et al*. 2005)

stabilizing the TS, hence lowering the activation energy and accelerating the reaction (Figure 1-6). For decades, experimental evidence support the idea that the stabilization of the transition state is the origin of the rate enhancement by enzymes and the primary basis for substrate specificity.[48]

A transition state analog (TSA) is a molecule that resembles the transition state structure and binds the enzyme much more tightly than corresponding substrate and product. Studies of enzymatic reaction mechanisms can provide opportunities for rational design of powerful transition state inhibitors.

1.4 Enzyme Catalytic Mechanisms

Enzymes affect the rate of reactions, instead of equilibriums. The rate of a chemical reaction primarily depends on the energetic barrier between the substrate and the product, the activation energy ($\Delta G_N^{\ddagger}$). Enzymes act by lowering the activation energy (Figure 1-6) and allow for rate enhancement of the reaction through one or more catalytic mechanisms: 1) general acid and base catalysis, 2) covalent catalysis, 3) proximity and orientation effects, and 4) preferential binding of the transition state.[45, 49, 50]

General Acid and Base Catalysis

The most common biochemical reactions involve proton transfer at some point during the reaction, in which acid and base groups are required for catalysis. Reactions catalyzed by protons (from hydronium ion H_3O^+) or hydroxide ion (enclosed by three H_2O molecules) in water are the specific acid and base catalysis.

However, in the majority of enzyme catalyzed reactions, the Brϕnsted-Lowry acidic and basic groups of enzymes, or cofactors promote the reactions, which are the general acid and base catalysis.[45]

Amino acid with acidic and basic side chains are commonly involved in general acid and base catalysis. In the active sites, reactive side chains are in the close proximity to the substrate, and positioned precisely controlled relative to the substrate, resulting in rate enhancement of 10^2 to 10^5.[43] The efficiency of general acid and base catalysis primarily depends on the pK_a of side chains participating in reactions, which will be greatly perturbed by the local environment of the active site.[42]

A characteristic feature of general acid and base catalysis is that the transition state of the substrate is stabilized by the catalytic groups involved in proton transfer. Representations of these transition states are shown in Figure 1-7. In this case, the hydrolysis of ester bonds requires formation of a transition state, where an electron is partially transferred from water to the ester. The transition state can be stabilized by a acidic group/electron-pair acceptor (HA) or a basic group/electron-pair donor (B:).[43] Some enzymes simultaneously employ both general acid and general base mechanisms to catalyze a reaction, which has known as a concerted general acid and base catalysis.[45]

Covalent Catalysis

In covalent catalysis, enzyme-catalyzed reactions go through the formation of a transient covalent intermediate between the enzyme and the substrate. Formation of

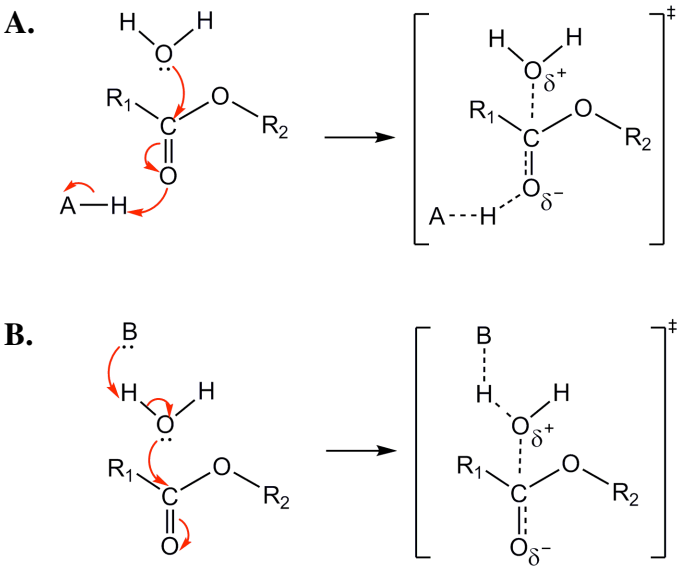

Figure 1-7. The transition states for ester hydrolysis catalyzed by general acid (A) and general base (B) mechanisms. Figure modified from Nelson, D.L. & Cox, M.M., 2005.

the covalent intermediate brings the reaction along the reaction coordinate toward the transition state, and lowers the activation energy of the reaction. The covalent catalysis mechanism breaks the reaction into the formation and the breakdown of the covalent intermediate instead of catalyzing the single reaction directly.[49] Several families of enzymes performs this type of mechanism, such as serine proteases (acyl-serine intermediates), cysteine proteases (acyl-cysteine intermediates), protein kinases and phosphatases (phosphor-amino acid intermediates), *etc*.[42] Covalent catalysis is performed mainly through nucleophilic and electrophilic pathways.

Nucleophilic Catalysis

Nucleophilic catalysis involves a nucleophilic attack on a substrate (group being transferred), resulting in a transient covalent intermediate with an electrophilic reaction center that is much more reactive than the ground state substrate.[42] The covalent intermediate can then be attacked by a water or an other molecule to form the product and regenerate the functional group of the enzyme.[42] Groups being transferred normally include acyl groups, phosphoryl groups and glycosyl groups.

The reaction rate of nucleophilic catalysis depends on the nucleophilicity (electron-donation ability) of the attacking group and the susceptibility of the substrate (electrophile).[42] The nucleophilicity is primarily determined by the basicity of the group (the tendency of a group to donate an electron pair to a proton). The nucleophilic reactivity of a group increases with its basicity. Thus, the reaction rate of most nucleophilic catalysis is normally correlated with the pK_a of the nucleophile.

Besides pK_a, the chemical nature of the nucleophile, including oxidation potential, polarity, ionization potential, electronegativity, and the group size, *etc*. would also determine the reaction rate, features that distinguish nucleophilic catalysis from general base catalysis.[42, 49] Table 1-1 lists enzyme side chains widely function as nucleophiles and examples of covalent intermediates formed during the reactions.

Electrophilic Catalysis/Metal Ion Catalysis

In electrophilic catalysis, a substrate reacts with an electrophile and a covalent intermediate forms. There are no efficient electrophiles among the amino acids. Therefore, enzymes often recruit electron-deficient organic cofactors or metal ions, which are coordinated with the substrate or side chains of amino acids as the electrophiles.

A variety of enzymes utilize divalent metal ions (Fe^{2+}, Cu^{2+}, Zn^{2+}, Mn^{2+}, Mg^{2+}, and Ca^{2+}, *etc*.) in the active sites as electrophilic catalysts. Metal ions participate in electrophilic reactions in several ways: 1) they can electrostatically stabilize or shield the negatively charged group of the substrate or the transition state; 2) they can preferentially bind and help orient reactive groups of the substrate properly for reaction, and also act as a bridge that mediates the interaction between a substrate and a nucleophilic group; 3) they can perturb the pK_a and hence the reactivity of nearby nucleophiles; 4) some metal ions can function as an electron carrier in the oxidation-reduction reactions by reversible changes in the metal oxidation states.[43]

Table 1-1: Nucleophiles of the amino acid side chains and the covalent intermediates formed during catalysis . (Adapted from Frey, 2007)

Amino acid	Nucleophile	Example enzyme	Covalent intermediate
Serine	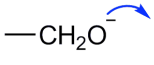	Serine proteases	Acyl-enzyme
Cysteine	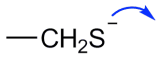	Cysteine proteases	Acyl-enzyme
Aspartate	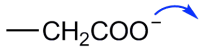	Coenzyme A transferases	CoA-enzyme
Lysine	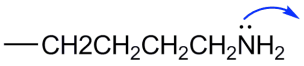	Pyridoxal-containing enzymes	Schiff bases
Histidine	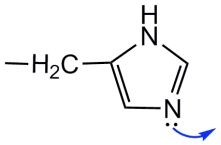	Phosphoglycerate mutase	Phosphoryl enzyme
Tyrosine	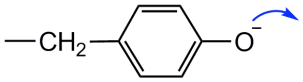	Glutamine synthase	Adenyl enzyme

The ε-amino group of lysine can react with carbonyl groups of substrates or coenzymes to form imines with higher electrophilic reactivities, which would promote the reactions. Pyridoxal phosphate and thiamine pyrophosphate are commonly used coenzymes for electrophilic catalysis.[49]

Proximity and Orientation Effects

The general acid and base, or the covalent catalysis chemistry performed in the enzyme active site would most likely have counterparts in the organic chemistry reaction, which go through the same transition states. Therefore, the great rate enhancement of enzyme is in the binding process that happens in the active site. The substrate in the active site must go through desolvation and loss of degrees of freedom.[42] Binding of a substrate to the active site through a series of weak interactions would bring the reactant toward the transition state. Those interactions can also stabilize the transition state and destabilize the corresponding ground state.

In the theory of the proximity and orientation effect, rate acceleration is derived from facts that the reactive groups of enzymes and substrates must be positioned in an orientation optimal for reaction. Proximity is proposed to increase the effective concentrations of substrate when bound in the enzyme active site, which by itself counts for relatively a small portion of rate acceleration.[45] The reactant maximizes its reactivity by changing its geometry such that reacting groups are positioned in a proper way, leading to the electronic energy minimum of its transition state, and this orientation effect can result in large rate enhancements.[45, 51] In other

words, the preorganization of the substrate to a reactive conformation followed by the stabilization by the enzyme active site would be sufficient to proceed to the transition state ($ES^{\ddagger}$).

In a single substrate reaction, the rate is greatly increased when the population of the substrate adapts a reactive conformation or a near-attack conformation (NAC).[52] Dr. Thomas Bruice and his colleagues define NAC as a reactive ground state conformer that is similar to the transition state (increase of enthalpy due to the formation of new inter or intramolucular interactions), where bond-breaking and bond-making have not been initiated. NAC is considered as a door from the ground state on the way to the transition state. When an enzyme catalyzes a bimolecular reaction, two molecules are brought in close proximity, resulting in a loss of translational and rotational motion (loss of entropy),[53] thereby lowering the activation energy and achieving significant rate enhancement.

Preferential Binding of The Transition State

The catalytic mechanisms described so far only account for a certain degree of rate enhancement. The major source of catalytic power comes from a preferential binding of the transition state rather than the corresponding ground state or product.[54] A thermodynamic cycle representing relationship between various states in the uncatalyzed and catalyzed single-substrate reaction is shown in Scheme 1:

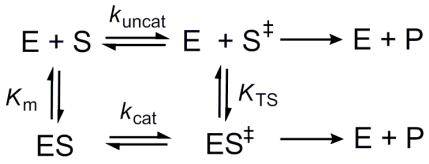

Scheme 1 (Adapted from Mader *et al*., 1997)

where k_{uncat} is the first-order rate constant for uncatalyzed conversion of substrate to product; K_{TS} is the hypothetical dissociation constant for the transition state. According to this cycle, the hypothetical binding of a transition state to its enzyme can be expressed as $K_{TS}/K_m = k_{uncat}/k_{cat}$.[55] This equation indicates that the more tightly an enzyme binds to a substrate in the transition state relative to the ground state, the faster the rate of enzyme catalyzed reaction relative to its counterpart reaction in solution. The enzyme active site provides an electrostatic environment that can accommodate developing charge in the transition state.[48, 56]

An enzyme can recognize the ground state of the substrate. The binding of the substrate induces the conformational change in the enzyme, which can constrain the substrate and then promote the bond breaking and formation.[46] Since an enzyme preferentially binds the transition state of the substrate, the transition state analogue that resembles the geometry of the transition state is a competitive inhibitor for the enzyme. Therefore, the transition state structure can provide a template for the synthesis of the transition state inhibitor.

This dissertation focuses on mechanistic studies of the two enzymes PchB and PchA responsible for salicylate biosynthesis in *P. aeruginosa*. Structural analysis was

also performed in order to assist in the elucidation of catalytic mechanisms for PchB and PchA. The goal of this work is to provide the catalysis and structural information to support the future work of the design of inhibitors against salicylate biosynthesis in pathogenic bacteria.

References

1. Richard, P. et al. Pseudomonas aeruginosa outbreak in a burn unit: role of antimicrobials in the emergence of multiply resistant strains. *J Infect Dis* **170**, 377-83 (1994).
2. Mendelson, M.H. et al. Pseudomonas aeruginosa bacteremia in patients with AIDS. *Clin Infect Dis* **18**, 886-95 (1994).
3. Govan, J.R. & Deretic, V. Microbial pathogenesis in cystic fibrosis: mucoid Pseudomonas aeruginosa and Burkholderia cepacia. *Microbiol Rev* **60**, 539-74 (1996).
4. Bottone, E.J. Yersinia enterocolitica: the charisma continues. *Clin Microbiol Rev* **10**, 257-76 (1997).
5. Hoogkamp-Korstanje, J.A. Antibiotics in Yersinia enterocolitica infections. *J Antimicrob Chemother* **20**, 123-31 (1987).
6. Perry, R.D. & Fetherston, J.D. Yersinia pestis--etiologic agent of plague. *Clin Microbiol Rev* **10**, 35-66 (1997).
7. Wandersman, C. & Delepelaire, P. Bacterial iron sources: from siderophores to hemophores. *Annu Rev Microbiol* **58**, 611-47 (2004).
8. Kammler, M., Schon, C. & Hantke, K. Characterization of the ferrous iron uptake system of Escherichia coli. *J Bacteriol* **175**, 6212-9 (1993).
9. Halliwell, B. & Gutteridge, J.M. Oxygen toxicity, oxygen radicals, transition metals and disease. *Biochem J* **219**, 1-14 (1984).
10. Raymond, K.N., Dertz, E.A. & Kim, S.S. Enterobactin: an archetype for microbial iron transport. *Proc Natl Acad Sci U S A* **100**, 3584-8 (2003).
11. Hantke, K. Regulation of ferric iron transport in Escherichia coli K12: isolation of a constitutive mutant. *Mol Gen Genet* **182**, 288-92 (1981).
12. Ratledge, C. & Dover, L.G. Iron metabolism in pathogenic bacteria. *Annu Rev Microbiol* **54**, 881-941 (2000).
13. Gray-Owen, S.D. & Schryvers, A.B. Bacterial transferrin and lactoferrin receptors. *Trends Microbiol* **4**, 185-91 (1996).
14. Schryvers, A.B. & Stojiljkovic, I. Iron acquisition systems in the pathogenic Neisseria. *Mol Microbiol* **32**, 1117-23 (1999).
15. Boulton, I.C., Gorringe, A.R., Shergill, J.K., Joannou, C.L. & Evans, R.W. A dynamic model of the meningococcal transferrin receptor. *J Theor Biol* **198**, 497-505 (1999).
16. Bruns, C.M. et al. Structure of Haemophilus influenzae Fe(+3)-binding protein reveals convergent evolution within a superfamily. *Nat Struct Biol* **4**, 919-24 (1997).
17. Stoebner, J.A. & Payne, S.M. Iron-regulated hemolysin production and utilization of heme and hemoglobin by Vibrio cholerae. *Infect Immun* **56**, 2891-5 (1988).
18. Pickett, C.L., Auffenberg, T., Pesci, E.C., Sheen, V.L. & Jusuf, S.S. Iron acquisition and hemolysin production by Campylobacter jejuni. *Infect Immun* **60**, 3872-7 (1992).

19. Bracken, C.S., Baer, M.T., Abdur-Rashid, A., Helms, W. & Stojiljkovic, I. Use of heme-protein complexes by the Yersinia enterocolitica HemR receptor: histidine residues are essential for receptor function. *J Bacteriol* **181**, 6063-72 (1999).
20. Arnoux, P. et al. The crystal structure of HasA, a hemophore secreted by Serratia marcescens. *Nat Struct Biol* **6**, 516-20 (1999).
21. Rossi, M.S. et al. Identification and characterization of the hemophore-dependent heme acquisition system of Yersinia pestis. *Infect Immun* **69**, 6707-17 (2001).
22. Letoffe, S., Delepelaire, P. & Wandersman, C. Free and hemophore-bound heme acquisitions through the outer membrane receptor HasR have different requirements for the TonB-ExbB-ExbD complex. *J Bacteriol* **186**, 4067-74 (2004).
23. Kikuchi, G., Yoshida, T. & Noguchi, M. Heme oxygenase and heme degradation. *Biochem Biophys Res Commun* **338**, 558-67 (2005).
24. Boukhalfa, H. & Crumbliss, A.L. Chemical aspects of siderophore mediated iron transport. *Biometals* **15**, 325-39 (2002).
25. Drechsel, H. & Jung, G. Peptide siderophores. *J Pept Sci* **4**, 147-81 (1998).
26. Takase, H., Nitanai, H., Hoshino, K. & Otani, T. Impact of siderophore production on Pseudomonas aeruginosa infections in immunosuppressed mice. *Infect Immun* **68**, 1834-9 (2000).
27. Lamont, I.L., Beare, P.A., Ochsner, U., Vasil, A.I. & Vasil, M.L. Siderophore-mediated signaling regulates virulence factor production in Pseudomonasaeruginosa. *Proc Natl Acad Sci U S A* **99**, 7072-7 (2002).
28. Heesemann, J. et al. Virulence of Yersinia enterocolitica is closely associated with siderophore production, expression of an iron-repressible outer membrane polypeptide of 65,000 Da and pesticin sensitivity. *Mol Microbiol* **8**, 397-408 (1993).
29. Mootz, H.D., Schwarzer, D. & Marahiel, M.A. Ways of assembling complex natural products on modular nonribosomal peptide synthetases. *Chembiochem* **3**, 490-504 (2002).
30. Sieber, S.A. & Marahiel, M.A. Molecular mechanisms underlying nonribosomal peptide synthesis: approaches to new antibiotics. *Chem Rev* **105**, 715-38 (2005).
31. Bleuel, C. et al. TolC is involved in enterobactin efflux across the outer membrane of Escherichia coli. *J Bacteriol* **187**, 6701-7 (2005).
32. Ferguson, A.D. & Deisenhofer, J. TonB-dependent receptors-structural perspectives. *Biochim Biophys Acta* **1565**, 318-32 (2002).
33. Cox, C.D. & Graham, R. Isolation of an iron-binding compound from Pseudomonas aeruginosa. *J Bacteriol* **137**, 357-64 (1979).
34. Cox, C.D. Effect of pyochelin on the virulence of Pseudomonas aeruginosa. *Infect Immun* **36**, 17-23 (1982).
35. Reimmann, C. et al. Essential PchG-dependent reduction in pyochelin biosynthesis of Pseudomonas aeruginosa. *J Bacteriol* **183**, 813-20 (2001).

36. Patel, H.M. & Walsh, C.T. In vitro reconstitution of the Pseudomonas aeruginosa nonribosomal peptide synthesis of pyochelin: characterization of backbone tailoring thiazoline reductase and N-methyltransferase activities. *Biochemistry* **40**, 9023-31 (2001).
37. Crosa, J.H. & Walsh, C.T. Genetics and assembly line enzymology of siderophore biosynthesis in bacteria. *Microbiol Mol Biol Rev* **66**, 223-49 (2002).
38. Gehring, A.M. et al. Iron acquisition in plague: modular logic in enzymatic biogenesis of yersiniabactin by Yersinia pestis. *Chem Biol* **5**, 573-86 (1998).
39. Miller, D.A., Luo, L., Hillson, N., Keating, T.A. & Walsh, C.T. Yersiniabactin synthetase: a four-protein assembly line producing the nonribosomal peptide/polyketide hybrid siderophore of Yersinia pestis. *Chem Biol* **9**, 333-44 (2002).
40. Kerbarh, O., Ciulli, A., Howard, N.I. & Abell, C. Salicylate biosynthesis: overexpression, purification, and characterization of Irp9, a bifunctional salicylate synthase from Yersinia enterocolitica. *J Bacteriol* **187**, 5061-6 (2005).
41. Wolfenden, R. & Snider, M.J. The depth of chemical time and the power of enzymes as catalysts. *Acc Chem Res* **34**, 938-45 (2001).
42. Frey, P.A., and Hegeman, A.D. Enzymatic Reaction Mechanisms (Oxford University Press, New York, 2007).
43. Nelson, D.L. & Cox, M.M. Lehninger Principles of Biochemistry (2005).
44. Karplus, M. Molecular dynamics simulations of biomolecules. *Acc Chem Res* **35**, 321-3 (2002).
45. Voet, D. & Voet, J.G. Biochemistry (Wiley, 2004).
46. Schramm, V.L. Enzymatic transition states and transition state analog design. *Annu Rev Biochem* **67**, 693-720 (1998).
47. Pauling, L. Molecular architecture and biological reactions. *Chem.Eng. News* **24**, 1375-1377 (1946).
48. Warshel, A. et al. Electrostatic basis for enzyme catalysis. *Chem Rev* **106**, 3210-35 (2006).
49. Jencks, W.P. Mechanism of Enzyme Action. *Annu Rev Biochem* **32**, 639-76 (1963).
50. Cannon, W.R. & Benkovic, S.J. Solvation, reorganization energy, and biological catalysis. *J Biol Chem* **273**, 26257-60 (1998).
51. Dafforn, A. & Koshland, D.E., Jr. Proximity, entropy and orbital steering. *Biochem Biophys Res Commun* **52**, 779-85 (1973).
52. Bruice, T.C. & Lightstone, F.C. Ground state and transition state contributions to the rates of intramolecular and enzymatic reactions. *Acc. Chem. Res.* **32**, 127-136 (1999).
53. Jencks, W.P. Binding energy, specificity, and enzymic catalysis: the circe effect. *Adv Enzymol Relat Areas Mol Biol* **43**, 219-410 (1975).
54. Pauling, L. Nature of forces between large molecules of biological interest. *Nature* **161**, 707-9 (1948).

55. Mader, M.M. & Bartlett, P.A. Binding Energy and Catalysis: The Implications for Transition-State Analogs and Catalytic Antibodies. *Chem Rev* **97**, 1281-1302 (1997).
56. Kienhofer, A., Kast, P. & Hilvert, D. Selective stabilization of the chorismate mutase transition state by a positively charged hydrogen bond donor. *J Am Chem Soc* **125**, 3206-7 (2003).

CHAPTER 2

Mechanistic and Structural Studies of PchB, a bifunctional Isochorismate-Pyruvate Lyase/Chorismate Mutase from *Pseudomonas aeruginosa*

The work described in this chapter is currently being revised for resubmission to *Biochemistry*. "Structure-function analyses of isochorismate-pyruvate lyase from *Pseudomonas aeruginosa* (PchB) suggest differing catalytic mechanisms for the two pericyclic reactions of this bifunctional enzyme"
Qianyi Luo, Jose Olucha, and Audrey Lamb.

2.1 Introduction

Salicylate is a precursor of iron chelators, siderophores in pathogenic bacteria, such as yersiniabactin in *Yersinia* spp., mycobactin in *Mycobacterium tuberculosis*, and pyochelin in *Pseudomonas aeruginosa*.[1] Salicylate can be derived from chorismate via isochorismate as an intermediate. In *P. aeruginosa* salicylate is made from chorismate in a two-step process by two enzymes: isochorismate synthase (PchA) and isochorismate-pyruvate lyase (PchB),[2, 3] followed by the incorporation into siderophore pyochelin. PchB has no sequence similarity to other pyruvate lyases. Instead, PchB is a structural homologue of *E. coli* chorismate mutase (EcCM) with a sequence identity of 20%.[4] Therefore, it is not surprising that PchB has an adventitious chorismate mutase activity.[2]

Both the isochorismate-pyruvate lyase (IPL) and chorismate mutase (CM) activities of PchB catalyze pericyclic reactions, which are unusual in biological

systems. These two reactions take place in the same active site where product is formed from a single substrate in one chemical step through a pericyclic transition state (Figure 2-1). IPL activity eliminates the enolpyruvate side chain from isochorismate to produce salicylate and pyruvate using a concerted but asynchronous [1,5]-sigmatropic hydrogen transfer mechanism with the cleavage of C3-O7 linkage and the hydrogen atom transfer from C2 to C9 of the enolpyruvate side chain (Figure 2-1a).[5] The non-physiological role of PchB as a chorismate mutase is to catalyze a [3,3]-sigmatropic rearrangement of chorismate to prephenate, in which bond-breaking at C3-O7 linkage and bond-making between C1-C9 are concerted but asynchronous, leading to a transfer of the pyruvate tail from the C3 ether linkage to a C1-C9 linkage (Figure 2-1b).[6] This non-physiological CM activity of PchB has considerably lower catalytic efficiency relative to IPL activity.[2] The experimentally measured rate enhancement in the physiological CM over the corresponding reaction in solution is 10^6 ~ 10^7-fold,[7, 8] but the origin of the catalytic power for these enzymes remains controversial.

Chorismate mutases from different organisms share only low sequence similarity. Based on the secondary structure arrangement, chorismate mutases are classified into AroH and AroQ classes. AroQ enzymes are completely helical dimeric bundles with buried active sites made of amino acids from both monomers. PchB (*P. aeruginosa*), EcCM (*E. coli*), ScCM (*Saccharamyces cerevisiae)*, and MtCM (*M. tuberculosis*)[9-11] belong to AroQ class (Figure 2-2a & b). A well-studied example of the AroH class is the CM enzyme in *Bacillus subtilis* (BsCM). The BsCM is a

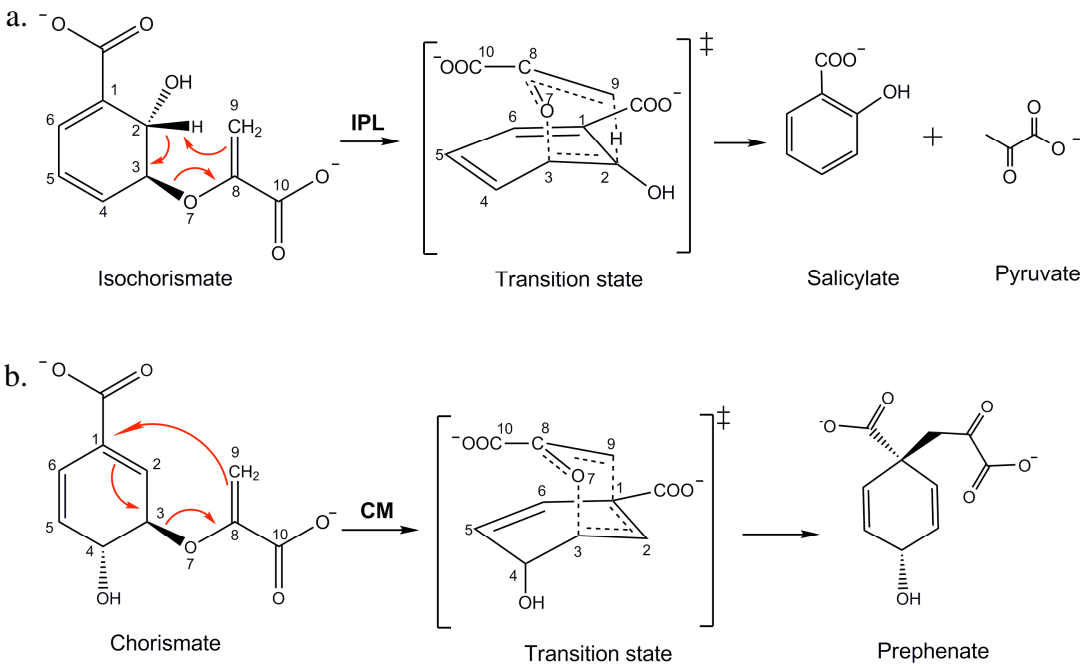

Figure 2-1: Reaction schemes of PchB catalyzed reactions. **a.** Isochorismate pyruvate lyase activity via [1,5]-pericyclic hydrogen transfer mechanism. **b.** Chorismate mutase activity via [3,3]-sigmatropic pericyclic rearrangement mechanism. Both CM and IPL have the transition states with aromatic characteristics.

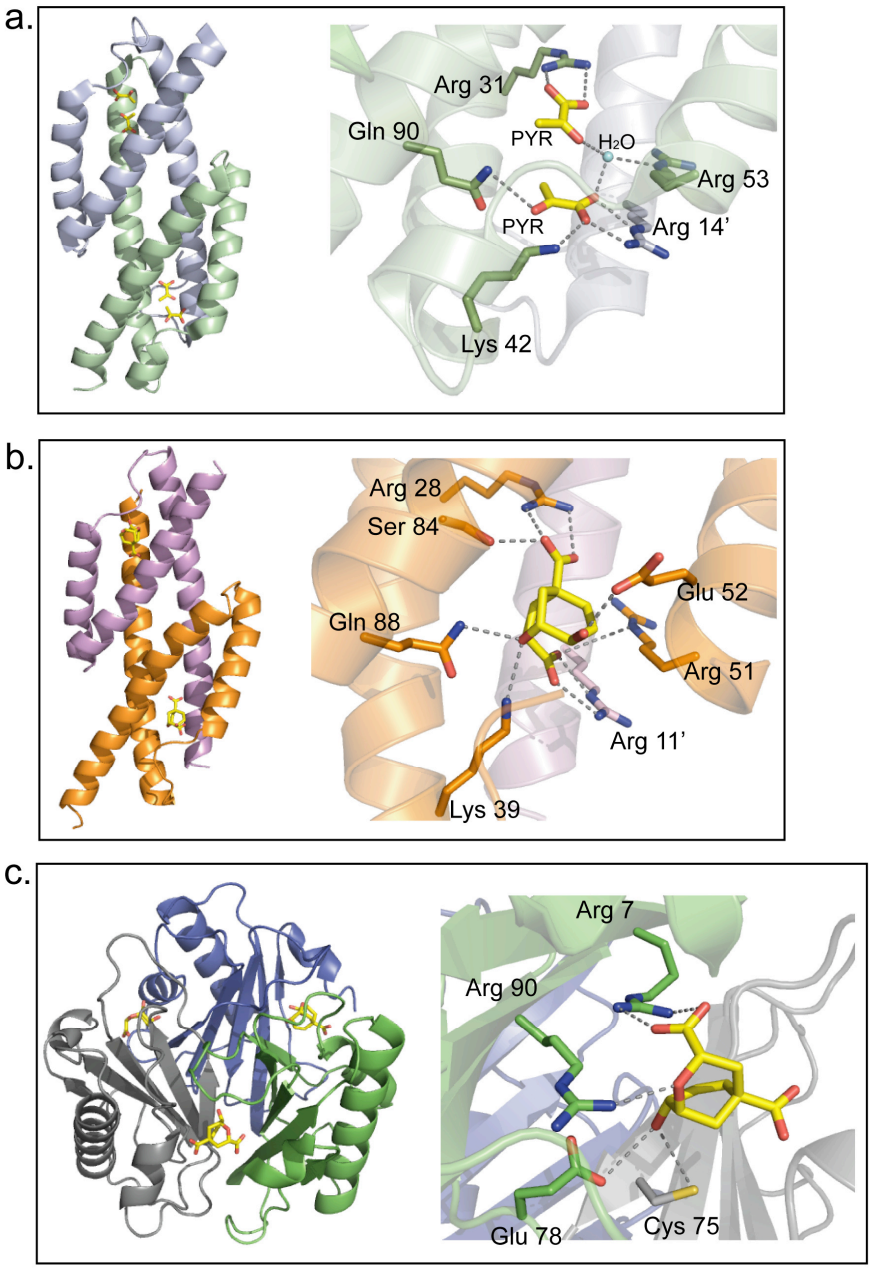

Figure 2-2: Structures of three chorismate mutases. **a.** PchB homodimer with two equivalent active sites, one of which is displayed. Two pyruvates are yellow sticks and H-bond to active site residues. (PDB code 2H9D); **b.** EcCM homodimer. One of the two equivalent active site is shown with the TSA bound. (PDB code 1ECM); **c.** BsCM homotrimer. Three active sites are located at the interface of subunits, where the TSA binds. (PDB code 2CHT). TSA, the transition state analog oxabicyclic acid is shown in yellow sticks in panels **b** and **c**. Figures were created using PyMOL.

homotrimer with three monomers folding into pseudo-α/β-barrel.[7, 8] Three equivalent active sites are located at the interfaces between the subunits (Figure 2-2c). Structures of chorismate mutase are diverse, however, by comparison of the active site architectures of EcCM and BsCM with a transition state analog (TSA) bound, Lee *et al*. considered that the active sites of CMs were comparable due to charge and shape complementarity.[9]

The detailed atomic structure of PchB has been determined. PchB is a structural homolog to EcCM. The structure of EcCM with TSA bound in the active site suggests that eight charged or polar amino acids are interact with TSA.[10] In PchB, only five of those amino acids are conserved, which leads to the ability to perform both IPL and CM reactions in the same active site. The major difference of the apo-PchB and pyruvate-bound PchB structures is present in a mobile loop between the first and second helices. This loop becomes fully ordered in the pyruvate-bound structure. A conserved residue lysine 42 in the loop was found to hydrogen bond to a pyruvate in the pyruvate-bound PchB structure (Figure 2-2a) and is proposed to be critical for catalysis.[4]

CM has become a popular model system to study the origin of the enormous catalytic power of enzymes experimentally and theoretically due to two advantages. First, the rearrangement of chorismate to prephenate that is catalyzed by CM has a counterpart in solution that proceeds in the same manner as that in active site. Studies have demonstrated that both catalyzed and uncatalyzed reactions undergo a concerted but asynchronous [3,3]-sigmatropic rearrangement through a chair-like pseudodiaxial

transition state (Figure 2-1a).[11-14] Second, there are no substrate-enzyme covalent bonds formed and broken during the intramolecular rearrangement of chorismate to prephenate. Only weak interactions involved.[15]

One way for CM to lower the activation energy and thus speed up the reaction is to electrostatically stabilize the polar transition state during catalysis.[16, 17] The x-ray crystallographic structures of several CMs have been solved. Analysis of the active site structures with TSA bound leads to a hypothesis that CM provides an active site that can accommodate the developing negative charge on the ether oxygen and the cyclohexadiene ring of the polar transition state via electrostatic and H-bonding interactions.[7, 9-11, 13] The positively charged amino acids in the CMs active sites are strategically arranged to orient chorismate to the pseudo-diaxial form previously to the chemical reaction.[18] Considerable mutagenesis studies that have been carried out on the EcCM,[19] BsCM,[20-23] and ScCM[24] support the electrostatic transition state stabilization hypothesis, suggesting that a positively charged amino acid residue (Lys39 in EcCM, Arg90 in BsCM, and Lys168 in ScCM) is positioned next to the ether oxygen of the breaking C3–O7 bond, stabilizing the developing negative charge of the transition state. Modification of Lys39 (EcCM) and Arg90 (BsCM) led to complete loss of mutase activities. Quantum mechanics/molecular mechanics (QM/MM) calculations also demonstrated electrostatic stabilization of the polar transition state to be dominant in catalysis.[25-28]

Another hypothesis that the substrate ground state conformation is important for catalytic efficiency in CM is mainly based on the computational studies. Dr. Thomas

Bruice and co-workers coined the term near attack conformation (NAC) to define a reactive substrate conformation for ground state that is required to enter the transition state. NAC is a true ground state conformation in which reacting atoms are within a distance that is less than/equals to the sum of their van der Waals radii and approach at an angle ±15° of the bonding angle in the transition state.[29] So one can consider that NAC is a transition-state-like ground state conformer[30] and a door through which reactants must pass on the way to the transition state.[31] Once enzyme binds and stabilizes the NAC, the catalysis can progress spontaneously without extra stabilization of the transition state.[29, 31-33]

PchB is a unique system for the experimentally testing the two hypotheses, transition state stabilization (TSS) and NAC, for the catalytic efficiency. PchB performs two pericyclic reactions (CM and IPL) in a single active site without any substrate-enzyme covalent intermediates involved. Two NACs are formed in PchB active site (Figure 2-3), which continue the progress toward two transition states (Figure 2-1). PchB with dominant IPL over CM activity is probably a consequence of the preorganization of the active site in a shape that prefers to constrain NAC for the IPL reaction over that for the CM reaction. However, the relative contributions of NAC and TSS to the overall rate enhancement in each reaction need to be investigated. The structure of PchB indicates that arginines deep in the active site organize the substrate, leading to generation of a NAC for catalysis. The mobile loop between the first two helices would have a relationship with catalysis due to the ordering of this loop upon substrate binding.[4] Lys42, the only active site residue

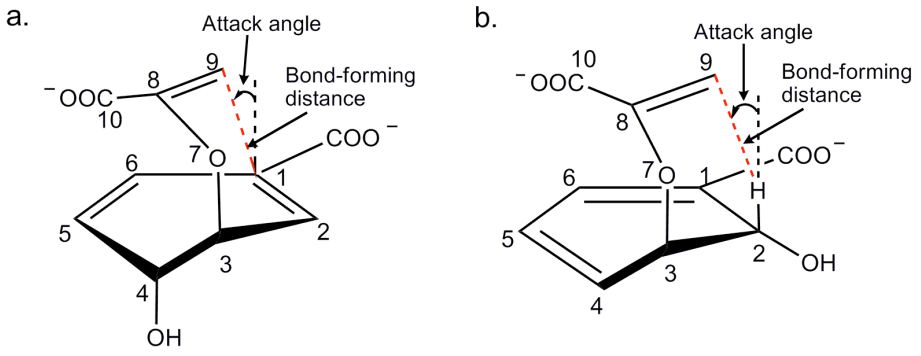

Figure 2-3: Two near attack conformations formed in PchB active site. **a.** Chorismate mutase reaction (modified from Zhang, X. *et al.*, 2005), **b.** Isochorismate-pyruvate lyase reaction.

found in the loop is proposed as a key factor for catalysis.[4] The strategic placement of Lys42 can promote bond breaking at C3-O7 of substrate and stabilize the developing negative charge at the ether oxygen in the transition states of CM and IPL reactions.

In this chapter, mutagenesis studies focusing on PchB Lys42 were carried out to elucidate the importance of positive charge and H-bond at position 42. The results obtained add further insight into the rate enhancement that arises from active site-constrain of a reactive substrate conformation and electrostatic stabilization of the transition state.

2.2 Materials and Methods

Site-Directed Mutagenesis of PchB

Site-directed PchB mutants, K42A, K42E, K42Q, K42H, A43P, and I87T were constructed from the plasmid pET29b-*pchB*,[4] using the QuikChange Site-directed Mutagenesis Kit from Stratagene. Primers and their corresponding complements were used (mutated codons were underlined):

K42A: 5′-GCG TCG CGC TTC <u>GCG</u> GCC AGC GAG GCG-3′

K42E: 5′-GCG TCG CGC TTC <u>GAG</u> GCC AGC GAG GCG-3′

K42Q: 5′-GCG TCG CGC TTC <u>CAG</u> GCC AGC GAG GCG-3′

K42H: 5′-GCG TCG CGC TTC <u>CAT</u> GCC AGC GAG GCG-3′

A43P: 5′-GCG TCG CGC TTC AAG <u>CCG</u> AGC GAG GCG GCG-3′

I87T: 5′-C ATC CAC TGG TAC <u>ACC</u> GCC GAG CAG ATC-3′

All mutations were confirmed by sequence analysis. Plasmids bearing each mutation

were transformed into *E. coli* BL21 (DE3) competent cells for protein overproduction.

Overexpression and Purification of Wild Type and Mutant PchB

Protein overexpression and purification were performed as previously described for the wild type PchB protein[4] with some modifications. The cells were grown in LB media at 37 °C with shaking at 250 rpm until OD_{600} reached ~ 0.8. Protein expression was induced with 0.2 mM isopropyl-β-D-thiogalactopyranoside (IPTG). After 3 hours, the cells were harvested by centrifugation (4,000 × g, 10 min, 4 °C). The pelleted cells were resuspended in 25 mM Tris-HCl pH 8.0 (buffer A) and lysed by sonication (Digital Sonifier, Branson). The cellular debris was removed by ultracentrifugation (142,000 × g, 45 min, 4 °C) and supernatant was applied to a Q Sepharose Fast Flow (Amersham Biosciences) column equilibrated with buffer A for anion-exchange chromatography. A linear gradient of 0 – 250 mM NaCl in buffer A was applied to the column and PchB protein eluted at approximately 100 mM NaCl. The fractions PchB were identified by SDS-PAGE, pooled, and concentrated with an Amicon stirred cell (YM-3 membrane). Four to five ml of sample was applied to a HiLoad 16/60 Superdex 75 gel filtration column equilibrated with 50 mM Tris-HCl, pH 8.0, 150 mM NaCl, 1 mM DTT, and 10% glycerol. The protein concentration was determined by Bradford assay. The resulting purity was determined to ~99% by SDS-PAGE. The purified protein was stored at – 80 °C for use in activity assays and crystallization trials.

Circular Dichroism Studies

Circular dichroism spectra were recorded on a Jasco J-815 spectrometer (Easton, MD) at 25 °C. Spectra were measured in 20 mM sodium/potassium phosphate pH 7.0 with a proteins concentration of 2 ~ 3.5 μM. The samples were measured in a quartz cuvette with a path length of 1 cm. Five wavelength scans from 190 nm to 260 nm in 1 nm steps (signal averaging time 1 s; bandwidth 1 nm) were recorded and averaged. The data were corrected by subtracting a buffer blank baseline from the average. Mean residue ellipticities (θ in degrees•cm^2•$dmol^{-1}$) were calculated as described.[34] The resulting data were smoothed and plotted with KaleidaGraph (Synergy Software).

Protein Crystallization

K42A was co-crystallized with salicylate and pyruvate at 18ºC using the hanging drop method. Before crystallization, K42A (3.8 mM) was incubated with 38 mM salicylate and 38 mM pyruvate on ice for 30 min. The drop was made by mixing 1 μl protein solution with 2 μl well solution consisting of 0.1 M TrisHCl pH 8.5, 2 M ammonium phosphate, and 13% glycerol. Crystals grew to about 1 × 0.7 × 0.4 mm in one week. I87T was crystallized at 25 ºC by the hanging drop method. Drops were made by mixing 1.5 μl of 19 mg/ml I87T protein solution with 1.5 μl of a reservoir solution composed of 0.1 M Bis-Tris Propane, pH 6.5, 0.14 M calcium chloride, 23% PEG 3350, and 10% glycerol. Long rod-shaped crystals with dimensions up to 0.37 × 0.06 × 0.05 mm were obtained in one week.

Data Collection and Structure Determination

For data collection, a K42A crystal from the drop was directly flash cooled in the stream of nitrogen gas at -160 ºC. The I87T crystal was transferred to cryoprotectant solution (0.1 M Bis-Tris propane, pH 6.5; 0.2 M calcium chloride, 30% PEG 3350; and 20% glycerol) and flash cooled in the nitrogen gas. X-ray diffraction data were collected at cryogenic temperature using a Rigaku RU-H3R rotating anode generator equipped with Raxis IV image plate detector at the University of Kansas Protein Structure Lab. The exposure time per image was 10 min at 1º oscillation steps with a crystal to detector distance of 150 mm. Diffraction data were indexed and scaled using HKL program suite.[35] Both K42A and I87T crystals belonged to the space group $P2_12_12_1$ with unit cell dimension a = 48.015 Å, b = 53.15 Å, c = 82.336 Å for K42A, and a = 54.5 Å, b = 74.7 Å, c = 88.5 Å for I87T. Data collection statistics are listed in Table 2-1.

The structure of K42A was determined using the molecular replacement program Phaser from the CCP4 program suite[36] and the PchB pyruvate-bound structure (PDB code 2H9D) as a model, with the water and ligands omitted. The I87T structure was determined by molecular replacement with the program Auto MolRep, also from the CCP4 package.[36] The PchB pyruvate-bound structure (PDB code 2H9D) was used as the search model. Model building proceeded using Coot[37] with cycles of maximum likelihood refinement using REFMAC[38], both in the CCP4 program package. Refinement statistics are in Table 2-1.

Table 2-1: Crystallographic statistics

	K42A with products	Apo I87T
Data Collection		
Resolution Range (Å)	41.5 - 2.5	100 - 2.15
Space Group	$P2_12_12_1$	$P2_12_12_1$
Unit Cell (Å)	a = 48.0, b = 53.2, c = 82.3	a = 54.5, b = 74.9, c = 88.5
Observations		
Unique	7706	20,232
Total	50,717	345,137
Completeness (%)[1]	99.9 (99.9)	99.2 (98.6)
Rsym[2]	0.101 (0.227)	0.108 (0.423)
% > 3 s (I)	85.7 (72.9)	80.4 (55.4)
Refinement		
Resolution Range (Å)	41.5 - 2.5	44.24 - 2.25
Number of Reflections	7,346	16,778
R-factor [3]	0.218	0.219
R_{free} [4]	0.276	0.256
Dimers/asymmetric unit	1	2
Number of atoms		
Protein, nonhydrogen	1580	2726
Nonprotein	48	77
Root mean square deviations		
Length (Å)	0.01	0.008
Angles (°)	1.22	1.02
Overall B factor ($Å^2$)	15.2	20.1

[1]Values in parentheses are for the highest resolution shell: 2.59 - 2.5 Å (K42A), 2.23 - 2.15 Å (I87T).

[2]$R_{sym} = S | I_{obs} - I_{avg} | / S I_{obs}$ where the summation is over all reflections.

[3]R-factor = $S | F_o - F_c | / S F_o$.

[4]For calculation of R_{free}, 4.5% (K42A) and 5.1% (I87T) of the reflections were reserved.

Isochorismate Preparation

Isochorismate was isolated from the CM-deficient *Klebsiella pneumoniae* 62-1 harboring the *entC* plasmind pKS3-02 as described[39] with some variations. Plasmid pKS3-02 was transformed into *K. pneumoniae* 62-1 by electroporation. Five ml of an overnight culture of *K. pneumoniae* 62-1/pKS3-02 in Nutrient broth was inoculated into 1 L of medium A[40] with shaking 250 rpm at 30°C until OD_{600nm} of 1.2 ~ 1.4. The cells were harvested by centrifugation (4000 × g, 10 min, 4 °C). The pellet was resuspended in 1 L of medium BN[39] and shaken at 250 rpm, 30 °C. After 14 ~ 16 h, supernatant was collected by centrifugation (4000 × g, 30 min, 4°C). Due to the fast decomposition rate at high temperature, all of the following steps were performed at 4 °C unless stated. The supernatant was titrated to pH 8.0 with 10 M NaOH. The supernatant was applied to the Dowex column (1 × 8, 200-400 mesh, Cl^-) with tap vacuum and washed with H_2O. After elution with 1 M NH_4Cl pH 8.5 at rate of 2ml/min, fractions with A_{280nm} above 200 mAU were combined, neutralized using HCl, and freeze-dried. The dried powder was extracted 3 times with 50 ml of methanol by sonication. Methanol extracts were pooled and rotary-evaporated. The residue was dissolved in 10 ml water.

Before large scale separation on HPLC, 20 µl of the sample was tested on an analytical HPLC column (Nucleosil 5u C18 100A, 150 × 4.6 mm) with a methanol gradient (0-5 min, 0% MeOH; 5-15, 10% MeOH; 15-25 min, 20% MeOH; 25-35 min, 30% MeOH; 35-48 min, 40% MeOH) as a mobile phase, running at 1 ml/min. The column output was recorded at 278 nm. Isochorismate eluted at 17 min with 20%

MeOH. Once sample was confirmed to contain isochorismate, a 5 ml sample aliquot was applied to a preparative column (Nucleosil 5u C18 100A column, 250 × 21.2 mm) in H_2O pH 2.5 (titrating with trifluoroacetic acid). A methanol gradient (0-35 min, 0-10% MeOH; 35-50 min, 10-20% MeOH; 50-85 min, 20-30% MeOH; 85-100 min, 30-45% MeOH) was used as mobile phase with a flow rate of 10 ml/min. Isochorismate eluted with 20.6% MeOH at 52 min. Pooled fractions containing isochorismate were neutralized by NaOH, freeze-dried, and stored at -80 °C. The concentration of isochorismate was determined by UV spectroscopy using ε_{278} = 8, 300 M^{-1} cm^{-1}. ^{1}H-NMR spectrum of isochorismate in D_2O was recorded on Bruker Avance 500 MHz spectrometer.

Steady-State Kinetic Studies

The IPL activities of wild type and mutant PchB enzymes were measured in an assay buffer 50 mM Na/K phosphate pH 7.5 at room temperature. The reaction mixture (final volume 100 µl) contained 1~2 µM enzyme. The isochorismate concentration was varied in assays for wild type, I87T, and A43P enzymes (1-80 µM); and for K42A, K42H, and K42Q mutants (5-390 µM). Initial velocities were determined by measuring the fluorescence of the product salicylate at an excitation wavelength of 300 nm and an emission wavelength of 430 nm with a fluorescence spectrophotometer (Cary Eclipse, Varian) over 2 min. The amount of salicylate formed was determined from a standard curved with varied salicylate concentration (0-80 µM) in the reaction buffer. Kinetic constants V_{max}, K_m and k_{cat} were calculated

from Michaelis-Menten equation ($\upsilon=V_{max}[S]/(K_m+[S])$ using KaleidaGraph.

For CM activity, chorismate was recrystallized from 60-80% pure chorismate (Sigma) as described previously.[41] All steady-state kinetic measurements on CM were performed in 50 mM Na/K phosphate pH 7.5 at room temperature. Chorismate concentration was varied between 0.1 mM and 1.4 mM. The reaction mixture (final volume 100 µl) contained 50~80 µM enzyme. Initial velocities were determined by measuring the disappearance of chorismate at 310 nm ($\varepsilon_{310} = 370\ M^{-1}\ cm^{-1}$)[22] on a UV spectrophotometer (Cary 50 Bio, Varian). Steady-state kinetic parameters were derived from the initial velocities of chorismate disappearance with KaleidaGraph.

Temperature Dependence of PchB Catalyzed Reactions

To determine the enthalpy and entropy contributions for both CM and IPL reactions performed by PchB, CM and IPL Reactions were conducted at temperatures, from 5 °C to 45 °C for IPL, 10 °C to 45 °C for CM, and 25 °C to 60 °C for the isochorismate uncatalyzed reactions. Chorismate disappearance and salicylate accumulation were monitored as described previously in this chapter for steady-sate measurements. k_{cat} was determined using Michaelis-Menten kinetics at each temperature. The thermodynamic parameters were obtained from least-squares analysis of the collected data using the Eyring equation:[42]

$$k_{cat} = (\mathbf{k}T/\mathbf{h})\, e^{-[(\Delta H‡/RT) - (\Delta S‡/R)]}$$

where **k** = Boltzmann's constant, **h** = Planck's constant, R = ideal gas constant, and T = absolute temperature. All data analysis was performed with KaleidaGraph.

2.3 Results

Enzyme Production

The mutant enzymes were generated from pET29b-*pchB* and purified in yields of 175 to 250 mg per liter cell culture using an anion exchange followed by a size exclusion chromatography. All mutant enzymes eluted as a homodimer (~ 23 kDa) from size exclusion column as wild type enzymes. The purities of enzymes were ~99% as determined by SDS-PAGE (data not shown).

CD Spectra Measurements

To investigate effects of single mutation on the overall secondary structure of PchB, the CD spectra of mutant enzymes were recorded and shown in Figure 2-4. Spectra of all mutants and the wild type display maximum near 190 nm and minina at 208 nm and 222 nm, consistent with the characteristics of α-helical folding. Mutations at position 42 and 43 do not show a shoulder at ~ 210 nm in our CD spectra as the EcCM mutants did.[19]

PchB K42A and I87T Structures

The crystals of K42A and I87T belong to the space group $P2_12_12_1$. The structures were determined by molecular replacement using wild type pyruvate bound (PDB code 2H9D)[4] as a model with omission of waters and ions.

The K42A structure was determined to 2.5 Å with salicylate and pyruvate

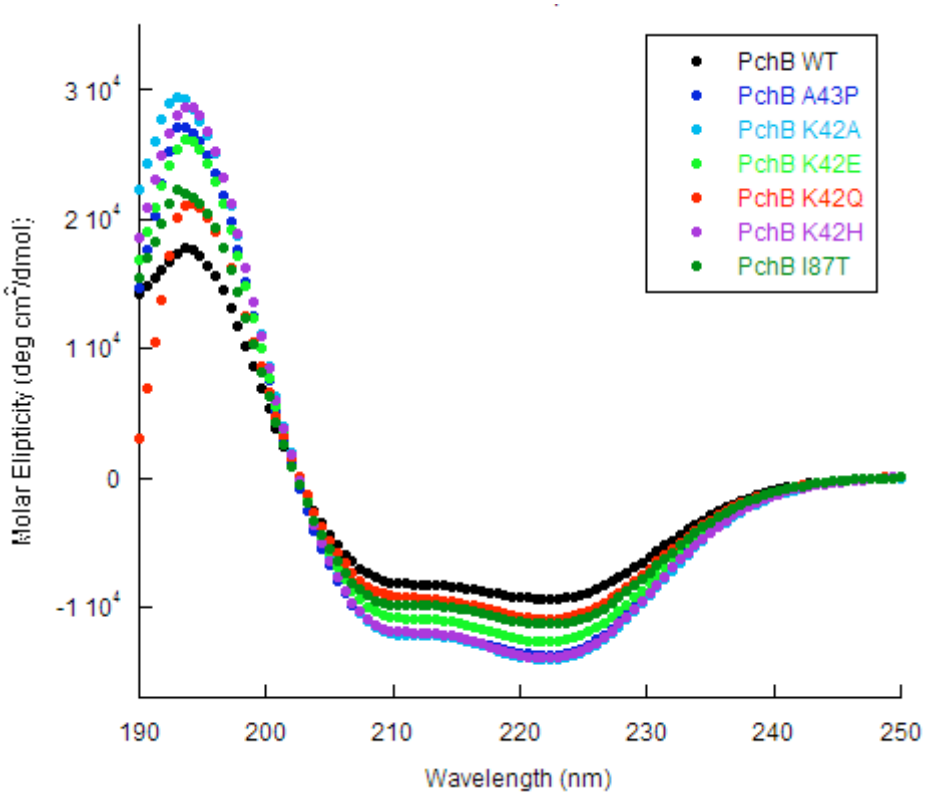

Figure 2-4: Overlay of the circular dichroism spectra of wild type and mutant PchB enzymes. Spectra were acquired for all the mutants and wild type enzymes studied. The spectra shown are the average of five scans, corrected for buffer blank and smoothed. The resulting spectra of mutants are very similar to that of the wild type PchB.

bound in the active site. Each asymmetric unit for K42A crystal contains one homodimer formed from two intertwined monomers (A and B). Both monomer A and B comprise residues 1 – 99. Two residues are disordered at the C termini of both monomers. The K42A structure is summarized in Table 2-2. The dimer has two closed active sites, and each contains one salicylate and one pyruvate. Salicylate binds more deeply in the active site, which is consistent with the prediction using wrong-ligand crystallographic refinement modeling.[4] The carboxylate group in salicylate is oriented by the side chain Arg31, and the pyruvate is oriented by Arg14 in the active site. The K42A structure is overlayed with wild type, and Figure 2-5a shows the superposition of the active sites. The overall root mean square deviation (RMSD) for the K42A monomer shown is 0.43 Å for 98 Cα positions, and for the dimer is 0.58 Å for 197 Cα atoms. These comparisons demonstrate that the integrity of the three-dimensional structure is well maintained after the mutation, which is also supported by the CD spectrum. The active site of K42A is conserved with RMSD of 0.21 Å for the Cα (position 42) in the shown monomer, and 0.46 Å for that in the opposing monomer. An electron density map for the active site can be found in Figure 2-5b.

The I87T structure was determined to 2.15 Å. The asymmetric unit contains 2 dimers. There are more disordered regions in I87T structure as compared to wild type. As summarized in Table 2-2, no electron density was observed in the regions between helices 1 and 2 from amino acid 44 to 55 in monomer A, 42 to 50 in monomer B, 40 to 53 in monomer C. One to nine amino acids at the N termini and three to eight

Table 2-2: Summary of K42A and I87T structures

	Ordered amino acids	Ions in active site
K42A		
Monomer A	1-99	salicylate and pyruvate
Monomer B	1-99	salicylate and pyruvate
I87T		
Monomer A	2-43, 56-94	none
Monomer B	10-41, 51-93	none
Monomer C	2-39, 54-98	none
Monomer D	2-98	none

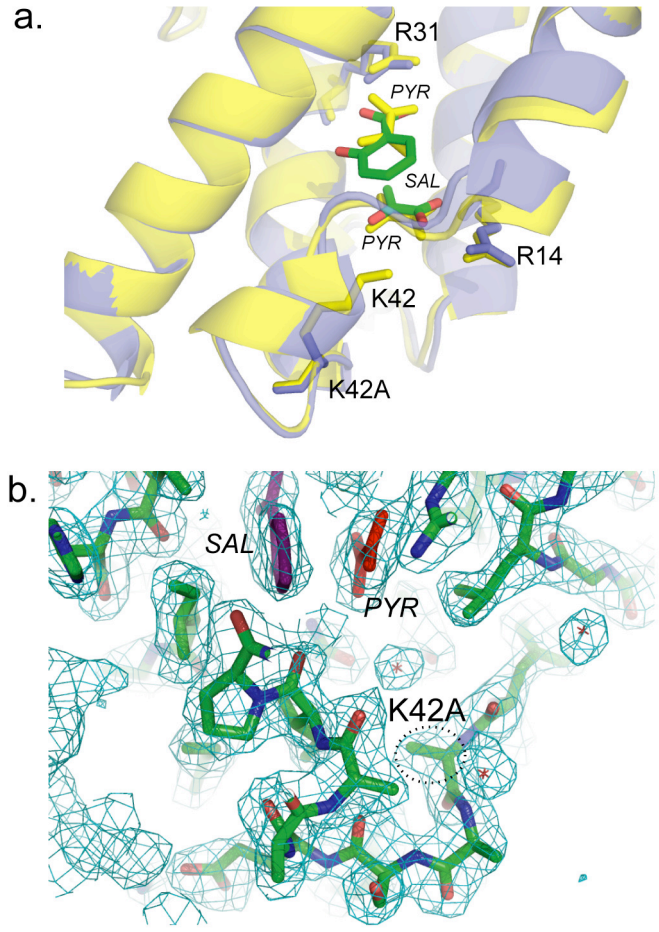

Figure 2-5: PchB K42A structure. **a.** Superposition of K42A (light purple) and pyruvate-bound closed wild type PchB (yellow; PDB code 2H9D) active sites. The salicylate and pyruvate molecules of the K42A structure are green sticks, and two pyruvates of the wild type structure are yellow sticks. **b.** An electron density map of the K42A active site. Figures were generated in PyMOL.

amino acids at C termini are disordered as well. The superposition of two I87T dimers from each asymmetric unit and the wild type structure is shown in Figure 2-6a. When ligands are not present in the active site, the mobile loops between the first two helices in monomer A, B and C have poorly defined structure. The disordered regions extended to several amino acids of helix 2 in A and C monomers. The electron density map of one active site is shown in Figure 2-6b. These unstructured regions may become ordered upon substrate binding.

Isochorismate Preparation

Isochorismate was isolated from *K. pneumoniae* 62-1/pKS3-02. The final purifying step was performed on HPLC system using methanol gradient as a mobile phase. A pre-run of sample was done on a small analytical HPLC C18 reverse phase column. The isochorismate eluted with 20% methanol at ~17 min followed by the chorismate peak at ~20 min (Figure 2-7a). A larger column was used for preparation of bulk isochorismate. Two peaks (52 min and 65 min) of 20-30% methanol from the preparative HPLC column (data not shown) were collected, acidified, and freeze-dried. Small amount of dried powder of two peaks were dissolved in D_2O, and ^1H NMR spectra were recorded. The spectrum for the 52 min peak (Figure 2-7b) matches the published data for isochorismate.[43] Due to the fast rate of uncatalyzed decomposition, the isochorismate sample in water was aliquoted and stored at – 80 °C.

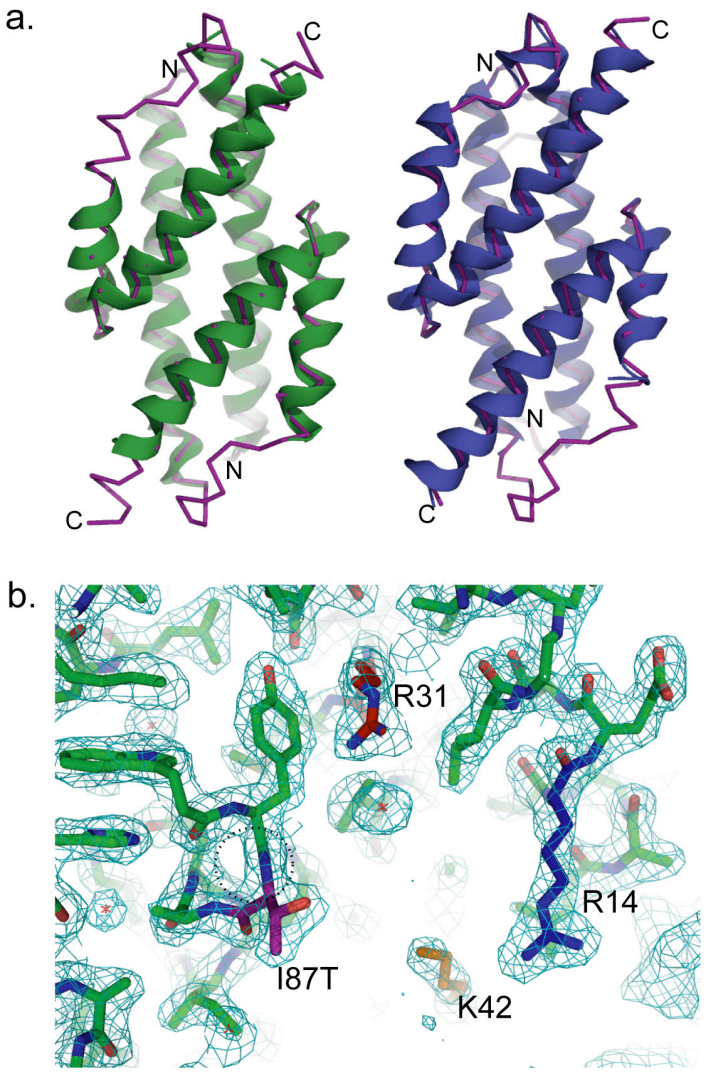

Figure 2-6: PchB I87T structure. **a.** Superposition of I87T two dimers (A and B in green, C and D in deep blue) from an asymmetric unit and the wild type pyruvate-bound closed structure (purple ribbon). **d.** An electron density map of the I87T active site with ordered Lys42 . Figures were generated in PyMOL.

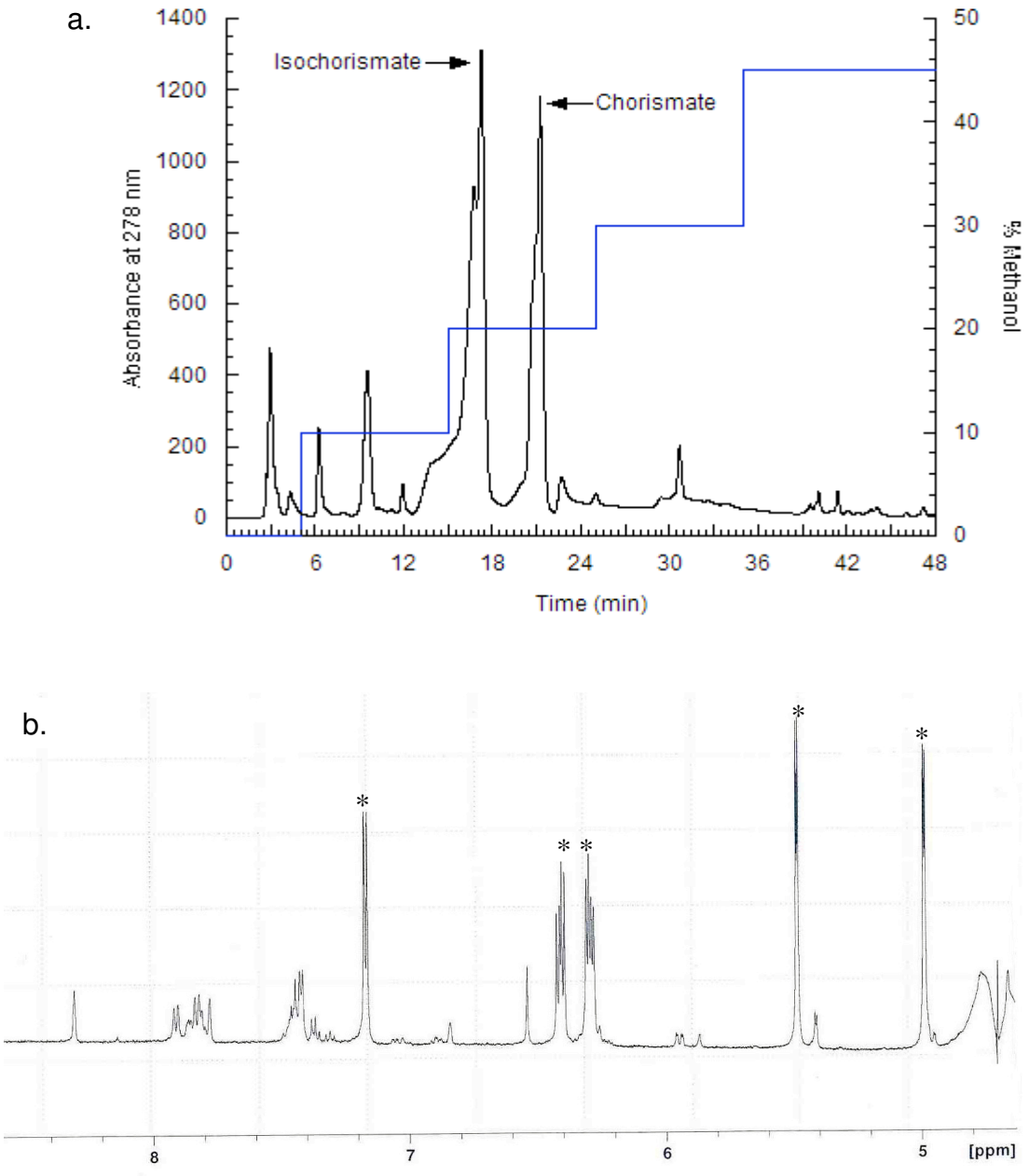

Figure 2-7: Separation of isochorismate. **a.** RP-HPLC analysis of the dried methanol extract that was dissolved in water. Isochorismate eluted at 20% methanol with retension time of 17 min followed by chorismate with retension time of 21 min, which was comparable to that described.[39] **b.** ^{1}H-NMR spectrum of the isochorismate peak from HPLC. Peaks for isochorismate are indicated by asterisks.

Determination of Steady-State Kinetic Parameters

To gain insight into the PchB reaction mechanisms, six mutants that differed from the wild type PchB by a single amino acid substitution were constructed and purified: K42A, K42E, K42Q, K42H, A43P, and I87T. Both CM and IPL activities were measured for wild type and each mutant. The steady-state kinetic parameters are summarized in Table 2-3a for CM, and 2-3b for IPL activities. Wild type PchB catalyzes CM reaction with k_{cat} of 1.41 min^{-1} and K_m of 120 μM, and IPL reaction with k_{cat} of 10.6 min^{-1} and K_m of 4.3 μM.

Both CM and IPL activities were detectable for all mutants except K42E and K42Q. Mutant K42E has no measurable CM or IPL activities, and K42Q has no CM activity but remains some IPL activity. Lys42 in the mobile loop is within electrostatic and H-bonding distance of the ether oxygen (O7) of substrate, and has been proposed to play a critical catalytic role.[4] Removal of both positive charge and hydrogen bonds at position 42 through K42A leads to approximately 100-fold reduction in k_{cat}/K_m for both CM and IPL activities. Removal of positive charge with hydrogen bonds intact through K42Q and K42H mutants results in a decrease in k_{cat}/K_m by ~ 60-fold for IPL reaction. K42H retains 3% catalytic efficiency on CM activities probably due to the partial protonation of the imidazole ring of histidine at pH 7.5, which results in little effect on k_{cat} but ~ 30-fold increase in K_m relative to wild type PchB. These large reduction in catalytic efficiency associated with mutations at Lys42 indicates that the electrostatic and hydrogen bonding abilities at site 42 are critical to both the k_{cat} and K_m of CM and IPL.

Table 2-3a: Comparison of steady-state kinetic parameters of chorismate mutase activities of wild type and mutant PchB

Enzymes	K_m (μM)	k_{cat} (min^{-1})	k_{cat} / K_m ($M^{-1}s^{-1}$)	% wild type (k_{cat} / K_m)
Wild type	120 ± 10	1.41 ± 0.03	201	100
K42A	720 ± 30	0.09 ± 0.00	2	1
K42E	*	*	-	-
K42Q	*	*	-	-
K42H	3770 ± 40	1.61 ± 0.02	7	3
A43P	186 ± 2	1.57 ± 0.01	141	70
I87T	440 ± 20	4.09 ± 0.07	155	77

* = below the limits of detection, 0.8 nmol for CM assay

Table 2-3b: Comparison of steady-state kinetic parameters of isochorismate-pyruvate lyase activities of wild type and mutant PchB

Enzymes	K_m (μM)	k_{cat} (min^{-1})	k_{cat} / K_m ($M^{-1}s^{-1}$)	% wild type (k_{cat} / K_m)
Wild type	4.3 ± 0.2	10.6 ± 0.1	41200	100
K42A	51 ± 3	1.47 ± 0.03	480	1
K42E	*	*	-	-
K42Q	66 ± 3	2.81 ± 0.05	714	2
K42H	57 ± 2	2.22 ± 0.04	640	2
A43P	5.3 ± 0.1	11.3 ± 0.3	36700	89
I87T	1.09 ± 0.05	0.85 ± 0.02	13000	32

* = below the limits of detection, 0.3 pmol for IPL assay

A43P mutant was designed to increase rigidity of the active site loop, which might suggest the overall contributions of active site loop motility to catalytic efficiencies. A43P has a k_{cat}/K_m of 70% of the wild type CM activity, and 89% of the wild type IPL activity. Two activities are covariant, with a slightly faster turnover rate (k_{cat}) and lower substrate binding affinity (K_m), which needs to be deconvoluted with the transient kinetics in the future.

The I87T mutant was previously identified as a mutation that was IPL defective but CM competent in PchB.[2] However, in our hands the I87T mutant has a catalytic efficiency (k_{cat}/K_m) of 32% of the wild type IPL activity, and 77% of the wild type CM activity.

Determination of the Activation Parameters

Tables 2-4 and 2-5 summarize the thermodynamic activation parameters calculated from the observed effects of temperature on the PchB catalyzed intramolecular rearrangements. The activation parameters for CM and IPL were determined by measuring the reaction rates of enzyme-catalyzed reaction in a temperature range of 10 to 45 °C for CM, and 5 to 45 °C for IPL. The rate constant of spontaneous rearrangement of isochorismate to salicylate was determined from 25 °C to 60 °C. Values for the enthalpy and entropy of activation ($\Delta H^{\ddagger}$ and $\Delta S^{\ddagger}$) were obtained by fitting rate constant versus temperature in to Eyring equation. Those resulting linear plots are shown in Figures 2-8 and 2-9. The enthalpy and entropy of activation for k_{cat} were found to be 15.9 kcal·mol^{-1} and -12.1 cal·mol^{-1}K^{-1} in PchB CM

Table 2-4: Activation parameters of the chorismate mutase reaction

chorismate mutase	$\Delta G^{\ddagger}$ (kcal·mol^{-1})	$\Delta H^{\ddagger}$ (kcal·mol^{-1})	$\Delta S^{\ddagger}$ (cal·mol^{-1}·K^{-1})	$T\Delta S^{\ddagger}$ (kcal·mol^{-1})
Uncatalyzed rearrangement[a]	24.5	20.7	-12.8	-3.8
PchB CM	19.5	15.9	-12.1	-3.6
KpCM[b] *Klebsiella pneumoniae*	16.2	15.9	-1.1	-0.3
BsCM[c] *Bacillus subtilis*	15.4	12.7	-9.1	-2.7
SaCM[b] *Streptomyces aureofaciens*	15	14.5	-1.6	-0.5

$\Delta G^{\ddagger}$ was calculated for 25 °C, T = 298.15 K

[a]Andrews, P.R., et al, *Biochemistry* **12**, 3492-98 (1973).

[b]Gorisch, H., *Biochemistry* **17**, 3700-05 (1978).

[c]Kast, P., et al, *Tetr Lett* **37**, 2691-94 (1996).

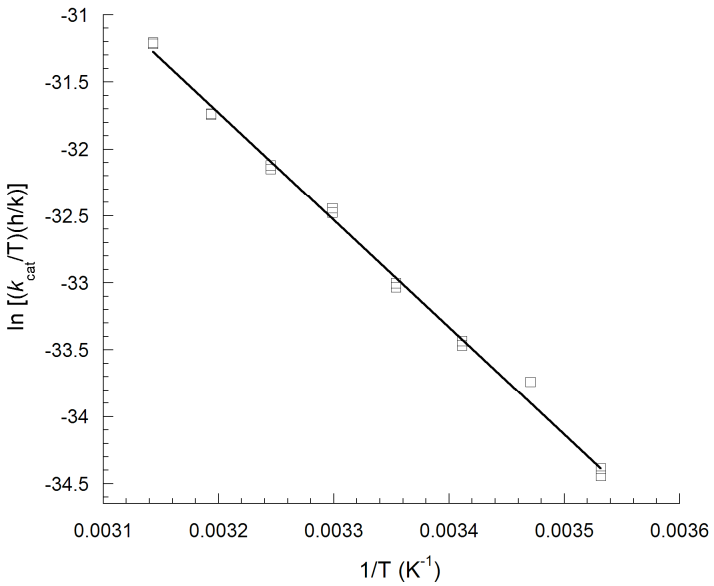

Figure 2-8: Temperature dependence of k_{cat} for chorismate mutase activity of PchB.

Table 2-5: Activation parameters of the isochorismate-pyruvate lyase reaction

Isochorismate-pyruvate lyase	$\Delta G^{\ddagger}$ (kcal·mol^{-1})	$\Delta H^{\ddagger}$ (kcal·mol^{-1})	$\Delta S^{\ddagger}$ (cal·mol^{-1}·K^{-1})	$T\Delta S^{\ddagger}$ (kcal·mol^{-1})
Uncatalyzed rearrangement	25.5	21.4	-13.8	-4.1
PchB IPL	18.5	11.1	-24.8	-7.4

$\Delta G^{\ddagger}$ was calculated for 25 °C, T = 298.15 K

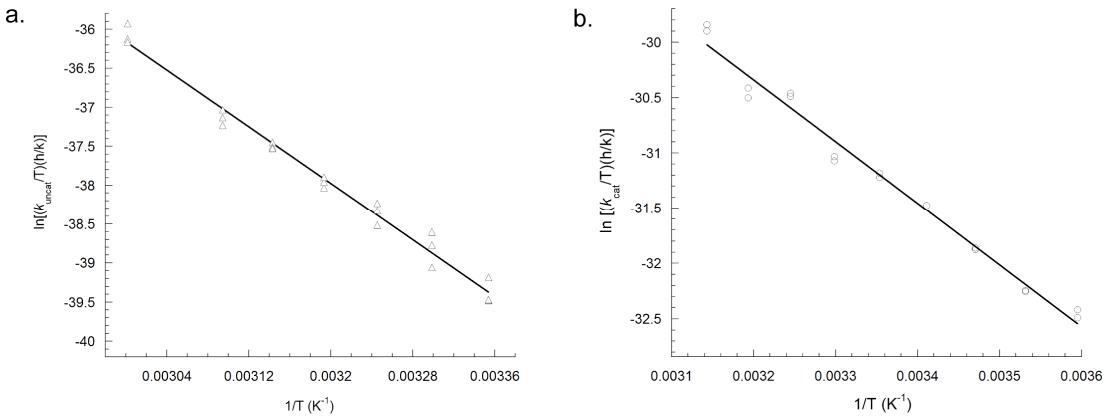

Figure 2-9. Temperature dependence of reaction rate for isochorismate rearrangement to salicylate. **a.** Uncatalyzed reaction in solution, **b.** Reaction catalyzed by PchB IPL activity.

activity, 11.1 kcal·mol^{-1} and -24.8 cal·mol^{-1}K^{-1}in PchB IPL activity. The activation free energy $\Delta G^{\ddagger}$ is 19.5 kcal mol^{-1} with the activation enthalpy ($\Delta H^{\ddagger}$) of 15.9 kcal mol^{-1} in PchB CM catalysis, which is lower than that found for uncatalyzed reaction in solution ($\Delta G^{\ddagger}$ is 24.5 kcal mol^{-1}, $\Delta H^{\ddagger}$ is 20.7 kcal mol^{-1}). This accounts for a rate acceleration of at least 10^3-fold by PchB CM ($\Delta\Delta G^{\ddagger}$ = 5 kcal mol^{-1}), which indicates that PchB is a less optimized for CM activity compared to most chorismate mutases[30] as the three described in Table 2-4 have $\Delta\Delta G^{\ddagger}$ in range of 8 ~ 9.5 kcal mol^{-1}. PchB has almost the same activation entropy ($\Delta S^{\ddagger}$ = -12.1 cal mol^{-1}K^{-1}) as the uncatalyzed rearrangement in solution ($\Delta S^{\ddagger}$ = -12.9 cal mol^{-1}K^{-1}) and is less favorable than CMs from *K. pneumonia* (KpCM) and *S. aureofaciens* (SaCM). Similar values of the entropic terms ($-T\Delta\Delta S^{\ddagger}$) was reported as 0.3 kcal mol^{-1} for KpCM and 0.5 kcal mol^{-1} for SaCM, in which their contributions to $\Delta\Delta G^{\ddagger}$ are 44% and 35%, for KpCM and SaCM catalyzed reactions, respectively. Whereas, PchB CM is more related to BsCM from the thermodynamic point of view. PchB has $-T\Delta\Delta S^{\ddagger}$ of 0.2 kcal mol^{-1}, and BsCM has 1.1 kcal mol^{-1}. The difference between $\Delta G^{\ddagger}_{cat}$ and $\Delta G^{\ddagger}_{uncat}$ ($\Delta\Delta G^{\ddagger}$) predominately arises from a difference in activation enthalpies ($\Delta\Delta H^{\ddagger}$).

2.4 Discussion

Chorismate mutase catalyses the [3,3]-Claisen rearrangement of chorismate to prephenate, the committed step in the biosynthesis of aromatic amino acids in microoganisms.[44] Because the chorismate rearrangement is not involved in covalent bonding with enzyme groups, CMs have been used as a model system to study

enzyme energetics for decades, but the source of catalytic power of these enzymes is still the subject of controversy. The two proposals gained the most attention: electrostatic transition state stabilization (TSS) and generation of a reactive substrate conformation. The electrostatic TSS proposal states that the charged/polar amino acid side chains in the active site are positioned precisely such that the active site preferentially binds the transition state over the ground state and stabilizes the developing negative charge in the TS, thus lowering the activation energy barrier. The reactive substrate conformation referred as a near attach conformation (NAC) by Hur and Bruice,[29] believes that the CM help in bringing the reacting atoms of chorismate to form a reactive substrate conformer - NAC, and once chorismate achieves this conformation the arrangement can proceed without addition of TSS.

PchB, a bifunctional enzyme in *P. aeruginosa*, has a physiological role as an isochorismate-pyruvate lyase and possesses weak chorismate mutase activity. PchB does not apply a general base mechanism to eliminate the pyruvate side chain from isochorismate as pyruvate lyases of other shikimic acid metabolites do.[45-47] Instead, the IPL activity of PchB uses a [1,5]-sigmatropic rearrangement mechanism.[5] Therefore, there are two pericyclic reactions that can happen in PchB active site, which indicates that during catalysis two NACs (Figure 2-3) will be formed, followed by formation of two transition states. Compared to the active sites of EcCM and BsCM (Figure 2-2), PchB active site has fewer charged/polar amino acids, which led to a hypothesis that the reduced electrostatic and hydrogen bonding interactions with substrate in PchB may provide this single active site with the ability to catalyze both

CM and IPL reactions.[4] Structures of apo- and pyruvate – bound PchB suggested that Lys42 and Gln90 might have stabilization effects on transition states. Lys42, the only active site amino acid found in a mobile loop, becomes ordered upon substrate binding,[4] which acts as a portal that helps with arranging the enolpyruvate side chains of substrates to form NACs, leading to aromatization in chorismate or pyruvate elimination from isochorismate. In this chapter, several single mutations on Lys42 were tested to explore the relative contributions of TSS and NAC for CM and IPL catalysis. The CD spectra of mutants and wild type PchB were comparable (Figure 2-4), which indicates that the structural integrity was well-maintained in each mutant. The x-ray crystallographic structure of K42A exhibited an intact active site architecture including an ordered active site loop and salicylate and pyruvate bound within the active site (Figure 2-5a and b). Therefore, variation in steady-state kinetic parameters of mutants is completely due to the modification of a single amino acid side chain without alteration of the active site.

CM activity of PchB and mutant enzymes was determined by spectrometrically measuring the disappearance of chorismate.[22] Reverse of charge at position 42 through K42E leads to no measurable CM activity, indicating that the negatively charged Glu42 may interrupt the shuttle of chorismate into the active site by repulsion of the C11 carboxylate group on chorismate, such that the enolpyruvate side chain can not be properly positioned over the cyclohexadiene ring to form a reactive pseudo-diaxial conformation and adopt the TS. Mutant K42A differed from wild type enzyme in its aliphatic side chain without charge or H-bonding ability. However,

K42A still has 1% of the wild type CM activity. An explanation for this 1% of residual activity is due to a contribution from NAC formation in the active site, since the active site of K42A still provides a shape in complementary to NAC. K42Q is a mutant with a neutural polar side chain and has no detectable CM activity, suggesting that the H-bonding ability of Gln42 was not enough for catalysis. Taking K42A into consideration, a possible reason is that H-bonding of Gln42 with the nearby Gln90 via a water molecule may alter the orientation of these two important residues relative to chorismate in a way that K42Q active site cannot provide the proper shape for NAC. Replacement of Lys42 by histidine with a titrable imidazole group on the side chain remains 3% of the catalytic efficiency, which results from ~ 5% of imidazole group was protonated at pH 7.5 (the reaction buffer) given that a calculated pK_a of 6.2 for the active site histine.[48] K42H has a little increase in k_{cat} (~ 1.2-fold) but leads to 32-fold increase in K_m. Therefore, a positive charge at position 42 is critical for CM catalytic efficiency, indicating that electrostatic TSS is critical for the CM activity. This conclusion can find the support in the pH dependence of K42H experiment that the CM activity in K42H was not detectable at pH values above 7.5.[48]

The IPL activities of PchB and mutants were determined by measuring the formation of product salicylate using fluorescence.[2] For each mutant, the IPL activity remains dominant over the corresponding CM activity. The IPL and CM activities of K42A and K42H are covariant, giving a k_{cat}/K_m of 1% and 2% of wild type IPL activity, respectively. The CM-deficient mutant K42Q has 2% of IPL activity relative to wild type, suggesting that substrate isochorismate probably is aligned in a different

way due to the relocation of a hydroxyl group from C4 to C2. This residual IPL activity results from NAC of isochorismate in K42Q active site.

The A43P mutant was designed to increase the rigidity of the active site loop by replacing an alaine with a bulky residue proline at position 43. A43P results in a 1.5-fold and a 1.2-fold reduction in k_{cat}/K_m relative to wild type CM and IPL, respectively. Both CM and IPL have a slightl increase in k_{cat} and K_m. The relationship of the active site loop and catalytic activity will be determined using transverse relaxation optimized NMR approach in the future by the next graduate student.

I87T was originally reported by Gaille *et al.* (2002) to be an IPL deficient and CM competent enzyme. However, according to our kinetic data, I87T has not completely lost IPL activity, but retains 32% of k_{cat}/K_m from wild type. Differences in the protein overproduction system and the sensitivity of the assay measurement probably count for the variation in kinetic observations, which Gaille group overexpressed I87T in *E. coli* and measured salicylate fluorescence in ethyl acetate after the reaction was stopped by concentrated HCl.[2] The structure of I87T displays more disordered regions compared to wild type pyruvate-bound closed structure (Figure2-6). This intrinsic disorder in the enzyme may play an important role in catalysis.[49]

Enzymes achieve rate enhancement by lowering the activation energy ($\Delta G^{\ddagger}$) compared to the uncatalyzed reaction in solution.[50] $\Delta G^{\ddagger}$ is given by

$$\Delta G^{\ddagger} = \Delta H^{\ddagger} - T\Delta S^{\ddagger}$$

Activation enthalpy $\Delta H^{\ddagger}$ is the difference between the transition state enthalpy and

the sum of reactants enthalpies in the ground state, representing the extent of bond-breaking and bond-making in the transition state. Activation entropy $\Delta S^{\ddagger}$ is the difference between the transition state entropy and the sum of the entropies in ground state reactants, which indicates the conformational change as the system progressing to the transition state. In order to achieve efficient catalysis, enzymes may increase the entropic term ($T\Delta S^{\ddagger}$) of $\Delta G^{\ddagger}$ by reducing the degree of freedom, or control the preorganization state in the active site for formation of ground state NACs.[51]

The rate enhancement of enzyme results from reduction in the activation enthalpy and/or the activation entropy.[11] Entropies of activation $\Delta S^{\ddagger}$ in PchB CM and BsCM are very similar to that in water, therefore the overall catalysis is due to enthalpic effects. In KpCM and SaCM, catalysis are dependent on both enthalpy and entropy, given that 44% and 35% of entropic contributions to catalysis, which supports the idea that enzyme catalysis arises from entropy loss upon substrate binding.[52] However, Warshel *et al.*[53] have shown that the binding of substrate to enzyme does not lead to loss of many degrees of freedom compared to the substrate in solution. One can suppose that the driving force for the rate enhancement of PchB CM is enthalpic. PchB preorganizes the active site for NAC and TS, lowering the free energy of the TS by electrostatic interactions to achieve the most catalytic efficiency.

References

1. Crosa, J.H. & Walsh, C.T. Genetics and assembly line enzymology of siderophore biosynthesis in bacteria. *Microbiol Mol Biol Rev* **66**, 223-49 (2002).
2. Gaille, C., Kast, P. & Haas, D. Salicylate biosynthesis in Pseudomonas aeruginosa. Purification and characterization of PchB, a novel bifunctional enzyme displaying isochorismate pyruvate-lyase and chorismate mutase activities. *J Biol Chem* **277**, 21768-75 (2002).
3. Gaille, C., Reimmann, C. & Haas, D. Isochorismate synthase (PchA), the first and rate-limiting enzyme in salicylate biosynthesis of Pseudomonas aeruginosa. *J Biol Chem* **278**, 16893-8 (2003).
4. Zaitseva, J., Lu, J., Olechoski, K.L. & Lamb, A.L. Two crystal structures of the isochorismate pyruvate lyase from Pseudomonas aeruginosa. *J Biol Chem* **281**, 33441-9 (2006).
5. DeClue, M.S., Baldridge, K.K., Kunzler, D.E., Kast, P. & Hilvert, D. Isochorismate pyruvate lyase: a pericyclic reaction mechanism? *J Am Chem Soc* **127**, 15002-3 (2005).
6. Rajagopalan, J.S., Taylor, K.M. & Jaffe, E.K. 13C NMR studies of the enzyme-product complex of Bacillus subtilis chorismate mutase. *Biochemistry* **32**, 3965-72 (1993).
7. Chook, Y.M., Ke, H. & Lipscomb, W.N. Crystal structures of the monofunctional chorismate mutase from Bacillus subtilis and its complex with a transition state analog. *Proc Natl Acad Sci U S A* **90**, 8600-3 (1993).
8. Chook, Y.M., Gray, J.V., Ke, H. & Lipscomb, W.N. The monofunctional chorismate mutase from Bacillus subtilis. Structure determination of chorismate mutase and its complexes with a transition state analog and prephenate, and implications for the mechanism of the enzymatic reaction. *J Mol Biol* **240**, 476-500 (1994).
9. Lee, A.Y., Stewart, J.D., Clardy, J. & Ganem, B. New insight into the catalytic mechanism of chorismate mutases from structural studies. *Chem Biol* **2**, 195-203 (1995).
10. Lee, A.Y., Karplus, P.A., Ganem, B. & Clardy, J. Atomic structrue of the buried catalytic pocket of *Escherichia coli* chorismate mutase. *J Am Chem Soc* **117**, 3627-3628 (1995).
11. Andrews, P.R., Smith, G.D. & Young, I.G. Transition-state stabilization and enzymic catalysis. Kinetic and molecular orbital studies of the rearrangement of chorismate to prephenate. *Biochemistry* **12**, 3492-8 (1973).
12. Hilvert, D., Carpenter, S.H., Nared, K.D. & Auditor, M.T. Catalysis of concerted reactions by antibodies: the Claisen rearrangement. *Proc Natl Acad Sci U S A* **85**, 4953-5 (1988).
13. Copley, S.D. & Knowles, J.R. The Uncatalyzed Claisen Rearrangement of Chorismate to Prephenate Prefers a Transition-State of Chairlike Geometry. *Journal of the American Chemical Society* **107**, 5306-5308 (1985).

14. Copley, S.D. & Knowles, J.R. The Conformational Equilibrium of Chorismate in Solution - Implications for the Mechanism of the Nonenzymatic and the Enzyme-Catalyzed Rearrangement of Chorismate to Prephenate. *Journal of the American Chemical Society* **109**, 5008-5013 (1987).
15. Bruice, T.C. A view at the millennium: the efficiency of enzymatic catalysis. *Acc Chem Res* **35**, 139-48 (2002).
16. Warshel, A. Energetics of Enzyme Catalysis. *Proceedings of the National Academy of Sciences of the United States of America* **75**, 5250-5254 (1978).
17. Warshel, A. et al. Electrostatic basis for enzyme catalysis. *Chemical Reviews* **106**, 3210-3235 (2006).
18. Warshel, A. et al. Electrostatic basis for enzyme catalysis. *Chem Rev* **106**, 3210-35 (2006).
19. Liu, D.R., Cload, S.T., Pastor, R.M. & Schultz, P.G. Analysis of active site residues in *Escherichia coli* chorismate mutase by site-directed mutagenesis. *J Am Chem Soc* **118**, 1789-1790 (1996).
20. Cload, S.T., Liu, D.R., Pastor, R.M. & Schultz, P.G. Mutagenesis study of active site residues in chorismae mutase from *Bacillus subtilis*. *J Am Chem Soc* **118**, 1787-1788 (1996).
21. Kast, P., Asif-Ullah, M., Jiang, N. & Hilvert, D. Exploring the active site of chorismate mutase by combinatorial mutagenesis and selection: the importance of electrostatic catalysis. *Proc Natl Acad Sci U S A* **93**, 5043-8 (1996).
22. Kast, P. et al. A strategically positioned cation is crucial for efficient catalysis by chorismate mutase. *J Biol Chem* **275**, 36832-8 (2000).
23. Kienhofer, A., Kast, P. & Hilvert, D. Selective stabilization of the chorismate mutase transition state by a positively charged hydrogen bond donor. *J Am Chem Soc* **125**, 3206-7 (2003).
24. Strater, N., Schnappauf, G., Braus, G. & Lipscomb, W.N. Mechanisms of catalysis and allosteric regulation of yeast chorismate mutase from crystal structures. *Structure* **5**, 1437-52 (1997).
25. Claeyssens, F., Ranaghan, K.E., Manby, F.R., Harvey, J.N. & Mulholland, A.J. Multiple high-level QM/MM reaction paths demonstrate transition-state stabilization in chorismate mutase: correlation of barrier height with transition-state stabilization. *Chem Commun (Camb)*, 5068-70 (2005).
26. Ranaghan, K.E. et al. Transition state stabilization and substrate strain in enzyme catalysis: ab initio QM/MM modelling of the chorismate mutase reaction. *Org Biomol Chem* **2**, 968-80 (2004).
27. Ranaghan, K.E. & Mulholland, A.J. Conformational effects in enzyme catalysis: QM/MM free energy calculation of the 'NAC' contribution in chorismate mutase. *Chem Commun (Camb)*, 1238-9 (2004).
28. Strajbl, M., Shurki, A., Kato, M. & Warshel, A. Apparent NAC effect in chorismate mutase reflects electrostatic transition state stabilization. *J Am Chem Soc* **125**, 10228-37 (2003).

29. Hur, S. & Bruice, T.C. Comparison of formation of reactive conformers (NACs) for the Claisen rearrangement of chorismate to prephenate in water and in the E. coli mutase: the efficiency of the enzyme catalysis. *J Am Chem Soc* **125**, 5964-72 (2003).
30. Schowen, R.L. How an enzyme surmounts the activation energy barrier. *Proc Natl Acad Sci U S A* **100**, 11931-2 (2003).
31. Zhang, X. & Bruice, T.C. A definitive mechanism for chorismate mutase. *Biochemistry* **44**, 10443-8 (2005).
32. Hur, S. & Bruice, T.C. Just a near attack conformer for catalysis (chorismate to prephenate rearrangements in water, antibody, enzymes, and their mutants). *J Am Chem Soc* **125**, 10540-2 (2003).
33. Hur, S. & Bruice, T.C. The near attack conformation approach to the study of the chorismate to prephenate reaction. *Proc Natl Acad Sci U S A* **100**, 12015-20 (2003).
34. The Biophysics Core Facility. The University of Colorado Health Sciences Center, Circular Dichroism Procedure. *http://biomol.uchsc.edu/cores/biophysics/circulardichroism.html*.
35. Otwinowski, Z. & Minor, W. Processing of X-ray diffraction data collceted in oscillation mode. *Methods Enzymol.* **276**, 307-326 (1997).
36. The CCP4 suite: programs for protein crystallography. *Acta Crystallogr D Biol Crystallogr* **50**, 760-3 (1994).
37. Emsley, P. & Cowtan, K. Coot: model-building tools for molecular graphics. *Acta Crystallogr D Biol Crystallogr* **60**, 2126-32 (2004).
38. Murshudov, G.N., Vagin, A.A. & Dodson, E.J. Refinement of macromolecular structures by the maximum-likelihood method. *Acta Crystallogr D Biol Crystallogr* **53**, 240-55 (1997).
39. Schmidt, K. & Leistner, E. Microbial production of (+)-trans-isochorismic acid. *Bioctechnol. Bioeng.* **45**, 285-291 (1995).
40. Gibson, F. Chorismic acid: purification and some chemical and physical studies. *Biochem. J.* **90**, 256-261 (1964).
41. Rieger, C.E. & Turnbull, J.L. Small scale biosynthesis and purification of gram quantities of chorismic acid. *Prep Biochem Biotechnol* **26**, 67-76 (1996).
42. Kast, P., AsifUllah, M. & Hilvert, D. Is chorismate mutase a prototypic entropy trap? - Activation parameters for the *Bacillus subtilis* enzyme. *Tetrahedron Letters* **37**, 2691-2694 (1996).
43. DeClue, M.S., Baldridge, K.K., Kast, P. & Hilvert, D. Experimental and computational investigation of the uncatalyzed rearrangement and elimination reactions of isochorismate. *J Am Chem Soc* **128**, 2043-51 (2006).
44. Gibson, F. & Pittard, J. Pathways of biosynthesis of aromatic amino acids and vitamins and their control in microorganisms. *Bacteriol Rev* **32**, 465-92 (1968).
45. Gallagher, D.T. et al. The crystal structure of chorismate lyase shows a new fold and a tightly retained product. *Proteins* **44**, 304-11 (2001).
46. Spraggon, G. et al. The structures of anthranilate synthase of Serratia marcescens crystallized in the presence of (i) its substrates, chorismate and

glutamine, and a product, glutamate, and (ii) its end-product inhibitor, L-tryptophan. *Proc Natl Acad Sci U S A* **98**, 6021-6 (2001).

47. Nakai, T. et al. Three-dimensional structure of 4-amino-4-deoxychorismate lyase from Escherichia coli. *J Biochem* **128**, 29-38 (2000).
48. Olucha, J., Luo, Q. & Lamb, A.L. pH dependence of *Pseudomonas aeruginosa* isochorismate-pyruvate lyase: Implications for transition state stabilization and the role of Lysine 42. *Submitted* (2009).
49. Vamvaca, K., Jelesarov, I. & Hilvert, D. Kinetics and thermodynamics of ligand binding to a molten globular enzyme and its native counterpart. *Journal of Molecular Biology* **382**, 971-977 (2008).
50. Voet, D. & Voet, J.G. Biochemistry (Wiley, 2004).
51. Bruice, T.C. & Lightstone, F.C. Ground state and transition state contribution to the rates of intramolecular and enzymatic reactions. *Acc. Chem. Res.* **32**, 127-136 (1999).
52. Page, M.I. & Jencks, W.P. Entropic contributions to rate accelerations in enzymic and intramolecular reactions and the chelate effect. *Proc Natl Acad Sci U S A* **68**, 1678-83 (1971).
53. Villa, J. et al. How important are entropic contributions to enzyme catalysis? *Proc Natl Acad Sci U S A* **97**, 11899-904 (2000).

CHAPTER 3

Salicylate Synthetic Enzymes in *Pseudomonas aeruginosa* and *Yersinia enterocolitica*

3.1 Introduction

Chorismate, the final product of the shikimate pathway, is a precursor for aromatic amino acids, vitamins K and E, menaquinones, siderophores and other metabolites in bacteria.[1] There are three important chorismate-utilizing enzymes that catalyze 1) isomerization of chorismate to isochorismate (isochorismate synthase, ICS), 2) replacement of the hydroxyl group at C4-chorismate by an amine (aminodeoxychorismate synthase, ADCS), or 3) removal of the C4 hydroxyl group followed by addition of amine at C2-chorismate (anthranilate synthase, AS). These enzymes are involved in the first committed step of menaquinone, siderophore, or tryptophan biosynthesis, so they are referred as MST family.[2] MST enzymes share high sequence homology and most MST members[3-6] are structurally homologous, and have a similar catalytic mechanism.[1] The absence of chorismate-dependent pathways in mammals makes chorismate-utilizing enzymes attractive targets for antimicrobial treatments for bacterial infections.

Derived from chorismate, isochorismate is an important intermediate of siderophore and menaquinone production in bacteria. Enzymes that catalyze these conversions belong to the Mg^{2+}-dependent MST family. Shown in Figure 3-1 are the

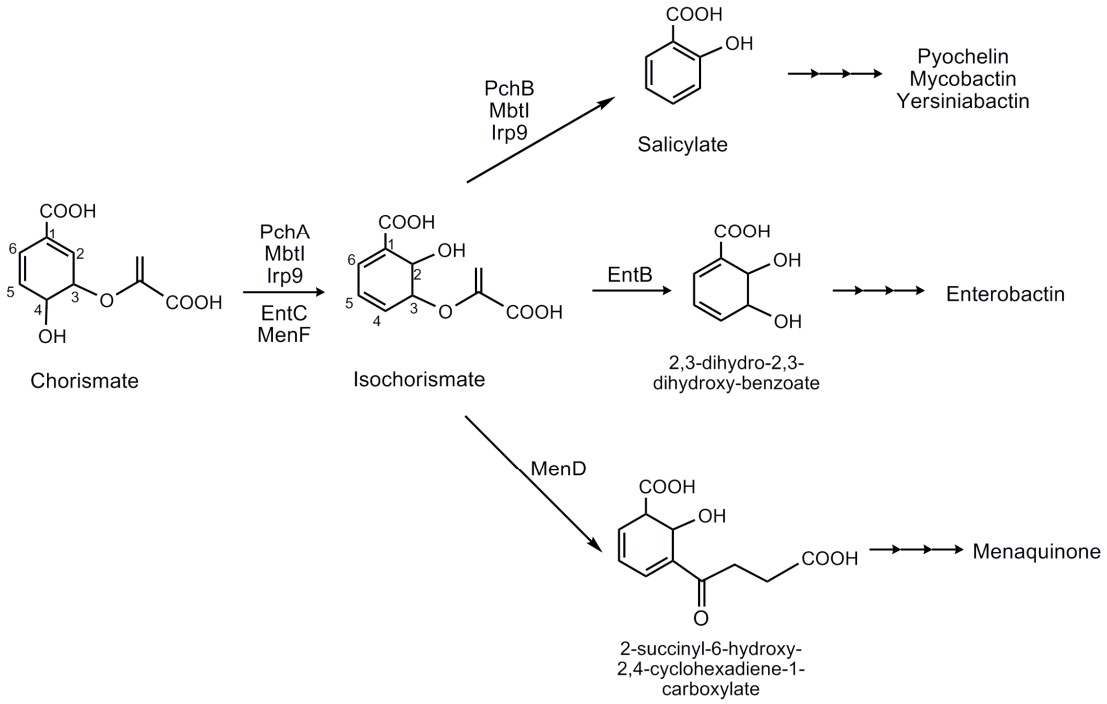

Figure 3-1: Conversion of chorismate to isochorismate and its incorporation into siderophores or menaquinone. Formation of isochorismate is the first committed step in formation of siderophores (pyochelin, mycobactin, yersiniabactin, and enterobactin) and menaquinone (vitamin K).

reactions of the most studied ICS enzymes including PchA in *P. aeruginosa*,[7] MbtI in *M. tuberculosis*,[5] Irp9 in *Y. enterocolitica*,[8] MenF and EntC in *E. coli*[9]. PchA, EntC and MenF are monofunctional ICS, whereas Irp9 and MbtI are salicylate synthases that perform a second reaction in which the pyruvate is eliminated from isochorismate to produce salicylate. In other words, in order for *P. aeruginosa* to utilize salicylate as a building block for siderophore pyochelin biosynthesis, a second enzyme (PchB) is required to remove the pyruvate tail from isochorismate (IPL activity) made by PchA to generate a salicylate.[10] It would be quite interesting to biochemically and structurally characterize the ICS PchA that will provide insight into the enzyme evolution in MST family and the search for inhibitors of salicylate synthesis.

EntC and MenF are two ICS in *E. coli* that catalyze an identical reaction, but their expression is regulated under different growth conditions, and are involved in different metabolism pathways. EntC is responsible for making isochorismate that is required for siderophore enterobactin biosynthesis under iron deficiency in *E. coli*, while MenF produces isochorismate for menaquinone synthesis under anaerobic conditions, which is essential for electron transport and ATP synthesis in *E. coli*.[11] PchA is 25% identical and 42% similar to EntC, and 34% identical and 50% similar to MenF (sequence alignment was performed in ClustalW[12]). The x-ray crystallographic structure of MenF has been determined,[2,6] which has an α/β overall fold (Figure 3-2a) similar to other chorismate-utilizing enzyme, such as anthranilate synthase in *Serratia marcescens*[3]. The MenF active site contains a sulfate ion that occupies the place where chorismate would bind and a magnesium ion that interacts

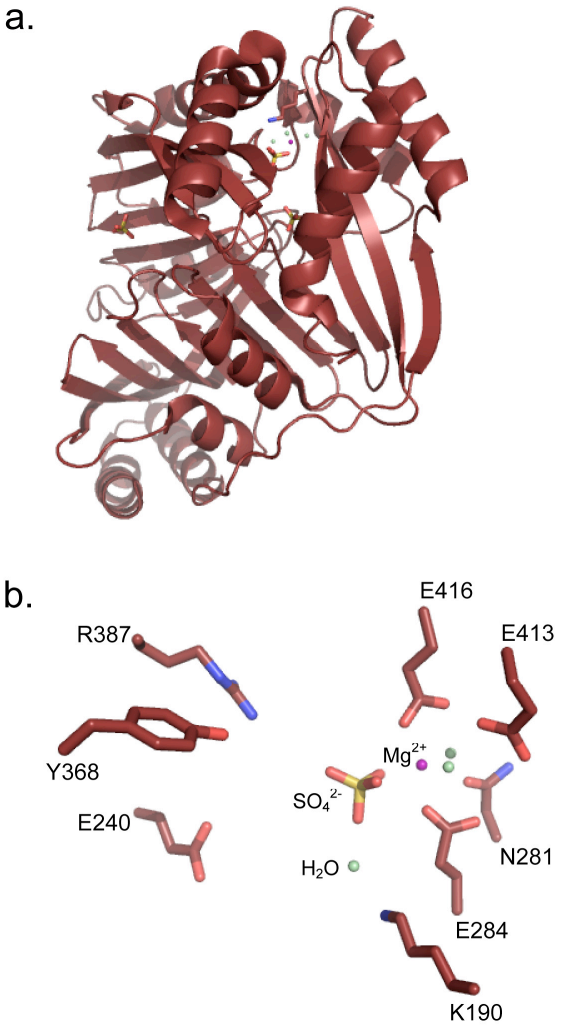

Figure 3-2: MenF overall and active site structures. **a.** Overall structure. MenF exhibits an α/β fold with antiparellel β-strands rapped around by α-helices. **b.** MenF active site structure. Sulfate ion is yellow stick and magnesium ion is purple sphere. Three important water molecules were found in the MenF active site, two involved in Mg^{2+} chelating and one is hypothesized to act as a nucleophile to attach C2-chorismate after activation by K190. Figures were created using PyMOL. (PDB ID 3BZN)

with the C1 carboxylate of chorismate (Figure 3-2b)[2]. Kolappan *et al.*[2] proposed the mechanism through which MenF rearranges chorismate to isochorismate (Figure 3-3). In the active site, Mg^{2+} is coordinated by two acidic residues E284 and E416 which in turn orients the C1 carboxylate group of chorismate. In contrast to anthranilate synthase, Mg^{2+} ion is not directly involved in catalysis.[1] The reaction starts with the activation of a water molecule by K190. The activated water acts as a nucleophile to attack the chorismate at the C2 carbon resulting in the S_N2'' rearrangement of 1-2 and 5-6 double bonds followed by elimination of the C4 hydroxyl group. E240 is in the proximity of C4-OH and thus expected to serve as a general acid to promote departure of the C4-OH.[2]

In contrast to *P. aeruginosa* which requires PchA and PchB to make salicylate, in some bacteria, the salicylate is generated from chorismate in a single step catalyzed by the bifunctional enzyme salicylate synthase, including Irp9 in *Y. enterocolitica* and MbtI in *M. tuberculosis*.[5,8] PchA shares 28% identity and 47% similarity to Irp9, and 30% identity and 47% similarity to MbtI, whereas PchB has no sequence similarity to these two enzymes. Studies have demonstrated that Irp9 and MbtI are bifunctional salicylate synthases with both isochorismate synthase and isochorismate-pyruvate synthase activities, and that isochorismate is a detectable intermediate during the catalysis.[4,5,8,13] Both Irp9 (Figure 3-4a) and MbtI x-ray crystallographic structures have the same fold as that previously described for MenF. The Irp9 active site with salicylate and pyruvate bound is shown in Figure 3-4a. Mg^{2+} coordinates with Glu directly or through a water molecule, and the salicylate carboxylate. The role of a

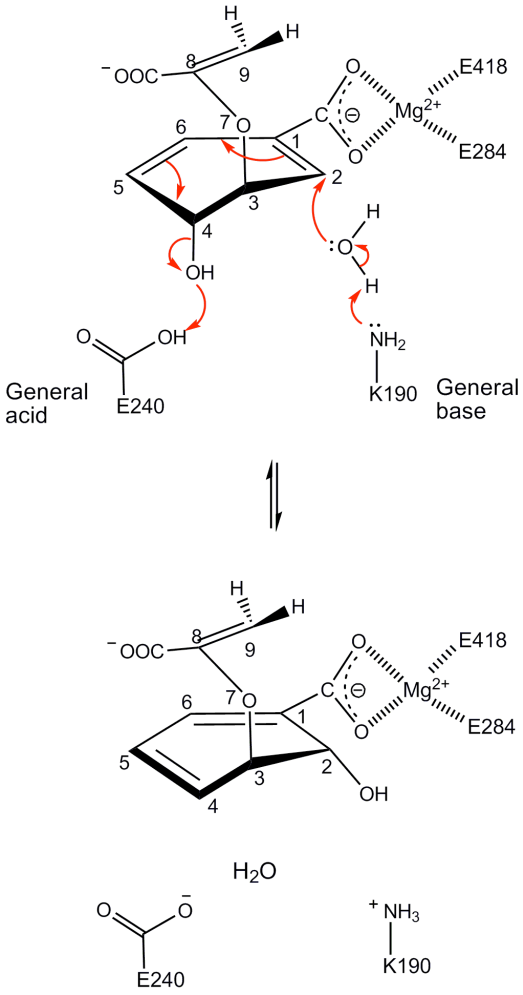

Figure 3-3: General acid and base catalysis proposed by MenF. (Modified from Kolappan *et al*. 2007)

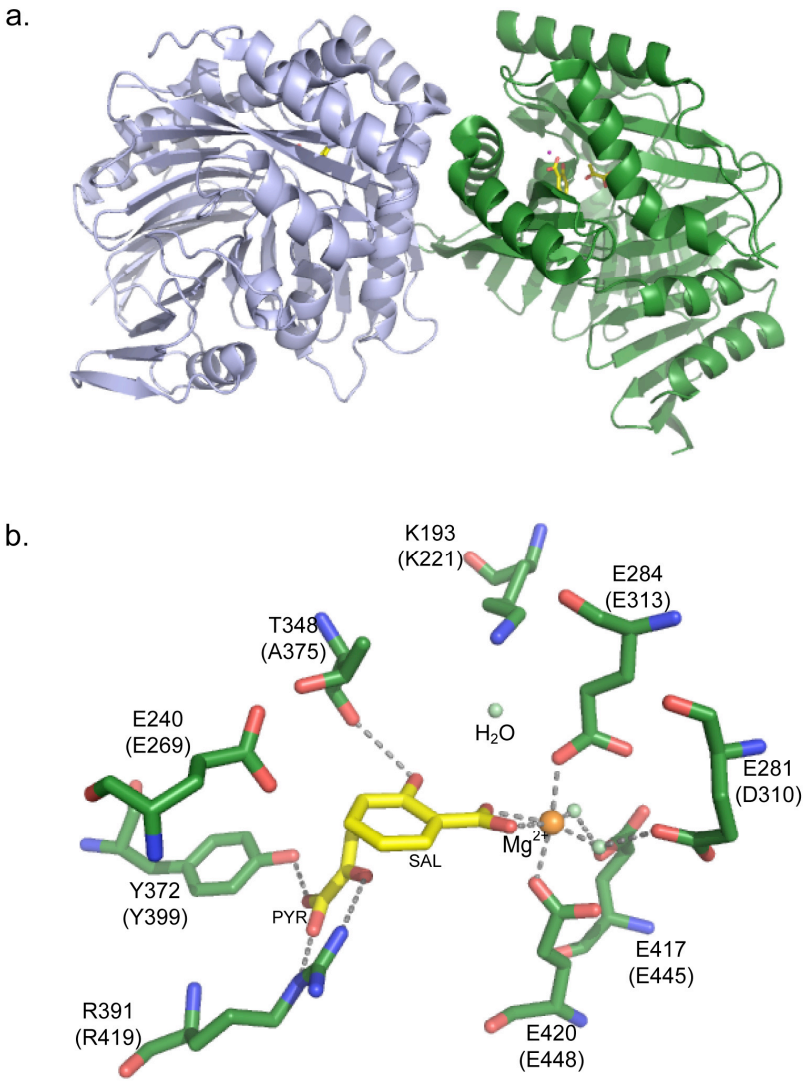

Figure 3-4: Salicylate synthase Irp9. **a.** Overall structure of Irp9. Irp9 is a dimeric Mg^{2+}-dependent salicylate synthase and has a α/β fold similar to MenF. **b.** The active site of Irp9 with salicylate and pyruvate bound. The corresponding amino acid residues in PchA are shown in parenthesis. (PDB code 2FN1). Figures were created with PyMOL.

divalent cation in the active site of salicylate synthase is proposed to orient the carboxylate on C1 chorismate without direct involvement in catalysis.[2,4]

According to structural and mechanistic studies on ICS and salicylate synthase in conjunction with sequence analysis (Figure 3-5 and Table 3-1), a reaction mechanism for MST family has been proposed[13] which can extend to PchA. It is proposed that nucleophilic addition of water to C2 promotes departure of C4-OH from chorismate. As shown in Figure 3-5, the active site residues of five displayed enzymes are highly conserved except for two (labeled with asterisks). The first nonconserved residue is Ala (A375 in PchA) that is conserved in ICS but is substituted by Thr in salicylate synthase, which might result in the loss of capability to eliminate enolpyruvate from isochorismate (IPL-deficient) in the ICS. The H-bonding of the backbone carbonyl of T348 to hydroxyl group of salicylate in Irp9 (Figure 3-4b)[4] may be shift compared to Ala, which was hypothesized to be critical for the IPL activity through alignment of isochorismate in the active site for the IPL reaction. The second nonconserved residue is Asp/Asn (D310 in PchA) in ICS but Glu in salicylate synthase. The role of this Glu in salicylate synthase is to coordinate Mg^{2+} through H_2O. The replacement of Glu by Asp/Asn with a shorter side chain might lead to a change in isochorismate orientation through pulling Mg^{2+} more deep in the active site, which may control the retention of the enolpyruvate on isochorismate.

To test these hypotheses, four active site mutations were constructed and kinetically analyzed in this chapter. Crystallization trials of PchA and Irp9 were

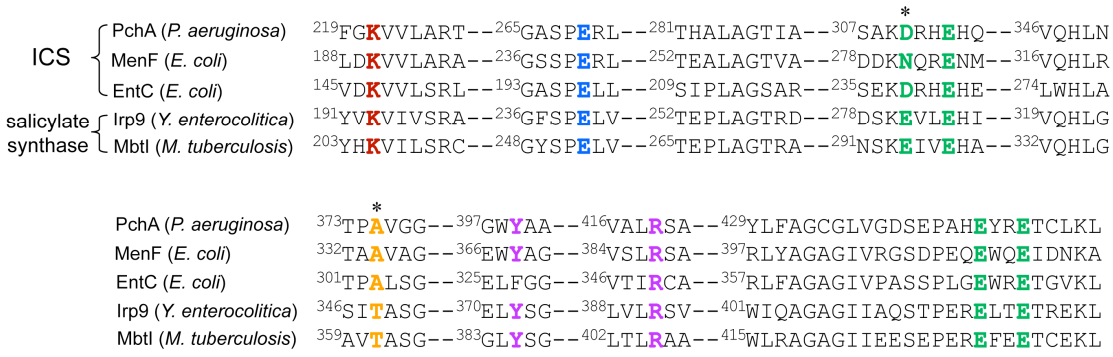

Figure 3-5: Active site sequence alignment of five chorismate-utilizing enzymes from MST family. Important residues are highlighted in colors. Residues K (red) and E (blue) were found to be general base and general acid in MenF and conserved in all aligned enzymes. Residues (E in green) coordinating Mg^{2+} are highly conserved. Backbone carbonyl of T (orange) H-bonds to hydroxyl group in salicylate. Y and R (in purple) orient carbonyl group in pyruvate. Sequence alignment was performed with ClustalW. Residues selected were based on MenF (PDB code 3BZN), Irp9 (PDB code 2FN0 and 2FN1), and MbtI (PDB code 2I6Y) active site structures.

Table 3-1: Comparison of active site amino acids of PchA and its homologues

	Isochorismate Synthase		Salicylate Synthase	
	PchA (*P. aeruginosa*)	MenF (*E. coli*)	Irp9 (*Y. enterocolitica*)	MbtI (*M. tuberculosis*)
General base for ICS activity	K221	K190	K193	K205
General acid for ICS activity	E269	E240	E240	E252
Coordinate Mg^{2+} ion through H_2O	D310 E445	N281 E413	E281 E417	E294 E431
Coordinate Mg^{2+} ion	E313 E448	E284 E416	E284 E420	E313 E434
Orient pyruvate	Y399 R419	Y368 R387	Y372 R391	Y385 R405
Orient salicylate hydroxyl group	A375	A344	T348	T361

carried out in an attempt to obtain structural information that will help with elucidation of PchA reaction mechanism and rational design of inhibitor of salicylate biosynthesis, and hence development of treatments for *P. aeruginosa*, *Yersinia* sp. and *M. tuberculosis* infections.

3.2 Material and Methods

3.2.1 Protein Production and Characterization

Cloning of *pchA* and *irp9*

pchA Constructs

pchA gene was amplified from *P. aeruginosa* PAO1 genomic DNA using PCR with Herculase polymerase (Statagene). The primers, restriction enzymes, and vectors used for each clone are summarized in Table 3-2. The amplified PCR fragments were digested with corresponding restriction enzymes, and inserted into selected vectors (Novagen). The insert was confirmed by nucleotide sequence analysis. The resulting plasmid was transformed into BL21 (DE3) *E. coli* competent cells (Novagen) for protein overproduction later.

Site-directed Mutagenesis

Mutation was introduced into pET28b-*pchA* construct using the QuikChange site-directed mutagenesis kit (Stratagene). Two complementary primers with a single mutation was used for each mutant (Table 3-2). The mutation was confirmed with DNA sequence analysis. The resultant plasmid was transformed into BL21 (DE3)

Table 3-2: Primers for cloning and mutagenesis

Protein	Primer	Primer sequence	Restriction Enzyme	Plasmid
PchA	forward	5'-AAT TAT ATA CAT ATG AGC CGG CTG GCG CCC CTG-3'	*NdeI*	pET29b
	reverse	5'-ATA ATA CAG ATC TGG GGC GAC GCC GCG CTG CAA GG-3'	*BglII*	
PchA/PchB	*pchA* -forward	5'-GGA ATT CGA TGA GCC GGC TGG CGC CCC TG-3'	*EcoRI*	pETDuet-1[1]
	pchA -reverse	5'-CCC AAG CTT TCA GGC GAC GCC GCG CTG-3'	*HindIII*	
	pchB -forward	5'-GGG AAT TCC ATA TGA AAA CTC CCG AAG ACT GC-3'	*NdeI*	
	pchB -reverse	5'-GAA GAT CTT CAT GCG GCA CCC CGT GTC-3'	*BglII*	
PchB/PchA	*pchB* -forward	5'-CAT GCC ATG GGC AAA ACT CCC GAA GAC TGC ACC-3'	*NcoI*	pETDuet-1[2]
	pchB -reverse	5'-ACG CGT CGA CTC ATG CGG CAC CCC GTG TC-3'	*SalI*	
	pchA -forward	5'-GGA ATT CCA TAT GAG CCG GCT GGC GCC CCT GA-3'	*NdeI*	
	pchA -reverse	5'-AAA ACT CGA GTC AGG CGA CGC CGC GCT GCA-3'	*XhoI*	
PchA	forward	5'-AAT TAT ATA CAT ATG AGC CGG CTG GCG CCC CTG-3'	*NdeI*	pET28b
	reverse	5'-CCC AAG CTT TCA GGC GAC GCC GCG CTG-3'	*HindIII*	
PchAt	forward	5'-GGA ATT CCA TAT GCA CGC CTT GCG CGG CAC C-3'	*NdeI*	pET28b
	reverse	5'-AAA ACT CGA GTC TAT GAG CTT CCC GCA TGG CAC-3'	*XhoI*	
Irp9	forward	5'-GGA ATT CCA TAT GAA AAT CAG TGA ATT TCT ACA C-3'	*NdeI*	pET29b
	reverse	5'-AAA ACT CGA GCA CCA TTA AAT AGG GCG CAA TG-3'	*XhoI*	
PchA K221A	forward	5'-GGG ACG CTT CGG CGC GGT CGT GCT GGC-3'	n.a.	pET28b-*pchA*
	reverse	5'-GCC AGC ACG ACC GCG CCG AAG CGT CCC-3'		
PchA E269A	forward	5'-GCG CCT CCC CGG CAC GCC GCC TCC G-3'	n.a.	pET28b-*pchA*
	reverse	5'-CGG ACC AGG CGT GCC GGG GAG GCG C-3'		
PchA D310E	forward	5'-GAC AGC GCC AAG GAG AGG CAC GAA CAC C-3'	n.a.	pET28b-*pchA*
	reverse	5'-GGT GTT CGT GCC TCT CCT TGG CGC TGT C-3'		
PchA A375T	forward	5'-GCA TCC GAC CCC CAC GGT GGG CGG CTA CC-3'	n.a.	pET28b-*pchA*
	reverse	5'-GGT AGC CGC CCA CCG TGG GGG TCG GAT GC-3'		

Restriction sites are highlighted in red; Mutated codon are highlighted in green.

[1]pETDuet-1 vector contains two multiple cloning sites (MCS). *pchA* and *pchB* were insterted into MCS1 and MCS2, respectively.

[2]*pchA* and *pchB* were insterted into MCS2 and MCS1, respectively

n.a.= not applicable

E. coli competent cells for protein overexpression.

irp9 Construct

irp9 gene was amplified by PCR from *Y. enterocolitica* (ATCC 9610) genomic DNA with the primer pair indicated (Table 3-2) and MasterMix (Eppendorf) with addition of 1.5 mM magnesium acetate solution provided. The amplified fragment was digested with *XhoI*/*NdeI* and ligated into the pET29b plasmid (Novagen). The desired plasmid encoded Irp9 (pET29b-*irp9*) with a C-terminal His_6 tag was confirmed by sequence analysis. This overexpression vector was then transformed into BL21 (DE3) *E. coli* cells for protein overproduction.

Protein Overexpression and Purification

C-terminal His_6-tag PchA

E. coli BL21 (DE3) cells harboring the pET29b-*pchA* construct were grown in Terrific Broth (TB) with 1% (v/v) glycerol and 50 μg/ml kanamycin at 37 °C, shaking at 225 × rpm. When the OD_{600} reached 0.6, the temperature was lowered to 18 °C for 30 min before induction. Protein expression was induced with the addition of IPTG to a final concentration of 0.2 mM. Incubation at 18 °C was continued for another 14 ~ 16 h. Cells were harvested by centrifugation (4,000 × g for 10 min at 4 °C) and resuspended in 25 mM Tris-HCl, pH 8.0, 500 mM NaCl (buffer A). The cells were disrupted by passing them through a French Press cell (35,000 psi) three times, and

cell debris was pelleted by centrifugation at 15,000 × g for 30 min at 4 °C. All of the following purification steps were performed at 4 °C. The lysate was applied to a chelating Sepharose Fast Flow column (Amersham) charged with Ni^{2+} and equilibrated with buffer A. PchA elution was carried out with a linear gradient of 5 mM – 300 mM imidazole in buffer A. Fractions containing PchA were combined and dialyzed against buffer 50 mM Tris-HCl pH 9.5, 1 mM EDTA, 10% glycerol (buffer B) overnight, which was followed by purification on Source 30Q (GE Healthcare) anion exchange chromatography. PchA eluted with a linear 0 – 500 mM NaCl gradient in buffer B. PchA fractions were identified by SDS-PAGE, pooled, concentrated, and further purified by a gel filtration column (HiLoad 16/60 Superdex 200) in 50 mM Tris-HCl, pH 8.0, 100 mM NaCl, 1mM DTT, 10% glycerol. The eluant peaks were analyzed on SDS-PAGE and PchA peak (52kDa) was pooled, concentrated, and stored at – 80 °C for future use.

N-terminal His_6-tag PchA and PchAt

Constructs pETDuet-1-*pchA/pchB*, pET28b-*pchA*, and pET28b-*pchAt* add a six-histidine tag to the N-terminal PchA and PchAt (a truncated PchA). The truncated PchA was generated by removal of flexible regions on both N- and C-termini according to the sequence alignment of PchA with Irp9 (Figure 3-6). *E. coli* cells with plasmid pETDuet-1-*pchA/pchB* were grown in LB broth containing 50 μg/ml with shaking at 225 rpm until the OD_{600} reached ~ 0.8. Protein expression was induced with an addition of IPTG to a final concentration of 0.2 mM for 3 hours. The cells

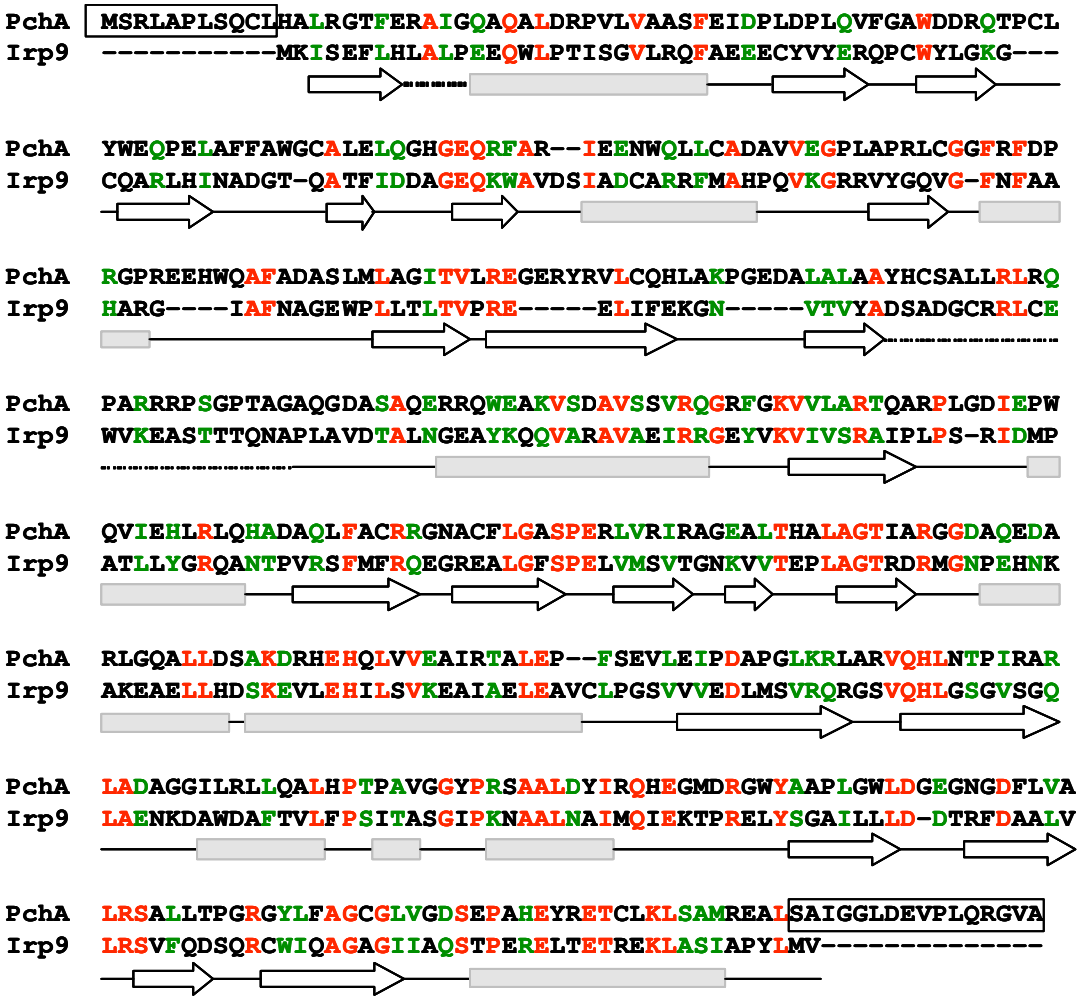

Figure 3-6: Sequence alignment of PchA and Irp9. Identical residues are in red, and similar residues are in green. PchA and Irp9 share 28% of sequence identity, and 47 % similarity. Secondary structure elements of Irp9 structure are shown: grey box, α-helix; white arrow, β-strand. Disorder loop in Irp9 is displayed as dotted lines. Loops are black lines. The amino acids highlighted in boxes are removed to generate a truncated PchA, referred as PchAt.

were pelleted by centrifugation (4,000 × g, 10 min, 4 °C) and resuspended in buffer, 25 mM Tris-HCl, pH 8.0, 500 mM NaCl. The purification steps were performed as described for C-terminal His_6-tag PchA.

Protein was overexpressed and purified from *E. coli* cells harboring plasmid pET28b-*pchA* or pET28b-*pchAt* conducted in a similar manner to C-terminal His_6-PchA with modifications. Six ml of overnight LB culture was inoculated in a 600 ml of TB medium containing 0.4% (v/v) glycerol and 50 μg/ml kanamycin in a 2L flask. Incubation was at 25 °C with shaking at 225 rpm until an OD_{600} of 0.4 was reached. Then temperature lowered to 20 °C with shaking at 225 rpm for another 12 ~ 14 h. The pellet were collected by centrifugation at 4,000 × g for 10 min at 4 °C and resuspended in buffer A1 (25 mM TrisHCl, pH 8, 500 mM KCl, 5 mM imidazole, 20% glycerol). The cells were disrupted with sonication. The first centrifugation was carried out at 15, 000 × g for 30 min. The supernatant was removed and saved for the later use. The pellet was resuspended with buffer A1 of same amount of supernatant and subjected to sonication again. This second debris was combined with the supernatant from first centrifugation and spun at 142, 000 × g for 1 h at 4 °C. The resulting supernatant was applied to a sepharose column charged with $NiCl_2$ and equilibrated in buffer A1. A step gradient of 15 mM, 45 mM, 150 mM and 300 mM imidazole in buffer A1 was applied to the column and the protein of interest eluted with 150 mM imidazole. Fractions were pooled and concentrated using an Amicon stirred cell with YM-30 membrane. Five ml of sample was applied to a HiLoad 16/60 Superdex 200 gel filtration column equilibrated with 50 mM TrisHCl, pH 8, 50 mM

KCl, 50 m Na Citrate, 10% glycerol. N-terminal His_6-PchA and His_6-PchAt were eluted as a monomer (~52kDa) from gel filtration column. The fractions containing protein of interest were pooled and concentrated by an Amicon stirred cell YM-30 or a Centriprep YM-30. The concentration of protein was determined by Bradford assay, and the purity was ~98%. The protein samples were kept at – 80 °C.

Un-His_6-tagged PchA

To obtain un-tagged PchA, *E. coli* BL21 (DE3) containing plasmid pETDuet-1-*pchB/pchA* was grown and collected as described for the construct pETDuet-1-*pchA/pchB*. Since *pchA* was inserted in MCS2 (multiple cloning site 2) of plasmid pETDuet-1-*pchB/pchA*, no His_6-tag was introduced to PchA. Purification was achieved by an anion exchange chromatography. The cell pellet was resuspended with buffer 20 mM TrisHCl, pH 8.5 and lysed by passing through French Press three times. The pellet was removed by centrifuging at 15, 000 × g at 4 °C for 30 min. The supernatant was applied to a Source 30Q anion exchange column equilibrated with 20 mM TrisHCl, pH 8. A linear gradient of 0 – 500 mM NaCl in 20 mM TrisHCl, pH 8 was applied to the column. The fractions were analyzed on SDS-PAGE for PchA.

The PchA protein without His-tag was also obtained by thrombin cleavage. The purified N-terminal His_6-PchA (expressed from pET28b-*pchA*) was incubated with thrombin in a ration of 2 units per mg PchA at room temperature for 2 h. The mixture was applied to nickel-charged column and eluted in the same manner as His_6-PchA purification on nickel column. The protein without His-tag flowed through the

column. Fractions containing PchA were pooled, concentrated, and further purified on gel filtration column in buffer 50 mM Hepes, pH 7.5, 150 mM NaCl, 10% glycerol.

PchA mutants

PchA mutants K221A, E269A, D310E and A375T were overexpressed, and purified in a two-step chromatography process, nickel affinity followed by gel filtration column as described for N-terminal His_6-PchA (pET28b-*pchA*).

Irp9 Overexpression and Purification

An overnight culture of BL21 (DE3) *E. coli* cells containing the Irp9 expression plasmid pET29b-*irp9* were inoculated to 1 liter LB medium with 50 μg/ml kanamycin. The cells were grown at 37 ºC with shaking at 225 × rpm to an OD_{600} of ~1.3. The temperature was then lowered to 18 ºC for 24 hr without IPTG induction. The cells were harvested by centrifugation. The pelleted cells were resuspended in 25 mM TrisHCl pH 8.0, 500 mM NaCl, 5 mM Imidazole (buffer A) and lysed by French Press (35, 000 psi). The cellular debris was removed by centrifugation (15,000 × g, 30 min, 4 °C) and supernatant was applied to a chelating Sepharose fast flow column charged with nickel chloride and pre-equilibrated in buffer A for nickel affinity chromatography. A step gradient of imidazole in buffer A was applied to the column and Irp9 protein eluted at 150 mM imidazole. The fractions containing Irp9 were pooled an applied to Superdex 200 size exclusion column equilibrated with 20 mM TrisHCl pH8.0, and 100 mM NaCl. After identification on SDS-PAGD, fractions

containing Irp9 were combined and concentrated with Centriprep (Millipore) YM-30.

Protein Determination

The protein concentration for all samples are determined by the method of Bradford with the Bio-Rad Protein Assay Dye Reagent. IgG was used as a standard.

Limited Proteolysis of PchA

To determine areas of PchA susceptible to proteolysis, PchA was treated with a variety of proteases, including trypsin, subtilisin, chymotrypsin, proteinase K, papain, and thrombin. PchA was incubated with each protease at 4 ^{o}C and room temperature (22 ^{o}C). The mixture (100 µl) contained 50 µg PchA and 0.5 µg protease in the cleavage buffer: 20mM TrisHCl, pH 7.8, 50 mM NaCl, 1 mM DTT, 5 mM $CaCl_2$ for trypsin, chymotrypsin, and subtilisin; 20mM TrisHCl, pH 7.8, 50 mM NaCl, 1 mM DTT for papain and proteinase K; 20 mM TrisHCl, pH 8.0, 100 mM NaCl for thrombin. Samples were collected at 5, 15, 30, 60, 120, and 240 min. Each sample was subjected to SDS-PAGE for analysis of the extent of cleavage.

3.2.2 Steady-State Kinetic Studies

Mg^{2+} Dependence of PchA activity

MST family are Mg^{2+}-dependent enzymes. The ICS activity of PchA was measured under a variety of divalent cation conditions using a coupled assay. The assay is required 20-fold excess of PchB to convert isochorismate made by PchA to

salicylate, which can be measured fluorescently.[7] The standard reaction mixture (200 µl) contained 50 mM TrisHCl, pH 7.5, 10% glycerol, 1 mM DTT, 10 µM PchA, 200 µM PchB, and 1 mM chorismate. To determine which divalent cations can support PchA activity, the standard reaction mixture without chorismate was preincubated with 1 mM EDTA for 10 min at room temperature followed by addition of 1 mM chorismate to initiate the reaction. Salicylate accumulation was monitored with an excitation wavelength of 300 nm and emission wavelength of 430 nm for 5 min. Ten mM $MgCl_2$, $CaCl_2$, $NiCl_2$, or $CoCl_2$ was added to each reaction with 1 mM EDTA, and salicylate formation was measured. Data were plotted with KaleidaGraph.

Steady-State Kinetics of PchA and Mutants

Coupled Isochorismate Synthase Measurement

The assay used to measure the steady-state kinetics of PchA and its mutant is coupled with 20-fold excess of PchB to convert isochorismate to salicylate and evaluate PchA ICS activity.[7] The reaction buffer for ICS contained 50 mM TrisHCl, pH 7.5, 10 mM $MgCl_2$, 1 mM DTT, and 10 % glycerol. The steady-state kinetic assays on wild type PchA were performed with 0.5 µM PchA and 10 µM PchB in the reaction buffer (100 µl) with chorismate concentration varying from 0.5 to 500 µM. The steady-state kinetic assays on mutants were performed with 1 µM PchA mutant enzyme and 20 µM PchB in the reaction buffer (100 µl) with chorismate concentration varying from 2 to 200 µM. Salicylate, a product of the coupled assay was measured by its fluorescence with an excitation of 300 nm and an emission of

430 nm. The amount of salicylate formed was determined from a salicylate standard curve with varied concentration of 0 – 80 μM salicylate in the reaction buffer. Kinetic constants V_{max}, K_m and k_{cat} were calculated from Michaelis-Menten equation using KaleidaGraph.

Chorismate Mutase Measurement

The CM activity on PchA mutant D310E was performed by the method described[10] at room temperature. The reaction mixture (400 μl) contained 50 mM TrisHCl, pH 7.5, 10 mM $MgCl_2$, 1 mM DTT, 10% glycerol, 50 μM D310E and chorismate with concentration varied between 0.1 and 5 mM. The reactions were initiated by the addition of chorismate. Every 15 seconds, 40 μl of reaction mixture was taken out and mixed with 20 μl 1M HCl to terminate the reaction. The reaction product prephenate was then converted to phenylpyruvate by incubation at 37 °C for 20 min. Phenylpyruvate concentration was determined at 320 nm under basic condition by the addition of 140 μl of 2.5 M NaOH (ε_{320} = 17,500 M^{-1} cm^{-1})[10] on a UV spectrophotometer. Steady-state kinetic parameters were derived from the initial velocities of prephenate accumulation with KaleidaGraph.

3.2.3 pH dependence of PchA catalysis

To determine the pH dependence of PchA catalysis, the k_{cat} and K_m of PchA ICS reaction was measured over a range of pH values. A multi-component buffer was used to cover the pH range of 6.0 through 9.5 and minimize buffer and ionic strength

effects. This buffer contains 50 mM MES, 25 mM Tris, 25 mM ethanolamine, 100 mM NaCl, named 1 × MTEN.[14] The kinetic assays were conducted in 1 × MTEN with varied pHs, 10 mM $MgCl_2$, 1 mM DTT, 10% glycerol, 0.5 μM PchA, 10 μM PchB. The following measurements and data analysis were performed in a identical manner as described in the *Coupled Isochorismate Synthase Measurement* section. Plots of log k_{cat} were generated with KaleidaGraph.

3.2.4 Protein Crystallization

Buffer Optimization

Dynamic Light Scattering (DLS)

Before DLS measurements, centrifugation of 30 min at 15, 000 × g in a table-top microcentrifuge was carried out to obtain a sample that is free of any dust or other particles. Protein samples used were at a concentration of ~ 1mg/ml in various buffer. The DLS data were recorded in a quartz cuvette with a light path of 5 mm using a PD2000 DLS (Precision Detectors). Five readings were recorded for each sample. Each reading was the average of 60 accumulated data points.

Solubility Screen

Protein solubility screens were carried out as described by Isaac *et al.*[15] with some modifications. 150 μl protein sample (~ 5 mg/ml) was incubated with 190 μl 40% PEG 8,000 at room temperature for 20 min, which precipitated protein from solution. The protein suspension was aliquoted to 18 μl followed by addition of 2 μl

buffer, salt or additive to a final concentration of 100 mM salt, 10% glycerol, or 1 mM EDTA. The mixture was incubated at room temperature for 20 min to allow for resolubilization of the protein. After centrifugation at 14, 000 rpm for 30 min, the 10 μl of supernatant was mixed with 1ml of 1 × Bio-Rad Protein Assay Dye and the absorbance at 595 nm was measured.

Protein Crystallization

Standard Crystallization

Protein crystallization was performed using hanging-drop, sitting-drop and sandwich-drop vapor diffusion methods and incubated at room temperature, 18 ºC or occasionally 4 ºC. The drop size is normally 3 μl with a protein to reservoir solution ratio of 1 to 1, 1 to 2, or 2 to 1 (v/v). The protein samples subjected to crystallization trials were either apo-, mixed with substrate or PchB.

Optimization

After initial screens, the crystallization hits would be subjected to cycles of optimization to improve the quality of initial crystals. Several standard optimization approaches were performed in this chapter.[16]

The first attempt was to refine around the initial successful condition with an increment matrix, such as pH versus salt, salt versus precipitant *etc*. Then temperature of crystallization would be optimized at 4, 11, 18, and 25 °C. A various additives can also introduce into crystallization condition. Table 3-3 listed the additives used in this

Table 3-3: Additives for crystallization optimization. (Adapted from Hampton Research)

Additive	Class
0.1M Cadmium chloride hydrate	Multivalent
0.1M Calcium chloride dihydrate	Multivalent
0.1M Cobalt(II) chloride hexahydrate	Multivalent
0.1M Magnesium chloride hexahydrate	Multivalent
0.1M Iron(III) chloride hexahydrate	Multivalent
0.1M Nickel(II) chloride hexahydrate	Multivalent
1.0M Ammonium sulfate	Salt
1.0M Potassium chloride	Salt
1.0M Lithium chloride	Salt
2.0M Sodium chloride	Salt
0.5M Sodium fluoride	Salt
1.0M Sodium iodide	Salt
0.1M Strontium thiocyanate	Salt
1.0M Sodium potassium tartrate dihydrate	Salt
1.0M Sodium citrate tribasic dihydrate	Salt
1.0M Cesium chloride	Salt
1.0M Sodium malonate pH 7.0	Salt
0.1M L-Proline	Amino Acid
30% v/v Dimethyl sulfoxide	Dissociating Agent
1.0M Glycine	Linker
0.3M Gly-Gly	Linker
0.1 M Taurine	Linker
0.1 M Betaine	Linker
1.0 Guanidine hydrochloride	Chaotrope
0.1 M Urea	Chaotrope
0.1 M TCEP hydrochloride	Chaotrope
0.1 M EDTA disodium salt dihydrate	Chelating Agent
5% w/v Polyvinylpyrrolidone K15	Polymer
10% w/v Polyethylene glycol 3,350	Polymer
30% w/v D-(+)-Glucose	Carbohydrate
30% w/v Sucrose	Carbohydrate
30% w/v D-(+)-Galactose	Carbohydrate
30% Ethylene glycol	Polyol
50% w/v PEG 400	Organic, Non-volatile
50% v/v Jeffamine M-600 pH 7.0	Organic, Non-volatile
40% v/v 1,6-Hexanediol	Organic, Non-volatile
30% v/v Ethanol	Organic, Non-volatile
30% v/v Methanol	Organic, Non-volatile
40% v/v 1,4-Butanediol	Organic, Non-volatile
40% v/v Acetonitrile	Organic, Non-volatile
1.0 M Sodium tartrate	Salt
40% v/v 1-Propanol	Organic, Non-volatile
30% Glycerol	
7% v/v 1-Butanol	Organic, Non-volatile
5% Ethyl acetate	Organic, Non-volatile
40% Acetone	Organic, Non-volatile

chapter. Alternate diffusion methods were conducted, including sitting-drop, sandwich-drop vapor diffusion methods. Seeding experiments including microseeding and macroseeding were also performed as described using ball-shaped PchA crystals (in sodium formate, pH 7.0) as seeds.[17]

3.3 Results and Discussion

Protein Production

Various constructs of PchA, such as N-terminal His_6, C-terminal H_6 PchA, PchA without tags, truncated PchAt were generated to improve yields of protein expression and produce suitable sample for crystallization experiments. Each protein was subjected to gel filtration as the last step of purification, which suggested that PchA is a monomer (52 kDa) in solution. Irp9 eluted as a dimer from gel filtration column which is consistent with published data.[8] PchA mutants K221A, E269A, D310E, and A375T have a superimposable elution profile of gel filtration to wild type (Figure 3-7), which suggested that single active site mutation acts as monomer in solution without causing oligomerization. The yield of PchA was improved from ~ 10 to 100 mg per liter of culture after a series of optimizations of *E. coli* growth conditions, protein expression conditions (such as temperature, IPTG concentration, and post-induction time), and buffers for chromatography. The best conditions determined so far can be applied to the constructs that use pET28b as a vector for PchA, which are summarized in Table 3-4. The purity of each PchA variant was determined to ~98% by SDS-PAGE.

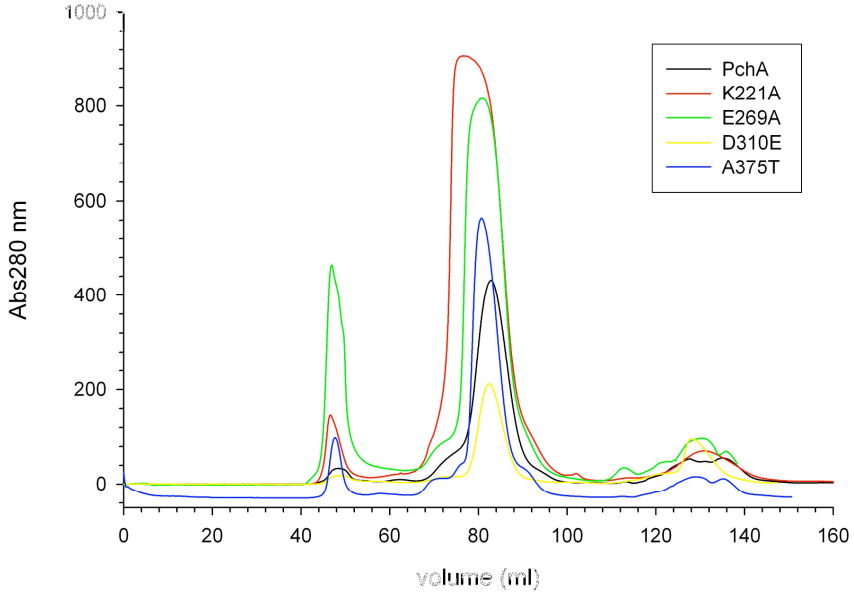

Figure 3-7: Superposition of wild type and mutants PchA elution profiles from Superdex 200 gel filtration chromatography. The elution volume at ~ 80 ml corresponds to a protein with a molecular weight of 52 kDa as PchA.

Table 3-4: Optimized conditions for PchA over-production and purification

Protein over-production	
Medium	Terrific broth with 0.4 % glycerol
Pre-induction temperature	25 °C
OD_{600} at induction	0.3 ~ 0.4
IPTG concentration	0 mM
Post-induction temperature	20 °C
Incubation time after induction	12 ~ 14 hours
Protein preparation for chromatography	
- Resuspend cell pellet in Buffer A1 - Lyse cells by sonication - Spin 1st lysate by regular spin (14, 000 rpm, 30 min, 4 °C) - Save supernatant and resuspend pellet in buffer A1 - Lyse sample by sonication - Combine 2nd lysate with 1st supernatant - Ultracentrifuge with 35,000 rpm, 1 h, 4 °C	
Protein purification	
Buffer A1 (for resuspending cells and Nickel column)	25 mM TrisHCl, pH8.0, 500 mM KCl, 5 mM imidazole, 20% glycerol
Buffer B (Nickel column)	25 mM TrisHCl, pH8.0, 500 mM KCl, 300 mM imidazole, 20% glycerol
Nickel Step Elution	- 10 % buffer B, 5 CV - 15 % buffer B, 5 CV - 50 % buffer B, 6 CV
Buffer for gel filtration	50 mM TrisHCl, pH8.0, 50 mM KCl, 50 mM Na Citrate, 10% glycerol

CV: column volume

Limited proteolytic analysis was conducted on PchA to identify flexible region on the protein, which might be a reason that interferes protein crystallization. If a small region on PchA could be removed after proteolysis, then the protein would be re-cloned to remove the regions and crystallization trials would be performed. Six proteases were tested and the aliquots from different time points were analyzed on SDS-PAGE. The goal was to determine if small region can be cleaved off from PchA without complete degradation. All proteases tested, including trypsin, subtilisin, chymotrypsin, proteinase K, papain, and thrombin, resulted in large degradation products with complete formation of small fragments on SDS-PAGE (data not shown), which was unsuitable for continued experiments.

Mg^{2+}-Dependence of PchA Catalysis

PchA homologs MenF and Irp9 require Mg^{2+} to align substrate and allow for catalysis to happen. Mg^{2+} is also evident in the structures of MenF and Irp9. To determine if Mg^{2+} is also required for PchA activity, 1 mM EDTA was pre-incubated with PchA reaction mixture. PchB is not a metal dependent enzyme; therefore the divalent cation condition would not affect the conversion of isochorismate to salicylate by PchB in the coupled reaction. The salicylate fluorescence was recorded over 5 min (Figure 3-8). The EDTA pre-treated sample did not have detectable salicylate formation over 5 min, indicating that PchA was not capable of making isochorismate from chorismate in the absence of Mg^{2+}. Various divalent cations were added to the EDTA pre-treated reaction mixture to determine which one could restore

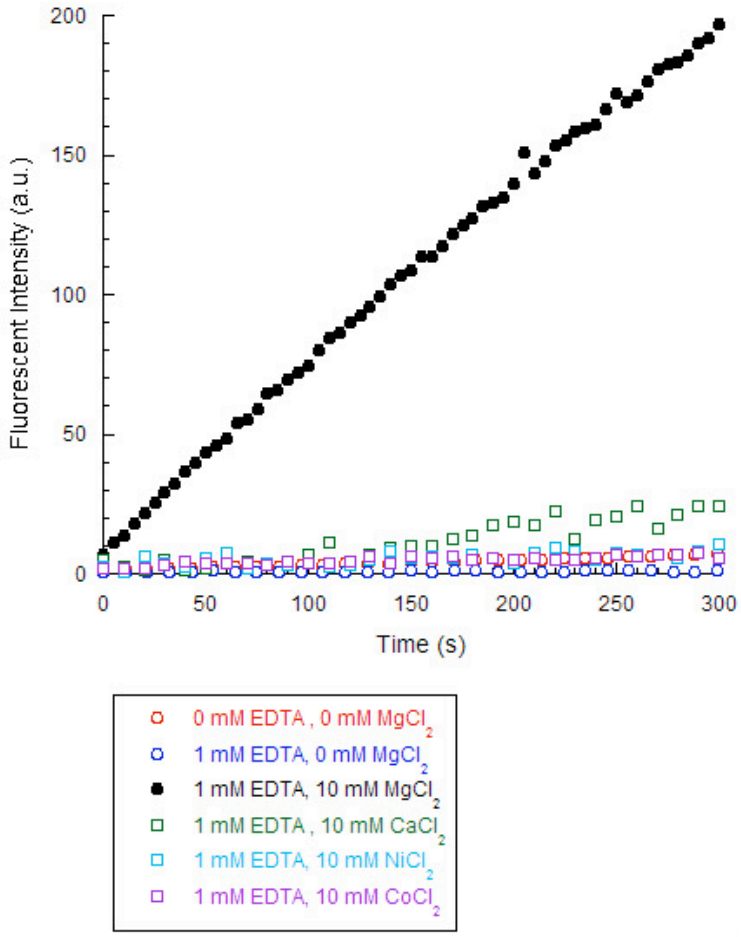

Figure 3-8: Mg^{2+}- dependence of PchA catalysis.

salicylate formation. Four divalent cations were examined: $MgCl_2$, $CaCl_2$, $NiCl_2$, and $CoCl_2$ with a final concentration of 10 mM in the reaction solution. $MgCl_2$ fully restores the catalytic function of PchA with an increase of ~ 200 a.u fluorescent intensity in 5 min. $CaCl_2$ restores a trace of catalysis, likely because its size and chemical properties are similar to Mg^{2+}. The data support that PchA requires Mg^{2+} to gain fully function.

Steady-State Kinetics

PchA isochorismate activity was measured using a coupled assay with PchB.[7] Since conversion of chorismate to isochorismate is the limiting step during this two-step process to produce salicylate, addition of 20-fold excess of PchB ensures all isochorismate is immediately converted to salicylate. Therefore, the kinetic measurement could represent the catalysis from PchA. In the reaction, 10 mM $MgCl_2$ was added to achieve fully active PchA.[7] The fluorescence of accumulated salicylate was recorded over 2 min with excitation wavelength of 300 nm and emission wavelength of 430 nm. To gain insight into the mechanism of PchA, four active site single mutations were constructed and purified for kinetic studies: K221A, E269A, A375T, and D310E.

Isochorismate differs from chorismate by the location of the hydroxyl group. It was proposed by Liu *et al.*[18] that the hydroxyl group of isochorismate came from water. A nucleophile from enzyme would facilitate the attack of water on C2 of chorismate. Later on, structures of MenF (K190) and Irp9 (K193) supported this idea

by trapping a water molecule in their active sites with a Lys nearby (Figure 3-2b, and 3-4b). However, mutation of K190A in MenF had no activity.[2] Lysine is a conserved residue in MST family and hence considered as a general base that helps with nucleophilic addition of water to C2-chorismate. We hypothesized that the corresponding K221 is the general base for PchA catalysis. The replacement of Lys by Ala in PchA results in an inactive enzyme (Table 3-5), which is consistent with result from homolog MenF. PchA catalysis is dependent on K221 that may be serve as the general base.

Glu is another conserved amino acid found in proximity to ligands in the active sites of MenF (E240) and Irp9 (E240). The mutations of E240A in Irp9 and E240Q in MenF led to complete loss of catalytic efficiencies.[2,4] This residue is in a position to interact with the C4-OH of chorismate, promoting departure of the hydroxyl group from C4 by serving as a general acid.[4] In PchA, the corresponding amino acid is Glu269. Mutation of E269 in PchA to Ala results in an inactive enzyme (Table 3-5), which suggests that Glu is required for catalysis at this position probably acting as the general acid. Further experiment of pH dependence of PchA catalysis was carried out to confirmed this reaction mechanism, which will be discussed later on.

As shown in Figure 3-5, Ala375 in PchA is conserved in ICS enzymes, whereas a Thr resides at this position in salicylate synthases. The backbone carbonyl group of Thr348 in Irp9 H-bonds to hydroxyl group of salicylate. It was suggested that this H-bond may be important to orient the isochorismate intermediate in salicylate synthase, leading to an IPL activity. One can suppose that change of Ala into Thr in ICS might

Table 3-5: PchA isochorismate synthase activity

	K_m (μM)	k_{cat} (min^{-1})	k_{cat} / K_m ($M^{-1}s^{-1}$)	% WT (k_{cat} / K_m)
Wild type	1.3 ± 0.03	3.3 ± 0.1	42000	100
K221A	n.a.	n.a.	-	-
E269A	n.a.	n.a.	-	-
A375T	120 ± 3	0.48 ± 0.01	69	0.16
D310E	2.2 ± 0.2	2.4± 0.1	18000	43

n.a. = no activity; n = 3

give rise to IPL activity in these enzymes. However, mutation of Ala344 into Thr in MenF did not result in gain of IPL activity but instead produced inactive enzyme.[2] The corresponding residue in PchA was mutated to Thr (A375T). The mutation decreases the ICS activity (k_{cat}/K_m) by ~ 600-fold with ~ 90-fold increase in K_m and ~ 7-fold decrease in k_{cat} (Table 3-5). The large decrease in catalytic efficiency was mainly due to increase in K_m, likely resulting from an slight alteration in active site architecture that lowers the substrate affinity and orientation.

Mutant D310E

Asp (D310 in PchA) is the second nonconserved amino acid (Figure 3-5), which is changed to Glu in salicylate synthase. The role of Glu is to coordinate Mg^{2+} through water. The shorter Asp in PchA may cause a shift of Mg^{2+} toward D310 in the active site and thus slightly shift the site of catalysis relative to the active site in salicylate synthase. We hypothesized that this change in active site could be the cause of loss of IPL activity in PchA. By replacing this Asp at the position 310 with Glu, the IPL activity may be created.

PchA D310E shows a reduction in ICS catalytic efficiency by ~ 60% (Table 3-5). To determine if this mutation has IPL activity, a reaction was performed in a similar manner as the coupled ICS assay in the absence of PchB. Salicylate formation was detected, indicating the recurrence of IPL activity in D310E. Chorismate mutase activity was also observed by measuring prephenate formation. The kinetic parameters for ICS and CM reactions catalyzed by D310E are summarized in Table

3-6. The catalytic efficiency for ICS is dominant over CM activity by ~ 3×10^3-fold in D310. Therefore, chorismate can bind to D310E in two orientations with formation of isochorismate (ICS) preferred over prephenate (CM). The K_m for ICS activity (2.2 μM) is much smaller than the K_m for CM activity (1521 μM) and the ICS reaction rate is ~5-fold fasted than the CM rate. The IPL activity of D310E is proposed to perform the pericyclic reaction in the same way as PchB does.

pH Profile of PchA

In order to examine the required protonation state of the reactive group and the acid base mechanism, the preliminary pH rate profiles of the kinetic parameter k_{cat} was determined over the pH range of 6 to 9.5 as shown in Figure 3-9. The reaction rate catalyzed by PchA decreases at both low and high pH with the highest rate at pH ~ 7.5. The bell-shaped pH curve indicates that two possible ionization groups relate to the reaction rate, one group getting protonated and the other getting deprotonated for maximal activity. One candidate is K221 as the general base activating water that acts as nucleophile attacking C2-chorismate. The other is E269 as the general acid to facilitate the removal of C4-OH on chorismate. pK_a for the two ionizable groups involved in catalysis can be obtained from inflection points in the graph of log k_{cat} versus pH and log (k_{cat}/K_m) versus pH using the equation described by Cook and Cleland.[19] In order to demonstrate the general acid and base reaction mechanism, the solvent deuterium isotope effects on isochorismate formation catalyzed by PchA wild type and mutants can be measured, which will indicate if the proton-transfer is

Table 3-6: D310E kinetics parameters

Activity	K_m (μM)	k_{cat} (min^{-1})	k_{cat} / K_m ($M^{-1}s^{-1}$)
WT PchA ICS	1.3 ± 0.03	3.3 ± 0.1	42000
D310E ICS	2.2 ± 0.2	2.4± 0.1	18000
D310E CM	1521 ± 469	0.48 ± 0.03	5.3

n=3

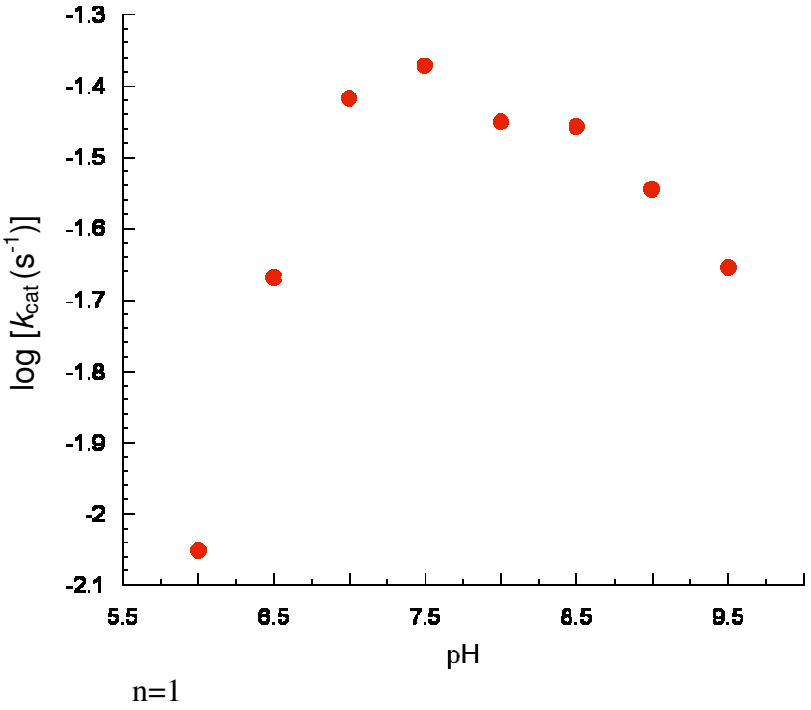

Figure 3-9: The pH dependence of the PchA reaction rate. PchA exhibits the highest reaction rate when the pH is 7.5. This preliminary pH curve is bell-shaped, indicating two ionization processes taken place during PchA catalysis. This data suggests the general acid and base catalysis conducted by PchA to convert chorismate to isochorismate.

rate-limiting. The results from mutagenesis, and preliminary pH-dependence of PchA kinetic parameters suggest that both K221 and E269 are critical for catalysis, most likely as the general base and acid.

PchA Crystallization

Buffer Optimization Screen

To improve PchA protein solubility for purification and crystallization, a buffer optimization screen was performed as described.[15] Protein precipitated by 40% PEG 8000 was resolubilized by the addition of 100 mM buffer, 100 mM salts, 10% glycerol, 1 mM DTT, 1 mM EDTA, respectively. Water was used as a blank. Additives promoting higher protein solubility would correspond to a larger absorbance reading at 595 nm. Results are summarized in Figure 3-10 for PchA and Figure 3-11 for PchAt. According to those results, buffer components were selected for different purification steps to achieve best outcome. Buffers for PchA purification are described in Table 3-4.

Crystallization Trials

To gain insight into the PchA mechanism for catalysis, we attempt to solve the atomic atomic structure of PchA by crystallography. Therefore, crystallization of PchA and mutants were carried out in this section. The crystallization screens that have been performed for PchA and truncated PchAt are summarized in Table 3-7. Among all the trial done, only one gave a positive result, which was crystallized in

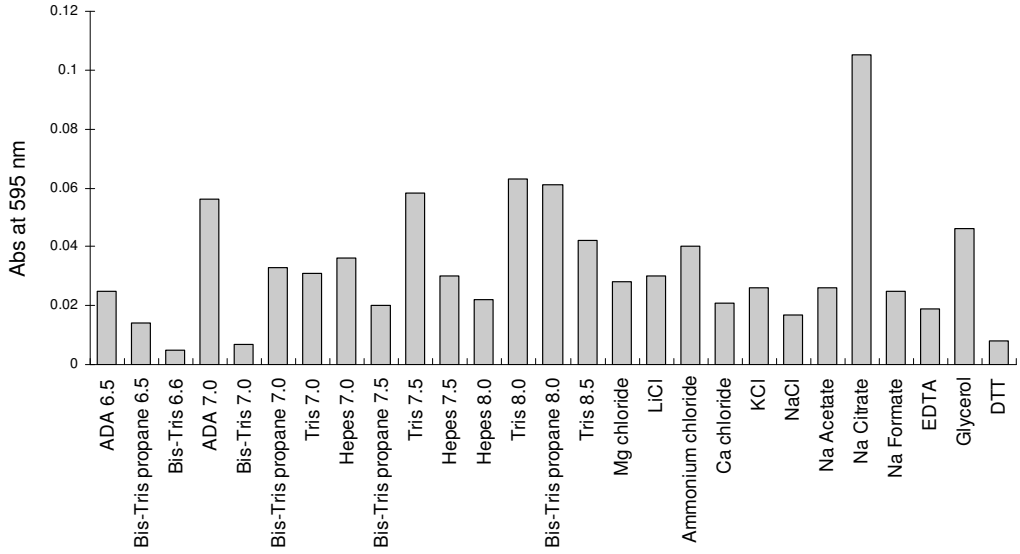

Figure 3-10: PchA buffer optimization screen.

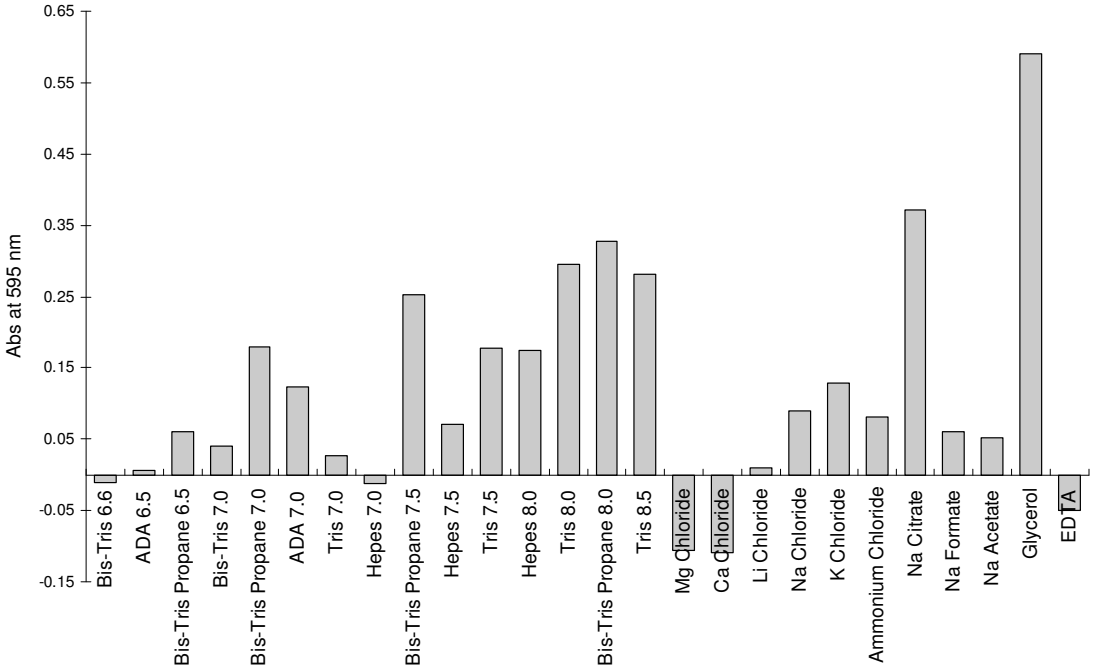

Figure 3-11: PchAt buffer optimization screen.

Table 3-7: Summary of PchA and PchAt initial matrix crystallization screens

Protein	Protein buffer	Additive/ other	Temp (°C)	Screens						
				Index™	SaltRx™	Crystal Screen™	Crystal Screen 2™	PEG/Ion Screen™	Wizard I	Wizard II
PchA 18 mg/ml	50mM Tris, pH8, 100 mM Nacl, 1 mM DTT, 10% Glycerol	None	25	×	×	×	×	×		
PchA 7 mg/ml	50 mM Hepes pH 7.5, 10 mM MgCl2, 1 mM DTT, 10 % Glycerol	None	25	×	×	×	×	×		
PchA 12 mg/ml	50 mM Tris pH 7.5	Chorismate	25	×	×	×	×	×	×	×
PchA 11 mg/ml	50mM Hepes pH 7.5,, 150 mM Nacl, 1 mM DTT, 10% Glycerol	PchB	25	×	×	×	×	×	×	
PchA (no His-tag) 17 mg/ml	50 mM Hepes pH 7.5, 150 mM NaCl, 10% Glycerol	None	25	×	×	×	×	×		
PchA (no His-tag) 10 mg/ml	50 mM Bis-Tris Propane, pH7.0, 150 mM NaCl	None	25	×	×		×	×		
PchA (no His-tag) 15 mg/ml	50 mM Tris pH 8.0, 150 mM NaCl	None	25	×	×	×	×	×	×	×
PchA 14 mg/ml	50 mM Hepes pH 7.5, 0.5 mM Na Formate, 1 mM DTT, 10% Glycerol	None	18	×	×	×	×	×		

Continued

Protein	Protein buffer	Additive/ other	Temp (°C)	Screens						
				Index™	SaltRx™	Crystal Screen™	Crystal Screen 2™	PEG/Ion Screen™	Wizard I	Wizard II
PchAt 14 mg/ml	50 mM ADA pH 7.0, 100 mM Na Citrate	None	25	×		×	×	×		
PchAt 17 mg/ml	50 mM Tris pH8.0, 100 mM Na Citrate, 10 % Glycerol	None	18	×	×	×	×	×		
PchAt (no His-tag) 12 mg/ml	50 mM Tris pH8.0, 100 mM Na Citrate, 10 % Glycerol	None	18	×	×	×	×	×	×	×
PchAt 18 mg/ml	50 mM Tris pH8.0, 100 mM Na Citrate, 10 % Glycerol	Salicylate & Pyruvate	18	×	×	×	×	×	×	×

×: screen performed.

3.5 M sodium formate, pH 7.0 from the initial matrix Index™ (Hampton Research) (Figure 3-12). A series of optimization cycle were conducted to change the morphology of this crystal, which all failed to change this ball-shaped crystal.

Irp9 Crystallization and Data Collection

Irp9, a PchA homolog, is the salicylate synthase in *Y. enterocolitica.* The goal was to solve the structure of Irp9 that would serve as a research model for PchA. The Irp9 clone was constructed, and the protein over-produced and purified. The activity assay suggested that Irp9 was capable of making salicylate from chorismate (data not shown). Initial matrix screens were conducted on Irp9, in which four conditions successfully gave rise to crystals. After optimization by fine increments, diffraction quality Irp9 crystals were obtained (crystallized in 0.1M TrisHCl, pH 8.0, 0.16 M $CaCl_2$, 13% PEG 3350) (Figure 3-13 inset). Native diffraction images were collected in the Protein Structure Lab at the University of Kansas. A single diffraction image is shown in Figure 3-13. The crystal diffracts to 2.55 Å. Data collection statistics are summarized in Table 3-8. However, at this point in our studies Kerbarh *et al.*[4] published the Irp9 structure. Comparision of our data to theirs revealed many similarities. The Irp9 eluted from gel filtration as a homodimer in our experiment in agreement with their structure of homodimer per asymmetric unit. Both have the same space group of $P2_1$. Our unit cell was with a = 56.69 Å, b = 161.26 Å, c = 58.93 Å, whereas with a = 56.74 Å, b = 145.67 Å, c = 58.81 Å in theirs.

In summary, we have demonstrated that PchA catalyzes isochorismate

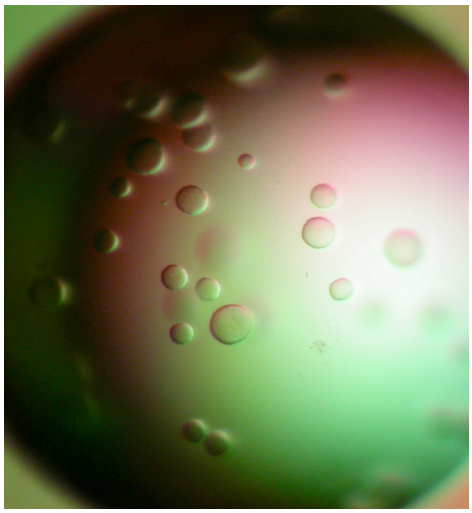

Figure 3-12: PchA crystallized in sodium formate, pH 7.0. The crystal was demonstrated as a protein crystal by blue dye and crushing techniques. The morphology of this ball-shaped crystal was not improved after a variety of crystallization optimization attempts.

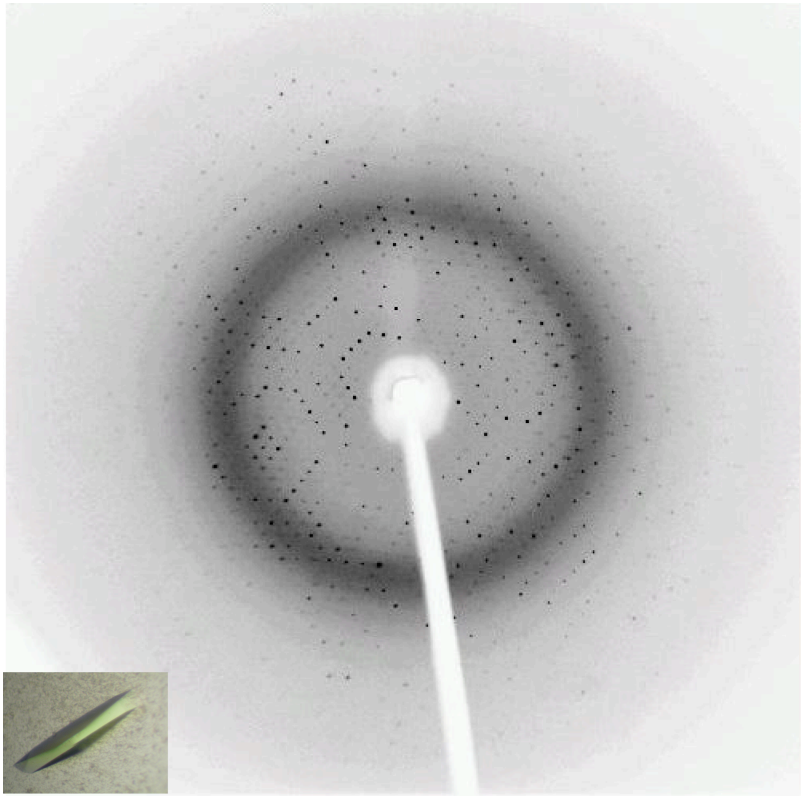

Figure 3-13: A diffraction image of Irp9. The inset of this figure is the Irp9 crystal subjected for data collection. This crystal diffracts to 2.5 Å.

Table 3-8: Data collection statistics

		Apo Irp9
Rsolution Range (Å)		50-2.55
Space Group		$P2_1$
Unit Cell (Å)		a = 56.69, b = 161.26, c = 58.93
		$\alpha = \gamma = 90°$, $\beta = 109.66°$
Obsrvations		
	Unique	23, 951
	Total	58, 296
Completeness (%)*		87.0 (73.8)
R_{sym} %		12.6 (39.9)
% $I > 3\sigma$		67.8 (46.5)

*Values in parentheses are for the highest resolution shell (2.64-2.55 Å)

formation by a general acid and base mechanism, in which Lys 221 and Glu 269 play roles as the general base and general acid, respectively, during catalysis. Our work also established a novel salicylate synthase from a isochorismate synthase by a single amino acid substitution on PchA. The mutant enzyme D310E will further our understanding of chorismate-utilizing enzymes.

References

1. He, Z., Stigers Lavoie, K.D., Bartlett, P.A. & Toney, M.D. Conservation of mechanism in three chorismate-utilizing enzymes. *J Am Chem Soc* **126**, 2378-85 (2004).
2. Kolappan, S. et al. Lysine 190 is the catalytic base in MenF, the menaquinone-specific isochorismate synthase from Escherichia coli: implications for an enzyme family. *Biochemistry* **46**, 946-53 (2007).
3. Spraggon, G. et al. The structures of anthranilate synthase of Serratia marcescens crystallized in the presence of (i) its substrates, chorismate and glutamine, and a product, glutamate, and (ii) its end-product inhibitor, L-tryptophan. *Proc Natl Acad Sci U S A* **98**, 6021-6 (2001).
4. Kerbarh, O., Chirgadze, D.Y., Blundell, T.L. & Abell, C. Crystal structures of Yersinia enterocolitica salicylate synthase and its complex with the reaction products salicylate and pyruvate. *J Mol Biol* **357**, 524-34 (2006).
5. Harrison, A.J. et al. The structure of MbtI from Mycobacterium tuberculosis, the first enzyme in the biosynthesis of the siderophore mycobactin, reveals it to be a salicylate synthase. *J Bacteriol* **188**, 6081-91 (2006).
6. Parsons, J.F., Shi, K.M. & Ladner, J.E. Structure of isochorismate synthase in complex with magnesium. *Acta Crystallogr D Biol Crystallogr* **64**, 607-10 (2008).
7. Gaille, C., Reimmann, C. & Haas, D. Isochorismate synthase (PchA), the first and rate-limiting enzyme in salicylate biosynthesis of Pseudomonas aeruginosa. *J Biol Chem* **278**, 16893-8 (2003).
8. Kerbarh, O., Ciulli, A., Howard, N.I. & Abell, C. Salicylate biosynthesis: overexpression, purification, and characterization of Irp9, a bifunctional salicylate synthase from Yersinia enterocolitica. *J Bacteriol* **187**, 5061-6 (2005).
9. Buss, K. et al. Clustering of isochorismate synthase genes menF and entC and channeling of isochorismate in Escherichia coli. *Biochim Biophys Acta* **1522**, 151-7 (2001).
10. Gaille, C., Kast, P. & Haas, D. Salicylate biosynthesis in Pseudomonas aeruginosa. Purification and characterization of PchB, a novel bifunctional enzyme displaying isochorismate pyruvate-lyase and chorismate mutase activities. *J Biol Chem* **277**, 21768-75 (2002).
11. Dosselaere, F. & Vanderleyden, J. A metabolic node in action: chorismate-utilizing enzymes in microorganisms. *Crit Rev Microbiol* **27**, 75-131 (2001).
12. Thompson, J.D., Higgins, D.G. & Gibson, T.J. CLUSTAL W: improving the sensitivity of progressive multiple sequence alignment through sequence weighting, position-specific gap penalties and weight matrix choice. *Nucleic Acids Res* **22**, 4673-80 (1994).
13. Zwahlen, J., Kolappan, S., Zhou, R., Kisker, C. & Tonge, P.J. Structure and mechanism of MbtI, the salicylate synthase from Mycobacterium tuberculosis. *Biochemistry* **46**, 954-64 (2007).

14. Yanchak, M.P., Taylor, R.A. & Crowder, M.W. Mutational analysis of metallo-beta-lactamase CcrA from Bacteroides fragilis. *Biochemistry* **39**, 11330-9 (2000).
15. Izaac, A., Schall, C.A. & Mueser, T.C. Assessment of a preliminary solubility screen to improve crystallization trials: uncoupling crystal condition searches. *Acta Crystallogr D Biol Crystallogr* **62**, 833-42 (2006).
16. McPherson, A. *Crystallization of biological macromolecules*, (1998).
17. Bergfors, T. Seeds to crystals. *J Struct Biol* **142**, 66-76 (2003).
18. Liu, J., Quinn, N., Berchtold, G.A. & Walsh, C.T. Overexpression, purification, and characterization of isochorismate synthase (EntC), the first enzyme involved in the biosynthesis of enterobactin from chorismate. *Biochemistry* **29**, 1417-25 (1990).
19. Cook, P.F. & Cleland, W.W. *Enzyme Kinetic and Mechanism*, (2007).

CHAPTER 4

High Throughput Screening of Inhibitors of Salicylate Synthesis in *Pseudomonas aeruginosa*

4.1 Introduction

Salicylate serves as a precursor for biosynthesis of some siderophores, including pyochelin in *P. aeruginosa*, yersiniabactin in *Yersinia* spp., mycobactin in *M. tuberculosis*. Chorismate is converted to salicylate either via a two-step process by PchA and PchB in *P. aeruginosa*, or via a single step by salicylate synthase enzymes in *Yersinia* spp. and *M. tuberculosis*. Derived from shikimate pathway, chorismate is the general precursor for a wide variety of other aromatic metabolites critical for bacteria and fungi growth, such as aromatic amino acids phenylalanine, tyrosine, and tryptophan; folate; ubiquinones; and menaquinones. These chorismate-utilizing pathways are attractive targets for the development of antimicrobial drugs because there are no similar pathways present in humans. Conversion of chorismate to various intermediates is the first committed step toward the generation of necessary compounds by five classes of chorismate-utilizing enzymes, including isochorismate synthase (ICS), anthranilate synthase (AS), aminodeoxychorismate synthase (ADCS), chorismate mutase (CM), and chorismate-pyruvate lyase (CL).

The ICS, AS, and ADCS enzymes catalyze conversions of chorismate to isochorismate, anthranilate, and aminodeoxychorismate, respectively. These three

chorismate-utilizing enzymes are related to each other by approximately 20% protein sequence homology. They share conserved active sites and display similar mechanisms.[1] Recent studies found that salicylate synthases convert chorismate to salicylate via an identifiable isochorismate intermediate and display similar active sites as ICS.[2-4] Members of CM share no sequence homology with the three chorismate-utilizing enzymes mentioned above. In addition enzymes of this family have relatively low sequence homologies among themselves. However, their active sites are conserved, catalyzing formation of prephenate for phenylalanine and tyrosine biosynthesis pathways through a conserved mechanism.[5,6] Given the importance of metabolites generated from chorismate and similarities of chorismate-utilizing enzymes, these enzymes are likely to be good targets for inhibition studies which will block the synthesis of aromatic metabolites, and hence bacterial growth and virulence.

In this chapter, the salicylate biosynthetic pathway in *P. aeruginosa* was subjected to the high throughput (HTS) experiment of searching small molecule inhibitors that would potentially serve as broad-spectrum antimicrobial reagents for *Pseudomonas*, *Yersinia*, and *Mycobacterium* infections, or as part of cocktail therapies for those infections. PchA and PchB are involved in salicylate synthesis from chorismate in *P. aeruginosa*. There are reasons why finding inhibitors for salicylate biosynthesis catalyzed by PchA and PchB is interesting. First, salicylate is required for siderophore assembly in *P. aeruginosa*, thus by cutting the supply of a crucial building block of iron chelators, *P. aeruginosa* would have problems with iron

uptake in the host environment. Second, through screening inhibition for the bi-enzyme reaction system, candidates that are capable of inhibiting salicylate formation may be relevant to homologous chorismate-utilizing enzymes of other pathogenic bacteria.

4.2 Materials and Methods

Protein Overproduction and Purification

PchB overexpression and purification were carried out as described using plasmid pET29b-*pchBs*.[7] For PchA purification, the plasmid pET28b-*pchA* was transformed into *E. coli* BL21 (DE3) competent cells. The overproduction and purification were as summarized in Table 3-4 (Chapter 3).

Chorismate Preparation

Bacterial Growth and Chorismate Accumulation

Chorismate was purified from *Klebsiella pneumoniae* 62-1 as described[8] with some modifications. Five ml of *K. pneumoniae* 62-1 overnight culture (grown at 30 °C with shaking at 250 rpm) was inoculated into 1 L of growth medium (Table 4-1) and incubated at 30 °C, shaking at 250 rpm until OD_{625} of ~ 2.0. The cells were collected by centrifugation at 6,000 × g for 10 min at 4 °C. The cell pellet was resuspended in 1 L accumulation medium (Table 4-1). The resuspension was then incubated at 30 °C with shaking of 250 rpm for 16 to 18 h. After centriguging the culture at 6,000 × g, 4 °C for 30 min, the supernatant was adjusted to pH 8.5 by

Table 4-1: Media for *K. pneumonia* 62-1 growth and chorismate secretion

Overnight Medium	
Nutrient Broth	0.4 g / 50 ml
Growth Medium (1 liter)	
Yeast extract	2 g
Casein hydrolysate	2 g
Citric acid	2 g
$MgSO_4 \cdot 7H_2O$	0.41 g
Na_2HPO_4	13.5 g
KH_2PO_4	1 g
NH_4Cl	2 g
Tryptophan	41 mg
Accumulation Medium* (1 liter)	
Glucose	10 g
Na_2HPO_4	19.2 g
KH_2PO_4	2.05 g
NH_4Cl	2.7 g
200 mM $MgCl_2$	425 µl
10 mM Tryptophan	1.5 ml

*No need to sterilize and prepare freshly

slowly adding 20 M NaOH on ice, which prevented the sample from heating.

Anion-exchange Chromatography of Accumulation Supernatant

Prior to purification, approximately 150 ml of Dower-Cl 1×8 resins (Sigma) was washed with 1 M of HCl, H_2O, 1 M NaOH, and then completely rinsed with H_2O. Unless othwise specified, the following steps were carried out at 4 °C due to the labile chorismate. The resin was mixed with the supernatant of 5 L accumulation culture and stirred for 30 min. The resin with chorismate bound was washed with 300 ml of H_2O three times before packed into an XK 50/20 column (GE Healthcare). The column was connected to an FPLC system and eluted with 3 CV (column volume) of 2 M NH_4Cl, pH 8.5 at 5 ml/min after equilibrium with 1 CV of H_2O. Each fraction of 10 ml was collected. Ten µl of each fraction was taken out and diluted by adding to 1 ml of H_2O followed by measurement of the OD_{275}. Fractions with the OD_{275} over 0.3 were pooled and acidified to pH 1.5 using 10 M HCl.

Organic Extraction and Crystallization of Chorismate

Chorismate was extracted three time from the acidified solution with equal volume of ice-cold ether. The ether extracts were pooled and dried with anhydrous $MgSO_4$ for 20 min on ice. After filtered to remove $MgSO_4$ solids, the ether extract was concentrated to less than 50 ml using rotary-evaporation at 22 °C. Light petroleum ether was slowly added to concentrated ether until the solution remained cloudy for a few seconds before clearing. The mixture was then cooled on ice to

allow chorismate to crystallize from the ether. Scratching against the glass wall was used to promote nucleation of chorismate crystals. After chorismate crystals were developed for 2 h, more light petroleum ether was added to promote the complete crystallization of chorismate. The yellow chorismate crystallites were filtered and vacuum-dried over P_2O_5 at 4 °C overnight.

Recrystallization of chorismate was conducted to remove yellow contaminants. The chorismate was dissolved in a minimal amount of ether with stirring. A small amount of activated charcoal was added to remove yellow impurities followed by removal of charcoal by regular filtration. The chorismate was the recrystallized from ether by the addition of an equal amount of methylene chloride and two volumes of hexane. The chorismate crystals were allow to develo at 4 °C for 2 h, followed by the addition of more hexane to ensure full recrystallization of chorismate. Chorismate crystals were filtered and dried over P_2O_5 under vacuum at 4 °C for overnight, then stored at – 80 °C.

Coupled Assay for HTS

In order to transform the assay from cuvette to a HTS microplate, the coupled assay[9] of PchA and PchB was modified from that previously described. The enzymes concentration versus substrate concentration were optimized using a matrix to obtain the best condition with linear production formation over at least 20 min. The reaction solution (70 µl) that gave the best result is composed of 50 mM TrisHCl, pH 7.5, 10 mM $MgCl_2$, 1 mM DTT, 10% glycerol, 20 µM PchA, 20 µM PchB, and 5 mM

chorismate. Salicylate accumulation was measured with excitation of 300 nm and emission of 430 nm using a Cary Eclipse fluorescence spectrophotometer (Varian) with a high-speed photomultiplier tube (PMT) detector voltage of 800 V.

HTS of Inhibitors of Coupled PchA and PchB Reaction

Purified PchA, PchB, chorismate and reaction buffers were sent to the High Throughput facility at The University of Kansas. The final assay development and validation, and the compound library screens were conducted by researchers at HTS facility.

4.3 Results and Discussion

The purpose of HTS is to identify inhibitors for PchA or PchB through screening for inhibition of salicylate production. To initiate screen of compound libraries, sufficient amounts of enzymes are required. Using the protocols described herein 15 g of PchA and 3.5 g of PchB were produced for these purpose.

Substrate chorismate is commercially available, however is extremely expensive with a price of $979 for 100 mg of 80% purity (Sigma). To produce 16 g of chorismate that HTS estimated would be required to do the screening with purity above 90%, *K. pneumoniae* 62-1 was used for biosynthesis of chorismate. *K. pneumoniae* 62-1 is a triple mutant that blocks the aromatic amino acid biosynthesis in this strain, leading to secretion of chorismate into medium in presence of tryptophan.[10] The average yield was ~ 400 mg/L of 60 to 70% pure chorismate (from

crystallization process).[8] The recrystallization process resulted in ~ 90% pure chorismate as evaluated by the HPLC analysis and ^{1}H-NMR spectrum (Figure 4-1), but decreased yields by half. The final yield of chorismate was ~ 200 mg/liter accumulation medium and a total of 15.6 mg 90% pure chorismate was produced.

A preliminary experiment was conducted to ensure that the enzymes and substrate were active in a 384-well plate used in the HTS experiment. Figure 4-2 shows the fluorescence of salicylate production over time, comparable to the reaction described in chapter 3. The pure chorismate was also subjected to NMR experiment. The proton NMR spectrum of chorismate indicates the highly pure chorismate, which is consistent with the published data.[11,12]

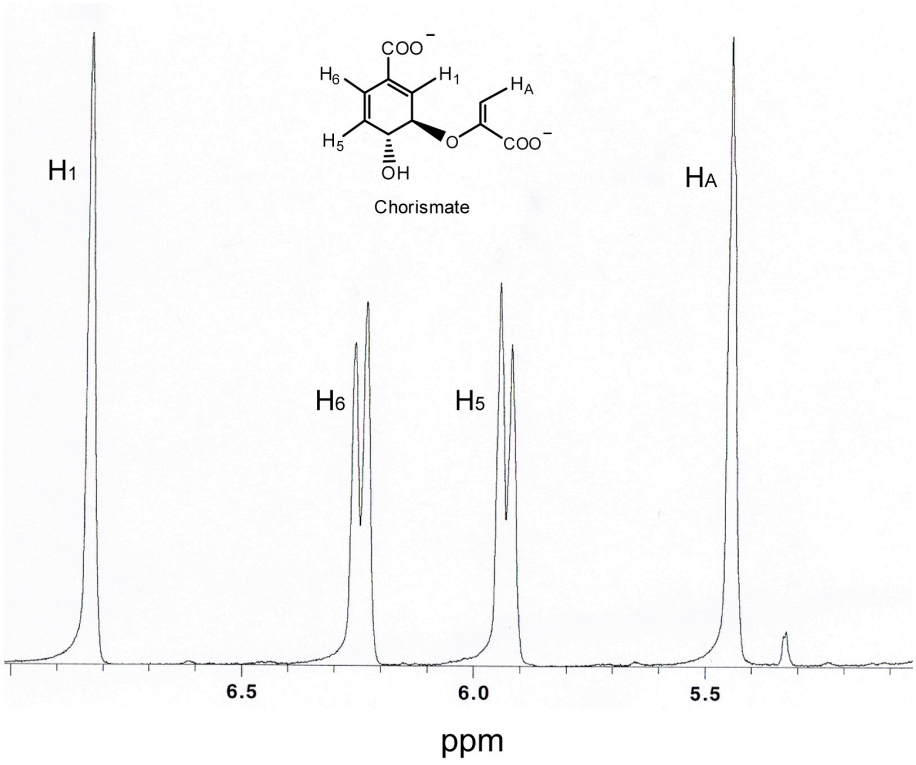

Figure 4-1: ^{1}H-NMR spectrum of chorismate purified from *K. pneumonia* 62-1. The resonances arising from chorismate H_1, H_5, H_6, and H_A in the region of 5.0 – 7.0 ppm. There is no presence of contaminants after 7.0 ppm.

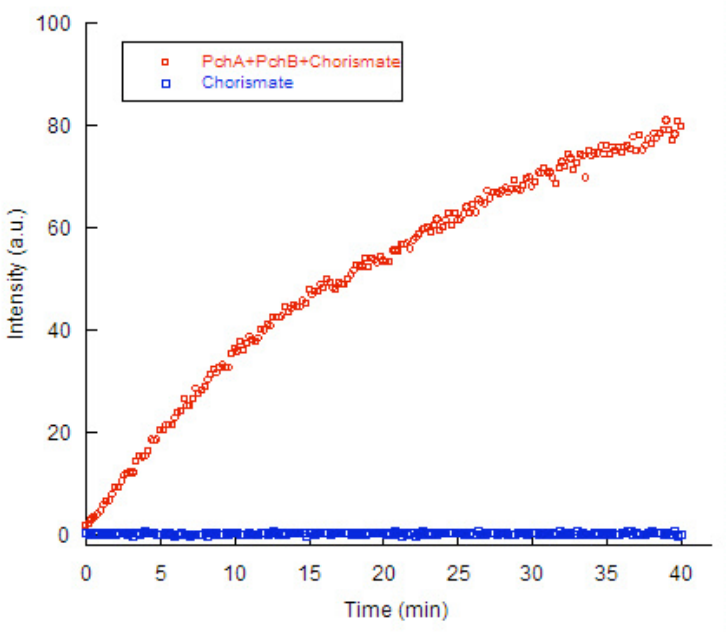

Figure 4-2: Coupled PchA and PchB assay using chorismate purified from *K. pneumoniae* 62-1. The fluorescent intensity of salicylate was monitored.

References

1. He, Z., Stigers Lavoie, K.D., Bartlett, P.A. & Toney, M.D. Conservation of mechanism in three chorismate-utilizing enzymes. *J Am Chem Soc* **126**, 2378-85 (2004).
2. Kerbarh, O., Chirgadze, D.Y., Blundell, T.L. & Abell, C. Crystal structures of Yersinia enterocolitica salicylate synthase and its complex with the reaction products salicylate and pyruvate. *J Mol Biol* **357**, 524-34 (2006).
3. Zwahlen, J., Kolappan, S., Zhou, R., Kisker, C. & Tonge, P.J. Structure and mechanism of MbtI, the salicylate synthase from Mycobacterium tuberculosis. *Biochemistry* **46**, 954-64 (2007).
4. Parsons, J.F., Shi, K.M. & Ladner, J.E. Structure of isochorismate synthase in complex with magnesium. *Acta Crystallogr D Biol Crystallogr* **64**, 607-10 (2008).
5. Davidson, B.E. Chorismate mutase-prephenate dehydratase from Escherichia coli. *Methods Enzymol* **142**, 432-9 (1987).
6. Lee, A.Y., Stewart, J.D., Clardy, J. & Ganem, B. New insight into the catalytic mechanism of chorismate mutases from structural studies. *Chem Biol* **2**, 195-203 (1995).
7. Zaitseva, J., Lu, J., Olechoski, K.L. & Lamb, A.L. Two crystal structures of the isochorismate pyruvate lyase from Pseudomonas aeruginosa. *J Biol Chem* **281**, 33441-9 (2006).
8. Rieger, C.E. & Turnbull, J.L. Small scale biosynthesis and purification of gram quantities of chorismic acid. *Prep Biochem Biotechnol* **26**, 67-76 (1996).
9. Gaille, C., Reimmann, C. & Haas, D. Isochorismate synthase (PchA), the first and rate-limiting enzyme in salicylate biosynthesis of Pseudomonas aeruginosa. *J Biol Chem* **278**, 16893-8 (2003).
10. Gibson, M.I. & Gibson, F. Preliminary studies on the isolation and metabolism of an intermediate in aromatic biosynthesis: chorismic acid. *Biochem J* **90**, 248-56 (1964).
11. Copley, S.D. & Knowles, J.R. The Conformational Equilibrium of Chorismate in Solution - Implications for the Mechanism of the Nonenzymatic and the Enzyme-Catalyzed Rearrangement of Chorismate to Prephenate. *Journal of the American Chemical Society* **109**, 5008-5013 (1987).
12. Rusnak, F., Liu, J., Quinn, N., Berchtold, G.A. & Walsh, C.T. Subcloning of the enterobactin biosynthetic gene entB: expression, purification, characterization, and substrate specificity of isochorismatase. *Biochemistry* **29**, 1425-35 (1990).

CHAPTER 5

Conclusion

During infections, pathogenic bacteria encounter an environment of iron starvation due to the strictly controlled iron homeostasis in mammal hosts. To cope with the requirement of iron for growth, colonization, and virulence, these bacteria have evolved several ways to extract iron from hosts. One of these is to excrete and reuptake siderophores, small organic compounds with extremely high affinity for ferric iron.[1] In *Pseudomonas aeruginosa* two siderophores, pyochelin and pyoverdin, are secreted during its infection and associated with its virulence.[2] Salicylate serves as a precursor for the phenolate-type siderophore, pyochelin. Since siderophore production is related to virulence, the inhibition of siderophore biosynthetic enzymes could lead to reduction in virulence and could provide a basis for the development of novel antimicrobial drugs.

This thesis focuses on two enzymes, PchA and PchB, which are responsible for salicylate biosynthesis in *P. aeruginosa*. The ultimate goal of this research is to elucidate how these enzymes promote chemical reactions in their active sites biochemically and structurally. Information obtained would provide a scaffold for the development of antimicrobial agents for *P. aeruginosa* infections, which could also extended to other pathogenic bacteria that also produce phenolate-type siderophore, including *Yersinia* sp. and *Mycobacterium tuberculosis.*

PchB has not only a physiological role as isochorismate-pyruvate lyase, IPL to transform isochorismate to salicylate, but also an adventitious activity as a chorismate mutase, CM to rearrange chorismate to prephenate.[3] Structural and mechanistic analyses of wild type PchB suggest that catalytic events of both IPL and CM take place in a single active site without formation of any covalent intermediates.[4] CMs, PchB structural homologues, have been in the center of studies for the origin of enormous catalytic power of enzymes. The transition state stabilization theory proposes that CM active site provides an electrostatic environment that would accommodate the developing negative charge in the transition state, such that the activation energy barrier is lowered, and hence achieve the rate acceleration.[5] The reactive substrate conformation believes that chorismate preorganized into a reactive conformer (defined as a near-attack conformation, NAC by Bruice and co-workers) that is constrained and stabilized by the enzyme active site, which will promote substrate progression to the transition state without any further requirement for energy inputs.[6]

An active site residue (Lys42) residing in the mobile loop between the first two helices is proposed to be critical for catalysis.[4] In chapter 2, PchB active site (Lys42) mutants were examined to determine the relative contributions of the transition state stabilization and reactive substrate destabilization during CM and IPL catalysis. For CM activity, a positive charge at position 42 is critical for efficient catalysis, indicating that the transition state stabilization serves as the major source of CM catalysis. However, in order to maximize catalytic efficiency, a reactive substrate

conformation is required to adapt in the active site for CM catalysis. For IPL activity, stabilizing the transition state and the reactive substrate conformer are required for catalysis, but not to the same extent. From this chapter, we conclude that while formation of a reactive substrate conformer is a prerequisite for pericyclic reactions catalyzed by PchB, electrostatic stabilization of the transition state would provide the means by which the enzyme obtain efficient catalysis.

PchA is an isochorismate synthase, catalyzing an isomerization of chorismate to isochorismate, which is the first step in salicylate biosynthesis in *P. aeruginosa*.[7] In *Yersinia* sp. and *M. tuberculosis*, salicylate synthesis only requires a single enzyme, salicylate synthase, to generate salicylate from chorismate via an isochorismate intermediate.[8, 9] The question addressed in chapter 3 is why PchA does not have the ability to perform the second reaction in salicylate synthesis pathway, even it has high sequence homology with salicylate synthases in *Y. enterocolitica* and *M. tuberculosis*. By comparing the sequence between PchA and structure-known salicylate synthase Irp9,[10] four active site amino acids achieved attention. Two conserved amino acids among chorismate-utilizing enzymes, K221 and E269 in PchA, are responsible for the general acid and base catalytic reaction mechanism. Replacements of these two sites by alanine resulted in complete loss of catalytic efficiency in PchA. The pH profile for PchA exhibits a bell-shaped curve, which suggests that two ionizable groups participate in catalysis. Taken together, these results suggest that activation of a water molecule by K221 as a general base promotes the nucleophilic attack on C2, and E269 acts as a general acid to facilitate departure of hydroxyl group from C4 on

chorismate, as proposed for mechanism of conversion of chorismate to isochorismate by PchA. The other two amino acids selected to study are non-conserved between salicylate synthase and isochorismate synthase. Our purpose is to investigate whether a mutation of non-conserved amino acid to the corresponding counterpart in salicylate synthase would be able to transform isochorismate synthase into salicylate synthase. PchA D310E gave promising results in that replacement of only a single residue, enzyme creates two additional activities, CM and IPL. These three activities, ICS, IPL, and CM can be deconvoluted by measuring the kinetic constants for each activity in the future. Additionally in the future structural determination of the PchA wild type and D310E could provide insight into the new hypothesis for reaction mechanism catalyzed by this mutant. The ICS MenF, salicylate synthase Irp9, and MbtI can serve as models for structure solution of PchA and D310E.

PchA, PchB, and chorismate have been prepared for high throughput screening, where various chemical compounds are tested for their ability to inhibit the salicylate synthesis *in vitro*. The compounds with highest IC_{50} against PchA or PchB will provide a starting point for designing antimicrobial agents for *P. aeruginosa* infection. Further improvement of these compounds could benefit from the detailed analyses of the reaction mechanism and structure of salicylate biosynthetic enzymes, PchA and PchB.

References

1. Wandersman, C. & Delepelaire, P. Bacterial iron sources: from siderophores to hemophores. *Annu Rev Microbiol* **58**, 611-47 (2004).
2. Lamont, I.L., Beare, P.A., Ochsner, U., Vasil, A.I. & Vasil, M.L. Siderophore-mediated signaling regulates virulence factor production in Pseudomonasaeruginosa. *Proc Natl Acad Sci U S A* **99**, 7072-7 (2002).
3. Gaille, C., Kast, P. & Haas, D. Salicylate biosynthesis in Pseudomonas aeruginosa. Purification and characterization of PchB, a novel bifunctional enzyme displaying isochorismate pyruvate-lyase and chorismate mutase activities. *J Biol Chem* **277**, 21768-75 (2002).
4. Zaitseva, J., Lu, J., Olechoski, K.L. & Lamb, A.L. Two crystal structures of the isochorismate pyruvate lyase from Pseudomonas aeruginosa. *J Biol Chem* **281**, 33441-9 (2006).
5. Warshel, A. et al. Electrostatic basis for enzyme catalysis. *Chem Rev* **106**, 3210-35 (2006).
6. Bruice, T.C. & Lightstone, F.C. Ground state and transition state contribution to the rates of intramolecular and enzymatic reactions. *Acc. Chem. Res.* **32**, 127-136 (1999).
7. Gaille, C., Reimmann, C. & Haas, D. Isochorismate synthase (PchA), the first and rate-limiting enzyme in salicylate biosynthesis of Pseudomonas aeruginosa. *J Biol Chem* **278**, 16893-8 (2003).
8. Liu, J., Quinn, N., Berchtold, G.A. & Walsh, C.T. Overexpression, purification, and characterization of isochorismate synthase (EntC), the first enzyme involved in the biosynthesis of enterobactin from chorismate. *Biochemistry* **29**, 1417-25 (1990).
9. Harrison, A.J. et al. The structure of MbtI from Mycobacterium tuberculosis, the first enzyme in the biosynthesis of the siderophore mycobactin, reveals it to be a salicylate synthase. *J Bacteriol* **188**, 6081-91 (2006).
10. Kerbarh, O., Chirgadze, D.Y., Blundell, T.L. & Abell, C. Crystal structures of Yersinia enterocolitica salicylate synthase and its complex with the reaction products salicylate and pyruvate. *J Mol Biol* **357**, 524-34 (2006).